Modeling of the interaction between neuronal populations involved in memory consolidation during the sleep-wake switch

Auteur : Preud'Homme, Chloé
Promoteur(s) : Drion, Guillaume
Faculté : Faculté des Sciences appliquées
Diplôme : Master en ingénieur civil biomédical, à finalité spécialisée
Année académique : 2020-2021
URI/URL : http://hdl.handle.net/2268.2/11559

Modeling of the interaction between neuronal populations involved in memory consolidation during the sleep-wake switch

Master thesis realized with the aim of obtaining the degree of Master in Biomedical Engineering

Chloé Preud'homme

Supervisor:
G. Drion

Jury members:
C. Phillips
D. Ruffoni
P. Sacré
V. Seutin

University of Liège
Faculty of Applied Sciences
Academic year 2020 - 2021

Modeling of the interaction between neuronal populations involved in memory consolidation during the sleep-wake switch

Chloé Preud'homme

Supervisor: G. Drion
Master in Biomedical Engineering, University of Liège
Academic year 2020-2021

Abstract

It has been shown experimentally that memory consolidation occurs during sleep and that three brain regions are involved in this process: the thalamus, the neocortex and the hippocampus. The hippocampus has been shown as being the short-term store of the representation, the neocortex as the long-term store and the thalamus as the coordinator of the consolidation during sleep. As an illustration, when an individual experiences a camping event in which he observes his tent and the trees, he can recall a representation of this event after a night of sleep at the sight of his tent. The representation has been consolidated in the long-term store, the connections between the two items are reinforced in the neocortex thanks to neuronal ensemble reactivations occurring in the hippocampus during sleep. It appears that the synchronization of their electrical behaviour is essential for the consolidation of the experience in the neocortex.

In order to deepen our knowledge about how memories are consolidated thanks to those organs, computational modeling is a powerful approach for testing various stimuli. However, the cellular communication between these three regions is computationally under-investigated.

Therefore, this present work aims to reproduce a simplified and faithful computational representation of global and local interactions in the context of memory consolidation. The global anatomy and the role of these brain regions are first highlighted and the oscillations of the sleep-wake cycle are examined. The neurophysiology of each cell types composing the different regions is deeply studied by exploring the literature. Then, the way the cells communicate is inspected in order to build a simplified but still representative cellular network connecting the three regions and demonstrating their communication during wakefulness and sleep. To that aim, conductance-based models are suitable modeling tools used for reproducing the electrical behaviour of the distinct types of cells constituting the thalamus, neocortex and hippocampus.

The behaviour of each cell taken individually is favourably reproduced with the aim of replicating the communication between each cell in the built network, which is performed successfully. Moreover, the network developed is robust to variability.

Liège, June 9^{th}, 2021

Chloé Preud'homme

Acknowledgements

Firstly, I am deeply grateful to my supervisor Professor Guillaume Drion for devoting his time in giving valuable guidance and feedback throughout the completion of this inspiring project.

I would also like to offer my special thanks to Kathleen Jacquerie for her availability, the helpful and constructive comments and suggestions.

Additionally, I would also like to express my gratitude to Professor Vincent Seutin for his availability and for the insightful discussions we had.

Then, I would like to express my gratitude to Caroline and Chloé who brought a lot of emotional support and with whom I could have enriching conversations helping me through the elaboration of this project.

Furthermore, I am extremely grateful to my friend Myriam for her encouragements and devotion. I would also like to acknowledge Charlotte, Myriam, Isabelle, Claire and Laura who supported me throughout the development of this project.

Finally, I would like to profoundly thank my family for their support and for always believing in me.

Contents

Chapter 1

Introduction

1.1 Motivations

The motivation behind this thesis arises from the will to better understand the principle of memory consolidation occurring during sleep. When experiencing a particular event, the features of the representation are encoded during wakefulness and are stored on a long-term basis during sleep. On the subsequent day, the consolidated representation can be retrieved. It has been highlighted that sleep protects memory from being erased [Klinzing et al. (2019a)]. This is due to an intrinsically organized brain activity during sleep emerging from the interconnection between three distinct brain regions playing essential roles in memory consolidation. These brain regions are the thalamus, the neocortex and the hippocampus. There exist theories highlighting experimentally the processes of encoding, consolidation and retrieval of experiences stemming from the interaction between these brain regions and the coupling of their rhythmic activity during sleep [Klinzing et al. (2019a)] and [Tononi and Cirelli (2014)]. To my knowledge, there has been no evidence in the literature that reproduces computationally the interaction between these three regions. It is well established that neurons' electrical activity can be reproduced with powerful modeling tools like the conductance-based model. However, the reproduction of the neuronal interconnection between the brain regions supporting memory consolidation is quite challenging as the brain counts 100 billion neurons and is the most complex organ of the human body. This thesis aims at further studying this ambiguous topic of experience encoding and memory consolidation by answering the following questions:

- How do the thalamus, the neocortex and the hippocampus interact?
- What is the specific role of these regions in memory consolidation?
- What are the principal cells of each region and how to provide a simplified but faithful model?
- How do these cells discharge during wakefulness and subsequent sleep?
- What is the neurophysiology of each type of cell?
- What is the architecture of each region?
- How do the principal neurons of each region interact during sleep and wakefulness and how can this interaction be modeled?

1.2 Structure

This thesis is divided into four main parts.

Part I introduces the notion and the different types of memory (CHAPTER 2). Then, it underlines the general anatomy, the role of the thalamus, the neocortex and the hippocampus and provides the

global interconnection between these regions (CHAPTER 3). It also offers an insight on neurophysiology and neuronal modeling by describing the anatomy of the cell, the neuronal membrane electrical behaviour given by conductance-based model and by investigating the communication process between two cells *i.e.* synapses and neurotransmitters (CHAPTER 4). Afterwards, the sleep-wake cycle is explored. The EEG oscillations, the sleep signatures and the cellular mechanism underlying these processes are clarified. Finally, the switch between wakefulness and sleep is explained by describing the action of neuromodulators and the different neuronal discharge modes. The strength of the connections are also altered by the brain state and the difference in the interconnection between the regions between wakefulness and sleep is presented (CHAPTER 5). The *Active systems consolidation theory* on which this project is based is presented and an analogy to this project is illustrated (CHAPTER 6).

Part II is devoted to research of the literature. On the one hand, analysis about the main types of cells of a region is lead. Models providing information about the corresponding types of currents, the order of magnitude of the related ionic conductances, the types of synaptic receptors and the approximate firing rate are investigated for the thalamocortical circuit and the hippocampal formation (CHAPTER 7 and 8). On the other hand, the connections between the main cell types of each region are examined in order to build the architecture of a neuronal network underlying the processes of encoding during awake states and memory consolidation during sleep. Moreover, the mnemonic role of hippocampal regions are underlined (CHAPTER 9).

Part III is dedicated to the modeling of the neuronal network built in PART II. Ionic conductances, synaptic receptors and the firing rates are respected. This allows the development of a physiological model tuned to obtain the desired pattern of activity of each cell in the network during wakefulness and sleep (CHAPTER 10). The robustness of the model is assessed by testing the variability of the ionic conductances of each cell which provides a more biological dimension to the network.

Part IV answers the questions that are asked in this context and that brought to the establishment of the network modeling. It also brings perspectives on possible improvements that could be added to the model. The addition of the subiculum and synaptic plasticity could be included, the latter to test the reinforcement of synaptic connections occurring during memory consolidation. Robustness could be further verified on more numerous circuits.

Part I

Background

Chapter 2

Memory

Memory can be defined as the capacity of an individual to retain and retrieve learned information which enables him to adapt his behaviour in response to a continuously changing environment [Bear et al. (2016)]. It is challenging to describe memory. Indeed, it depends on different aspects for example, the time of retention, the structure of the brain involved or the content of the memorization. Based on the latter, it is possible to define different types of memory and subcategories represented in FIGURE 2.1 [Rasch and Born (2013), G. Vandewalle (2019)].

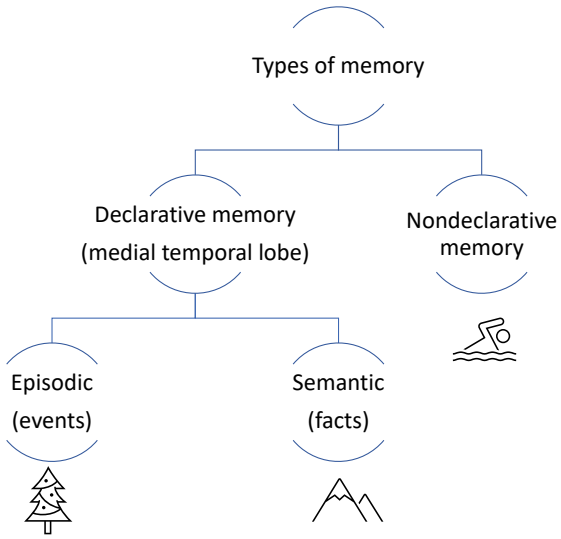

Figure 2.1 – Types of memory. - Based on the content of memorization, memory can be catgorized in declarative memory (relying on brain structures in the medial temporal lobe) and the nondeclarative memory. The declarative memory can be subcategorized into the episodic and semantic memory. The tree symbolizes a Christmas event, the mountains symbolizes the Everest peak and the swimmer represents the skill of swimming. - Adapted from [Bear et al. (2016)]

2.1 Declarative memory

What is declarative memory?

Declarative memory is the explicit type of memory that can be retained intentionally or unintentionally and can be retrieved with awareness [Rasch and Born (2013)]. It can be subcategorized into two distinct types: episodic and semantic memory.

- The **episodic type of memory** denotes the memory of autobiographical life events that can be remembered by only living it once but is subjected to forgetting. It consists in the contextualization of life experiences like a wedding or a Christmas evening.

- The **semantic memory** denotes the memory of facts that requires multiple trials to be remembered like knowing that Everest is the highest peak in the world. The context in which one learned this information is not remembered.

Declarative memory depends on a particular structure of the medial temporal lobe region: the hippocampus [Rasch and Born (2013)].

Memory consolidation and sleep

Most of the events and facts that are temporarily (seconds to few minutes) held in the brain and that are prone to decay constitutes the short-term memory. Only a small portion of the events experienced last for days, months, years known as the long-term memory storage. An experience is converted into a long-term memory thanks to the process of memory consolidation. The process underlying the formation of long-term memory is represented in FIGURE 2.2. Memory function is divided into three subprocesses: encoding of the information, the consolidation and then the recalling of the information. The consolidation of memory takes place during sleep and strengthen the newly encoded information into the preexisting long term memory: the neocortex [Rasch and Born (2013)].

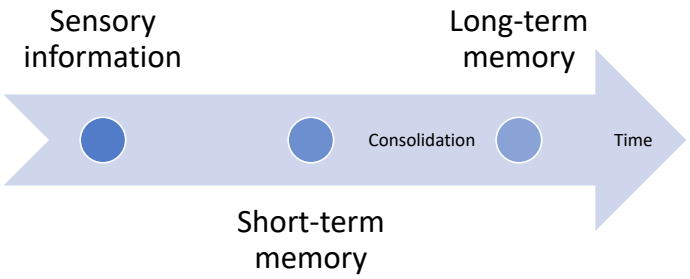

Figure 2.2 – Memory consolidation process. - Sensory stimulus experienced during the day is converted into short-term memory which in turn is consolidated into long-term memory. Adapted from [Bear et al. (2016)]

2.2 Nondeclarative memory

The nondeclarative memory is the implicit type of memory (see FIGURE 2.1). It is mainly concerned with the procedural memory for skills, habits, behaviour or conditioning. For example, one learned when he was young how to swim, he does not recall the event during which he learned but he still has the skills to swim which do not require consciousness [Bear et al. (2016)] The formation of nondeclarative memory does not rely on the medial temporal lobe but on other areas of the brain such as the striatum, cerebellum and motor or sensory cortices for the procedural memory and the amygdala and cerebellum for particular types of conditioning [Rasch and Born (2013)].

Chapter 3

Anatomy of the brain

The thesis focuses on the interaction between the neurons of the different organs involved in memory consolidation namely the thalamus, the neocortex and the hippocampus. This section aims at describing the general anatomy and the role of the three different organs.

3.1 Thalamus

3.1.1 General anatomy

The first major actor involved in memory consolidation is the thalamus. The thalamus is located below the hypothalamus and are both parts of the diencephalon which is inserted in between the brain stem and the neocortex as shown in FIGURE 3.1. The thalamus is divided into different zones which are relay

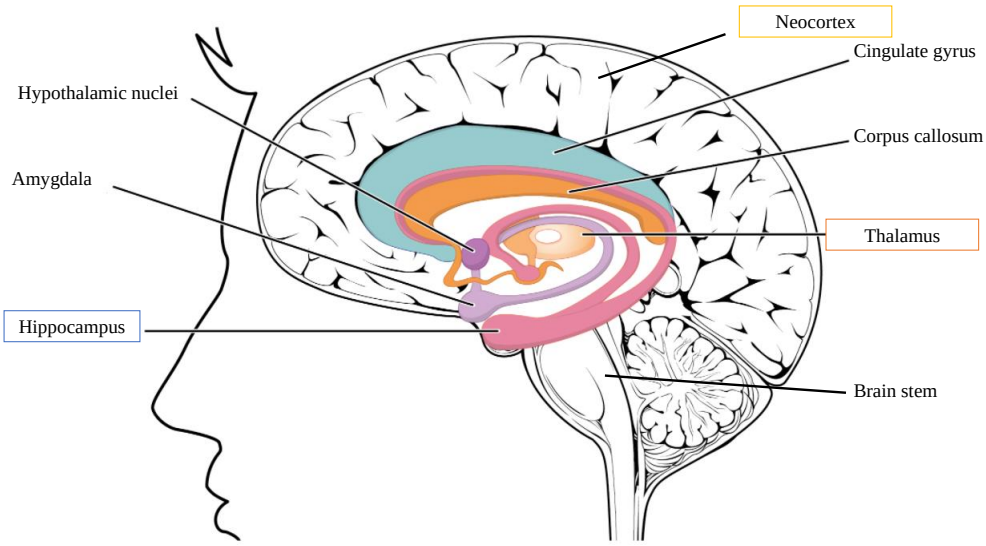

Figure 3.1 – Sagittal cut of the brain. - The thalamus (embedded in an orange box) is situated between the brain stem and the neocortex. The neocortex (embedded in a yellow box) constitutes the external layer of the brain and has two hemispheres linked by the corpus callosum. The hippocampus (embedded in a blue box) has the shape of a "seahorse" and forms a border on the brain stem. The coloured regions sit in the temporal lobe. - Adapted from [Giovannini (2017)]

thalamic nuclei each composed of excitatory relay neurons which are specialized and receive different types of sensory information (auditory, visual, vestibular, somatosensory and gustatory) *e.g.* lateral geniculate nucleus (LGN) is the relay nucleus for visual stimuli as shown in FIGURE 3.2. Other kinds of thalamic nuclei are the thalamic reticular nuclei (TRN) which is a thin sheet of inhibitory interneurons enveloping the rugby ball-shaped relay thalamic nuclei and inhibiting relay neurons. These neurons are the reticular neurons (RE). Excitatory and inhibitory neurons differ in the type of neurotransmitter they produce as will be explained further in SECTION 4.4.

3.1.2 Role

The thalamus acts as a gateway to the neocortex and its main purpose is to sort and relay the sensorial information except the olfactory information coming from the external world to the right part of the neocortex. The thalamus is essential for specifying the pattern of cortical areas [Bear et al. (2016)]. This external type of input to the relay thalamic nuclei are called drivers but there can also be inputs coming from other brain regions that modify the transmission of the external information which are known as modulators. Modulators can be inputs coming from the brain stem region, feedbacks from the cortex and from the TRN [Brain's explained (2017b)]. An example of a driver input can illustrate the role of relay of the thalamus and is represented in FIGURE 3.2. A visual stimulus is first generated by the photoreceptors present on the retina from the external light. The stimulus is vehiculated from the two retinae via the optical nerves to the optic chiasm where the nerves from both retinae cross each other. The information is then relayed to the LGN. The thalamic relay neuron of the LGN nucleus then project to specific regions of the primary visual cortex and also to the cells of perigeniculate nucleus (PGN) of the thalamic reticular nucleus which in turn sends inhibitory connections to the relay cell [Bear et al. (2016)]

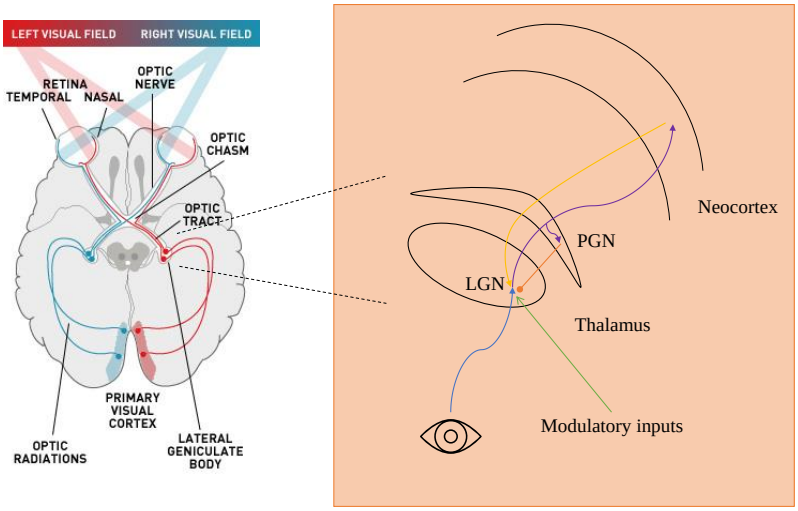

Figure 3.2 – Visual pathway (right) and TRN, thalamic relay cells and neocortex interconnection (left). -A visual stimulus formed by photoreceptors present in the retina travels to the thalamic relay cell, the LGN (blue arrow) which projects its axons to the PGN and the neocortex (purple arrows). The PGN in turn inhibits the LGN (orange dotarrow head). The neocortex excites the LGN (yellow arrow). A modulatory input can also influence LGN cells responses (green arrow). - Adapted from [Trusted Neurodiagnostics academy]

Moreover, the thalamus enables the brain to switch between two different states, wakefulness and sleep. Its role is therefore primordial in the sleep-dependent memory consolidation. During sleep, the thalamus can block incoming signals by synaptic inhibition while during wakefulness, the input can enter the brain [Steriade et al. (1993)]. The thalamus is also believed to be the coordinator of consolidation during sleep [Klinzing et al. (2019a)].

3.2 Neocortex

3.2.1 General anatomy

The neocortex corresponds to the external layer of the brain and possesses two hemispheres linked by the corpus callosum. It contains bumps and furrows which are almost the same in every individual to increase cortical surface [G. Vandewalle (2019)] (see FIGURE 3.1). The neocortex is composed of different types of cortical neurons that are organized in layers parallel to the surface of the brain [Bear et al. (2016)]. There are a total of six layers. The first level is called the molecular layer or pia

matter, it does not contain any cell bodies and there is also a level that contains *pyramidal neurons* of the neocortex which have larger dendrites, *i.e.* apical dendrites extending to the first level. Cortical neurons in each of these layers have a certain shape, certain connections between them and therefore certain functions which are not the same everywhere in the neocortex. Based on this, it is possible to delimit the neocortex into different zones which have different cell organization *i.e.* a different cytoarchitecture. Different looking cortical areas achieve different functions. These different zones are called Brodmann areas and each area has a different function in terms of processing the information. The related functions of each area are close to each other and each area with a particular function is assigned a number [G. Vandewalle (2019)]. For example, zone 17 is the visual cortex, zone 4 is the motor cortex. The thalamus contributes to this separation of the neocortex in zones [Bear et al. (2016)] as previously stated.

3.2.2 Role

The neocortex is the region of the brain that governs the processing of the sensorial information coming from the external world and enables the body to respond to sensorial stimuli. The processing of the information is quite complex and there are a lot of interconnections between different types of neurons and different brain areas. The neocortex enables the functional integration of the information as it has a hierarchical organization between the cortical areas. The primary sensory cortex is the first zone to receive the information and decodes the basic properties of the stimulus. Then, the unimodal sensory association cortex interprets the stimulus and has strong connections with the primary sensory cortex. Then, the multimodal association cortices unify multimodal perception, encode information in memory and allow motor coordination [G. Vandewalle (2019)]. Therefore, the neocortex is a map of the different areas that are precisely interconnected to perform specific function enabling to give a unified perception of the environment [Bear et al. (2016)]. The generation of action is generated in the motor cortex. While the ascending path had a hierarchical organization at the level of the cortices, the descending path has a dehierarchisation.

The information journey in the neocortex is represented in FIGURE 3.3.

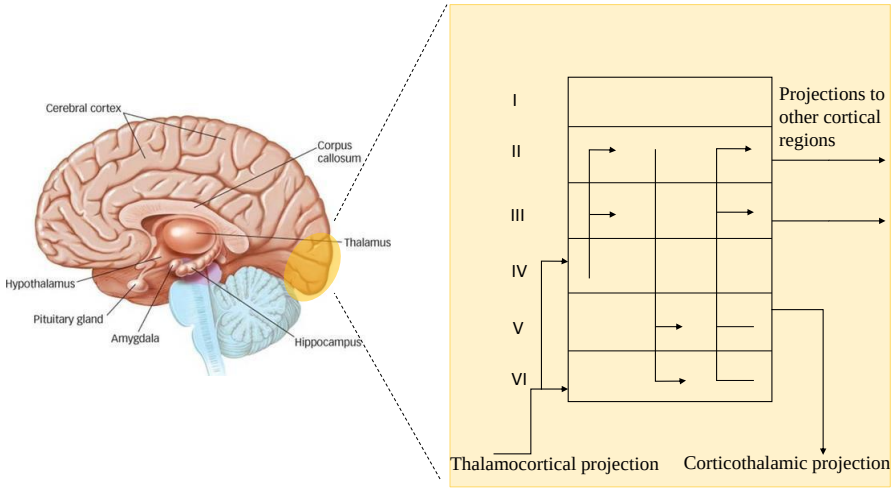

Figure 3.3 – Primary visual cortex column - The visual stimulus relayed by the LGN is send to the primary visual cortex in area 17 (left: highlighted in yellow) in layer IV and VI. Contacts are made between different layers of the cortical column: axons from neurons in layer IV project to layer II & III which project to layer V & VI which in turn project to layer II & III. Axons from layer II & III project to other cortical regions and axons from layer V project back to the LGN. - Adapted from [Mind fully well]

The path of the visual stimulus previously relayed by the thalamus can also be illustrated to understand the processing of a sensorial stimulus in the neocortex:

- The information is relayed from the LGN to the primary visual cortex in area 17 in specific layers

- LGN projections terminate principally in layer IV and VI of the cortical column [Wei et al. (2016), McCormick et al. (2015), Sherman (2001)].
- Neurons in layer IV and VI make contact with other cortical layers having distinct local, efferent and afferent connectivity [Brain's explained (2017a) Hill and Tononi (2005)]. The neuronal projection goes from layer IV to layer II & III which in turn project to layer V & VI then back to layer IV and layer II & III [Hill and Tononi (2005), Olcese et al. (2010), Brain's explained (2017a)].
- Layer V consists of corticothalamic neurons sending back their connections to the TRN and the thalamic relay nuclei [McCormick et al. (2015)].
- Layer II & III send projections to other regions of the cortex [Brain's explained (2017a)].

Furthermore, the neocortex is the site of long-term memory storage holding the consolidated representation during sleep [Langille (2019)].

3.3 Hippocampus

3.3.1 General anatomy

The hippocampus is a folded allocortical structure that is named after its shape of a "seahorse" and is located in the limbic lobe [Giovannini (2017)]. The allocortex constitutes a distinct piece of the cortex different from the neocortex due to its unique connections and specific neuron types which convey it with particular functions [Buzsaki (2006)]. The limbic lobe is named after its shape, limbus meaning "border" as it forms a border around the brain stem and it sits in the medial temporal lobe of the brain [Bear et al. (2016)]. It is composed of the cingulate gyrus, the medial temporal cortex and the hippocampus (see FIGURE 3.1). The role of the limbic system is multiple. It plays a role in the feeling and expression of emotions but also in behaviour, olfaction, motivation, adrenaline flow and memory consolidation. The latter function is believed to be accomplished by the hippocampus [Giovannini (2017)]. The hippocampus is composed of two layers of neurons folded onto each other. One layer is the tooth-shaped dentate gyrus and the other one is the C-shaped Ammon's horn which is divided into four parts: CA1, CA2, CA3, CA4, CA standing for "Corpus Ammonis". The CA3 region consists of two layers of neurons with recurrent projections [Buzsaki (2006)]. Usually, the parts of interest are the CA1 and CA3 zones [Bear et al. (2016), O'Mara et al. (2001)]. The hippocampal formation consists of the dentate gyrus, the CA1-CA3 zones, the subiculum and the entorhinal cortex [O'Mara (2005)]. The hippocampal formation is a connection network that can operate in a loop each stages integrating and processing information for the consolidation of memory as represented in FIGURE 3.4.

The sensory information flowing from the neocortical areas to the hippocampal formation pass through the parahippocampal cortex, perirhinal cortex, constituting together with the hippocampal formation, the medial temporal lobe [Bear et al. (2016)]. Their inputs comes from unimodal and polymodal association cortices (auditory, visual, somatosensory). Their mutual connections confer a higher degree of associative integration of the information [Lavenex and Amaral (2000)]. The hippocampal formation microcircuit is represented in FIGURE 3.4 and is the following:

1. Layers II and III of the entorhinal cortex (EC) receives input from association cortices of the neocortex and are the major input regions of the hippocampus [O'Mara et al. (2000)].
2. The information then flows from layer II of the entorhinal cortex via its projecting axons constituting the perforant path to the dentate gyrus and the CA3 region. Information also flows from layer III of the entorhinal cortex to the CA1 region and the subiculum [Xu et al. (2016), O'Mara (2005), O'Mara et al. (2000), O'Mara et al. (2000)]. Layer II and III constitute the superficial layer of the entorhinal cortex.
3. The information further integrated by the dentate gyrus is transmitted via the mossy fibres projecting to the CA3 region possessing recurrent excitatory connections

4. The information from CA3 flows to CA1 via the Schaffer collaterals.

5. Then the subicular complex subdivided into the subiculum itself and also the presubiculum and parasubiculum [O'Mara et al. (2001)] is the major output of the hippocampus and receives input from the CA1 region of the hippocampus which also directly project to the entorhinal cortex layer V and VI.

6. The information goes back to the deep layer V and VI of the entorhinal cortex constituting the way out of the hippocampal formation.

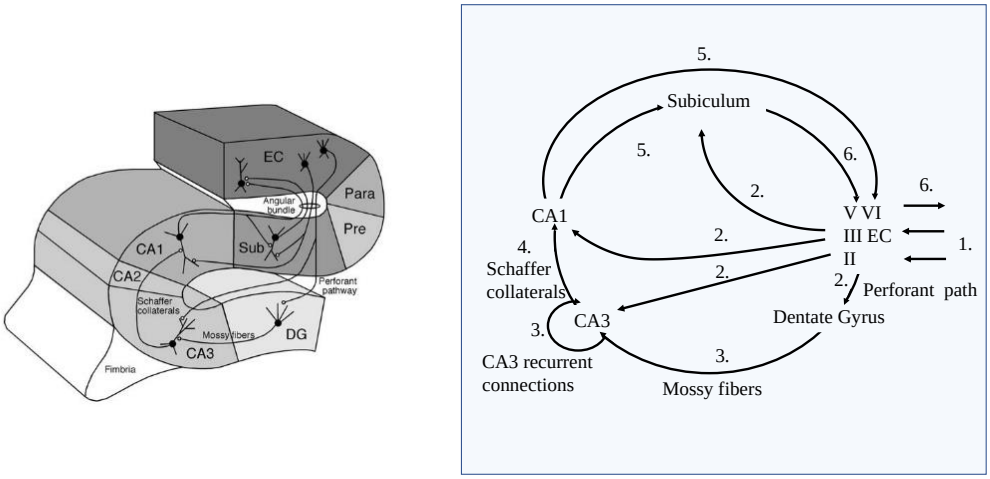

Figure 3.4 – Hippocampal microcircuit - 1. Layer II and III of EC receive projections from association cortices. 2. Neurons of layer II project to the dentate gyrus and the CA3 region via the perforant path. Neurons of EC layer III project to CA1 region and the subiculum. 3. The dentate gyrus sends its mossy fibers to CA3 cells and possesses recurrent collaterals. 4. CA3 cells connect to CA1 cells thanks to their Schaffer collaterals. 5. CA1 then projects to the subiculum and to the deep layers of the EC. The subiculum sends backprojection to CA1 region and to the deep layers of the EC. 6. Deep layers then project to neocortical areas.- Adapted from [Giovannini (2017)](left) and [Xu et al. (2016)](right)

3.3.2 Role

The hippocampal formation is a major contributor to declarative memory consolidation. It interacts with the neocortex and thalamus for the consolidation of memory. It functionally binds sensory information into an episodic gist like representation [Klinzing et al. (2019b)]. It does not hold the information but labels them as a data bank to provide spatio-temporal context of the events [Buzsaki (2006)]. The loop-like organization of the hippocampal formation enables the encoding and consolidation of the information in the neocortex. More particularly, it is a key player in the support of spatial memory to allow spatial navigation. Indeed, it has been demonstrated that some neurons of the hippocampal formation, known as place cells, code for every position in space [Buzsaki (2006)]. Therefore, information from every modality enters the entorhinal context and emerges from the hippocampal formation in the imagery form of a map that can be used for navigation in space [Buzsaki (2006)]. The role of the hippocampal formation in the medial temporal lobe was shown by the operation of the medial temporal lobe of patient H.M in 1953. H.M is famous in Neuroscience as his case helped discovered the role of the hippocampus in memory consolidation. H.M. experienced aggravating epileptic seizures. At age 27, 8cm of his medial temporal lobe was removed to calm the seizures including 2/3 of his hippocampus. The result was that he experienced anterograde amnesia. He couldn't recall any events occurring after his operation as soon as they happen which is basically the declarative memory. He also experienced some degree of retrograde amnesia and had no memory

of the events that happened just before his operation. This suggests that the hippocampus doesn't play a role in holding the information for a long period of time but rather is involved in the binding of the information for the consolidation of the declarative memory. It is a short term memory storage. Procedural and working memory did not seem affected by the loss of a part of the hippocampus [Bear et al. (2016)].

3.4 Global interconnection between the regions

FIGURE 3.5 depicts the global interconnections between the three regions previously described. The scenario illustrated throughout this thesis is the following:

1. An individual is camping in the forest and admires the environment around him. What he observes are his red tent and the huge green pine trees. Both items generate a stimulus conveyed throughout the brain simplified as being the stimulations corresponding to the trees (green) and the tent (red). The information reaches the thalamus in the same manner as described earlier in SUBSECTION 3.1.2

2. Axons from the LGN projects onto layer IV and VI of the primary visual cortex. Neurons inside the cortical column project into different layers as mentioned in SUBSECTION 3.2.2

3. The information leaves the neocortex via ascending projections arising from layer II & III and reaches the hippocampus passing through the perirhinal and parahippocampal cortex. The information arrives in the hippocampus and loops in the hippocampal microcircuit as explained in SUBSECTION 3.3.1

4. The information leaves the hippocampus and goes back to the neocortex via a reciprocal descendent path, thus passing by the parahippocampal and perirhinal cortex [Lavenex and Amaral (2000)].

FIGURES 3.2, 3.3 and 3.4 are zoom from FIGURE 3.5 corresponding to the regions orange, yellow and blue respectively.

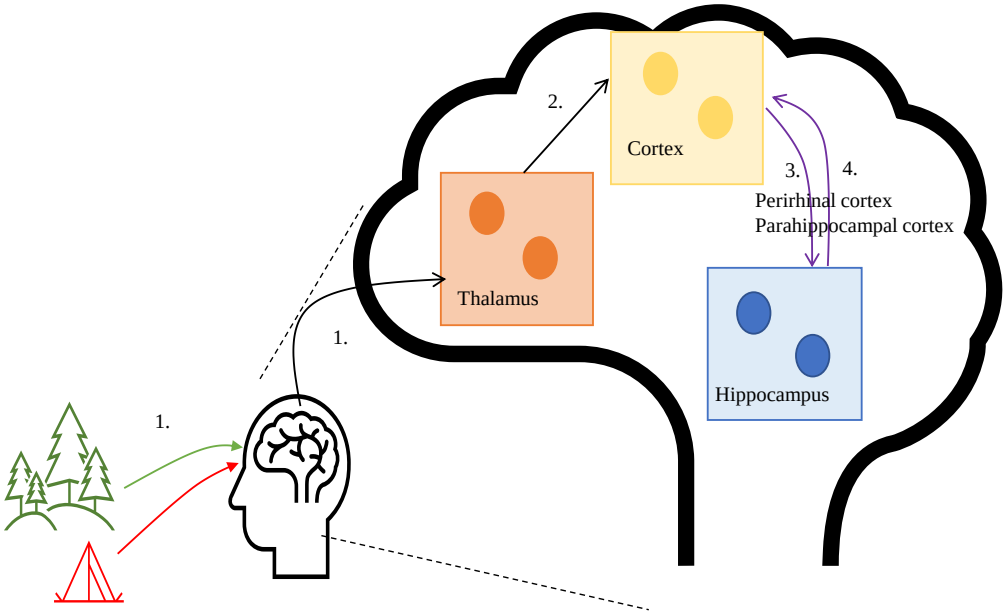

Figure 3.5 – Brain regions interconnection - 1. Stimulation from the camping event is conveyed from the external world to the thalamus (the tent in red and the trees in green) 2. Sensory information flows from the thalamus to the neocortex. 3. Then, it travels to the hippocampal formation passing by the perirhinal and the parahippocampal cortex. 4. Efferent projections from the hippocampal formation goes back to the neocortex. Purple arrows indicate that the afferent and efferent projections to and from the hippocampal formation are reciprocal.

Chapter 4

Elements of neurophysiology and neuronal modeling

The organs and living tissues of the human body are made of cells. The brain more specifically consists of particular cell types named the neurons. It is important to understand how neurons work and can be modeled individually before understanding how they interact with each other in a network or population within the brain [Bear et al. (2016)].

4.1 The cell

The neuron is an excitable cell that is the basic functional building block of the nervous system for transmitting information via the generation of electrical and chemical signals. A brain cell consists of four different parts involved in the reception, generation and transmission of signals [Giovannini (2017), Sépulchre (2008-2009)] which are represented in FIGURE 4.1.

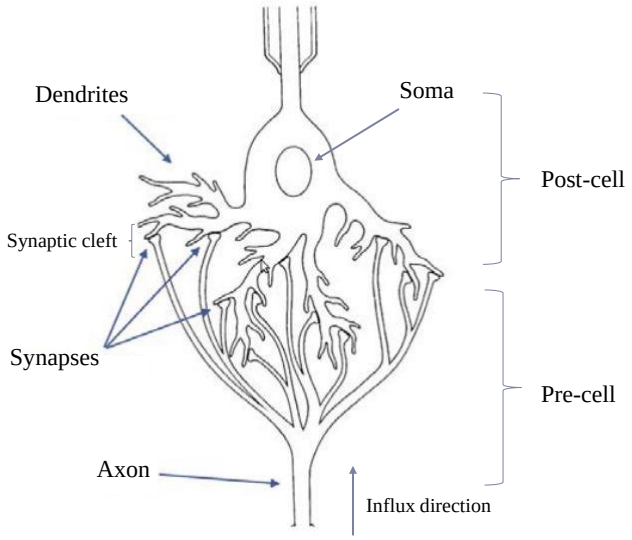

Figure 4.1 – Morphology of a neuron. - An action potential propagates in the axon of a pre-cell until the synapse and is transmitted through the synaptic cleft to the dendrites of a post-cell. Dendrites extend from the soma and forms a dendritic tree - Adapted from [Giovannini (2017)]

- The dendrites are the postsynaptic terminals of the neuron and are the receptors of the infor-

mation as they detect the neurotransmitters released from an anterior neuron. The dendrites extend from the soma and form a tree around it known as the dendritic tree. A classification of the neurons can be based on the different shapes of the dendritic tree [Bear et al. (2016)].

- The information is integrated by the soma and an action potential is generated if the intensity of the stimulation is sufficient. The generation of an action potential is explained in the APPENDIX A.1.
- The axon is connected to the soma and acts as the cable through which the action potential propagates.
- The synapses are the output of the axon. The electrical signal is converted into a chemical signal in the form of neurotransmitters vehiculated through the synaptic cleft which is the space between the pre and postsynaptic neuron via synaptic vesicles. The type of neurotransmitters varies according to the type of the neuron defining its function [Bear et al. (2016)] as seen in SECTION 4.4.

4.2 The neuronal membrane

The comprehension of the structure and function of the plasma membrane is primordial for understanding the generation and transmission of the electrical signal and therefore to perceive the communication principles between neurons [Bear et al. (2016)]

4.2.1 Biological architecture

The plasma membrane constitutes a phospholipid bilayer shielding the inside of the cell from the extracellular environment. It is also made of proteins embedded in the bilayer that is selectively permeable to specific ions. They are known as ionic channels if the ions can flow according to their electrochemical gradient or active transporters if the ions flow against their electrochemical gradient with the help of external adenosine triphosphate [Drion (2013)].

4.2.2 Membrane Potential

Neurons electrical behaviour depends on the transfer of charges carried by ions across the membrane via the ion channels or active transporters. Those ions are majoritarily sodium and potassium but can also be calcium or chlorine depending on the type of neurons and their function [Sépulchre (2008-2009)]. Membrane permeability and the resulting distribution of ions across the membrane generates a potential difference between the extracellular and intracellular medium. This potential is known as the membrane potential V_m ($=V_{in} - V_{out}$). A change of this potential due to an external stimulation gives rise to an electrical signal. When an ion flow through the membrane following its concentration gradient, it changes the potential across the membrane as the ions are charged particles and creates a difference in potential across the membrane by following their concentration gradient. Therefore, ions are going to flow through the membrane until an equilibrium is reached between the chemical and electrical driving force [Drion (2013)]. The potential for which the electrical and osmotic forces cancel each other is known as the resting potential of the membrane (approximately -70 mV) defined by the Nernst equation which is the following:

$$V_m = -\frac{RT}{zF} \ln \left(\frac{\sum_{\text{ion}^+} P_{\text{ion}} \left[\text{ ion }^+ \right]_{\text{out}} + \sum_{\text{ion}^-} P_{\text{ion-}} \left[\text{ ion }^- \right]_{\text{in}}}{\sum_{\text{ion}^+} P_{\text{ion}} + \left[\text{ ion }^+ \right]_{\text{in}} + \sum_{\text{ion}^-} P_{\text{ion}} \left[\text{ ion }^- \right]_{\text{out}}} \right)$$

where ion^+ denotes positively charged ions (Na^+, K^+, Ca^{2+} for example) and negatively charged ions (Cl^- for example). The relative permeability for the membrane of each ion is denoted by P_{ion}. R, T, z and F denote respectively the gas constant, the temperature in Kelvin, the valence of the ion and the Faraday's constant [Sépulchre (2008-2009)].

4.2.3 Conductance-based model

The neuronal membrane is particularly adequate to be mathematically modeled as a RC electrical circuit (see FIGURE 4.2) [Drion (2013)].

Its electrical analogy is established according to Kirchoff's law which gives that the current applied to stimulate the neuron is equal to the sum of all the ionic currents and the membrane capacitive current ($=C_m \frac{dV_m}{dt}$) where C_m is the constant capacity of the membrane and V_m is the membrane potential which varies with time resulting in the following formula [Izhikevich (2007)]:

$$C_m \dot{V}_m = -\sum_{i=1}^{n} g_{ion,i} \left(V_m - E_{ion,i}\right) + I_{app}$$

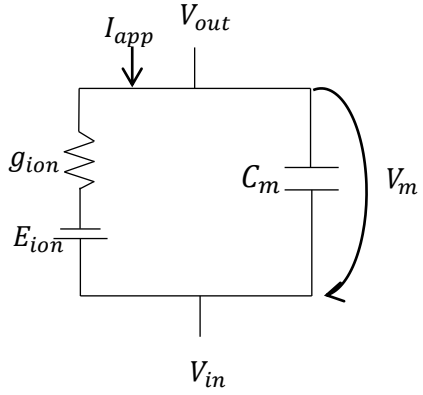

Figure 4.2 – Membrane modeled as an RC circuit. - g_{ion} corresponds to an ion channel, E_{ion} is the reversal potential of an ion, the capacitance C_m represents the membrane phospholipid bilayer and I_{app} is the applied current. - Adapted from [Jacquerie (2018)]

An ionic current can be expressed following Ohm's law as the product of nonlinear conductances g_{ion} and their corresponding driving force $(V_m - E_{ion})$ where E_{ion} is the reversal potential of the ionic current as follows: $I_{ion} = g_{ion}\left(V_m - E_{ion}\right)$. The ions flow through the membrane until V_m reaches E_{ion} [Drion (2013)]. The ionic currents are generated thanks to the presence of voltage-gated channels in the membrane through which the ions can go following their electrochemical gradients [Izhikevich (2007)]. The conductances g_{ion} of these channels are time and voltage-dependent. A **conductance-based model** is defined by the summation of specific voltage-dependent current sources I_{ion}. A current-specific channel is defined by the dynamic of its conductance g_{ion} and its ionic permeability. The dynamic of a particular conductance can be controlled by gating particles called gates that are dynamic variables in the model which are voltage-gated variables. An activation gate opens (activation) and closes (deactivation) when V_m increases and decreases respectively. An inactivation gate opens (deinactivation) and closes (inactivation) respectively as V_m increases and decreases respectively. $m_i \in [0,1]$ is the activation gate and $h_i \in [0,1]$ is the inactivation gate. The dynamics for both types of gates is defined as follows:

$$\dot{m}_{\text{ion}} = \frac{m_{\text{ion},\,\infty}\left(V_m\right) - m_{\text{ion}}}{\tau_{m_{\text{ion}}}\left(V\right)}$$

where τ_m is the activation/inactivation time constant and $m_{\text{ion},\,\infty}\left(V\right)$ is the fraction of open channel at equilibrium for a given voltage [Sépulchre (2008-2009)]. Providing the latter definitions, the **conductance-based model** can be characterized by the following ordinary differential equations

$$C_m \dot{V}_m = -\sum_{i} \bar{g}_i m_i^p h_i^q \left(V - E_i\right) + I_{app}$$

$$\dot{m}_i = \frac{m_{i,\infty}(V) - m_i}{\tau_m(V)} \quad \text{for } i = 1:n$$

$$\dot{h}_i = \frac{h_{i,\infty}(V) - h_i}{\tau_{h_1}(V)} \quad \text{for } i = 1:n$$

where p and q are two integers exponent.

4.3 Synapses

Two neurons communicate with each other via a particular junction called the synapse. The information flows from a presynaptic neuron which consists of an axon terminal to a postsynaptic neuron which

may be the dendrite or soma of the neuron. The transfer of the information occurs in different forms: electrical-chemical-electrical. An action potential circulating in the presynaptic neuron is transformed at the axon terminal in a chemical signal called a neurotransmitter. The neurotransmitter binds to a specific receptor at the postsynaptic dendrite which regulates the opening and closing of ionic channels. This mechanism enables a chemically controlled flow of ionic currents in and out of the postsynaptic neuron generating the transfer of an electrical signal in the postsynaptic neuron [Bear et al. (2016) [Giovannini (2017)]. The electrical signal can also be transmitted to a postsynaptic neuron through electrical synapses forming gap junctions, this type of synapses are not of interest for the purpose of this thesis.

4.4 Neurotransmitters

The type of neurotransmitter released by a presynaptic neuron affects the behaviour of the postsynaptic neuron when binding to the specialized receptor. A neuron is said to be excitatory if the neurotransmitter released generates an action potential by bringing the postsynaptic neuron to its threshold value. A neuron is said to be inhibitory if the neurotransmitters released prevent the postsynaptic neuron from generating an action potential by bringing it away from the threshold value [Giovannini (2017)].

4.4.1 Excitatory synaptic transmission

Glutamate is the principal excitatory neurotransmitter that binds to specific glutamate-gated ion channels classified as α-amino-3-hydroxy-5-methyl-4-isoxazolepropionic acid receptor ($AMPA$) or N-methyl-D-aspartate receptor ($NMDA$). $AMPA$ receptor is permeable to Na^+ and K^+ ions and $NMDA$ receptor is additionally permeable to Ca^{2+}. When glutamate is released by the presynaptic neuron, it binds to the $AMPA$ receptor which enables the flow of the extracellular sodium and intracellular potassium in and out of the cell respectively. This receptor is voltage-independent. Glutamate also binds to $NMDA$ receptor regulating the passage of Na^+, K^+ and Ca^{2+} as $AMPA$ receptors except that this is not sufficient to allow the flow of ions in the postsynaptic cell due to the presence of Mg^{2+} blocking the channel. The removal of the Mg^{2+} requires a depolarization of the membrane potential which is mediated by the $AMPA$ receptor. Thus, the flow of ions through the $NMDA$ receptors depends on the postsynaptic membrane potential and on the binding of glutamate [G. Vandewalle (2019), Bear et al. (2016), Giovannini (2017)]. The molecular mechanism behind the regulation of $AMPA$ and $NMDA$ receptors is represented in Figure 4.3.

The entry of positively charged ion currents in the cell through these receptors results in a depolarization of the membrane potential of the postsynaptic neuron. This transient depolarization is named an excitatory postsynaptic potential (EPSP) see Figure 4.3. The summation of EPSPs induces an important synaptic depolarization of the membrane potential that may lead to the generation of an action potential in the postsynaptic neuron if the threshold value is reached. The summation of EPSPs can either be spatial when the EPSPs are induced concurrently at different synapses of the same dendrite or temporal when EPSPs add up at the same synapse successively [Bear et al. (2016)].

4.4.2 Inhibitory synaptic transmission

The main inhibitory neurotransmitter is the γ-Aminobutyric acid ($GABA$) that can bind to two different classes of receptors: $GABAa$ and $GABAb$ receptors. When $GABA$ is released in the synaptic cleft by the presynaptic neurons and interacts with these receptors, the postsynaptic neuron does not fire an action potential or release neurotransmitter. $GABAa$ receptor is ionotropic. When $GABA$ binds to this receptor, a chloride channel opens leading to the inward flow of a negatively charged chloride ion which hyperpolarizes the membrane potential. $GABAb$ receptors are metabotropic G-protein-coupled receptor. This receptor is activated by the binding of $GABA$ and opens the K^+ channel indirectly coupled to it via G-protein mediation. The outward flow of positively charged potassium ions hyperpolarizes the membrane potential. This process is represented in Figure 4.4. The transient hyperpolarization of the membrane potential is called an inhibitory postsynaptic potential (IPSP) which diminishes the size of EPSPs and prevents the potential from reaching the threshold value for

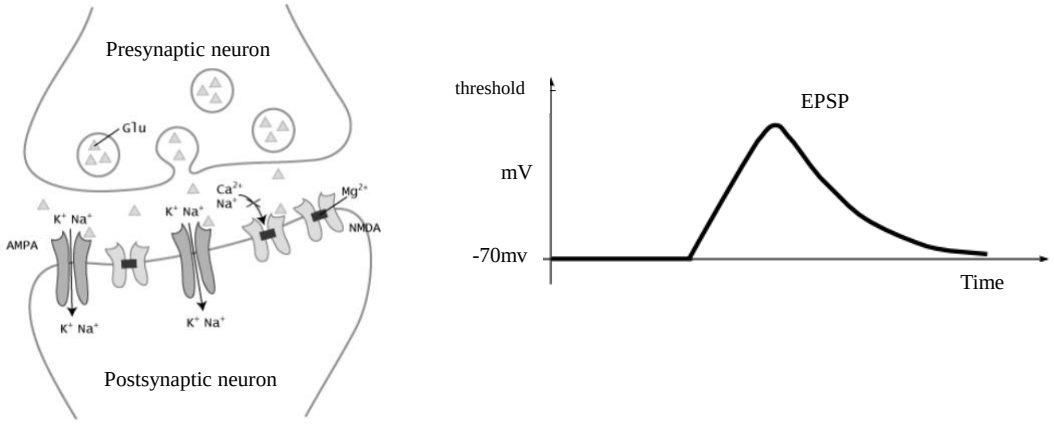

Figure 4.3 – Schematic of $AMPA$ and $NMDA$ receptors embedded in the cell membrane (left) - Trace of an EPSP (right). When glutamate is released from the presynaptic neuron vesicles, they interact with $AMPA$ and $NMDA$ receptors present in the postsynaptic cell membrane. The binding of glutamate to $AMPA$ receptors allows their opening and Na^+ and K^+ flow through the receptor. Glutamate also opens $NMDA$ receptors when the membrane potential is sufficiently depolarized by the opening of the $AMPA$ receptors allowing the removal of the blocking Mg^+ - The trace of the EPSP shows the depolarization of the membrane from its resting potential but below threshold, therefore not generating an action potential - Adapted from [Giovannini (2017)]

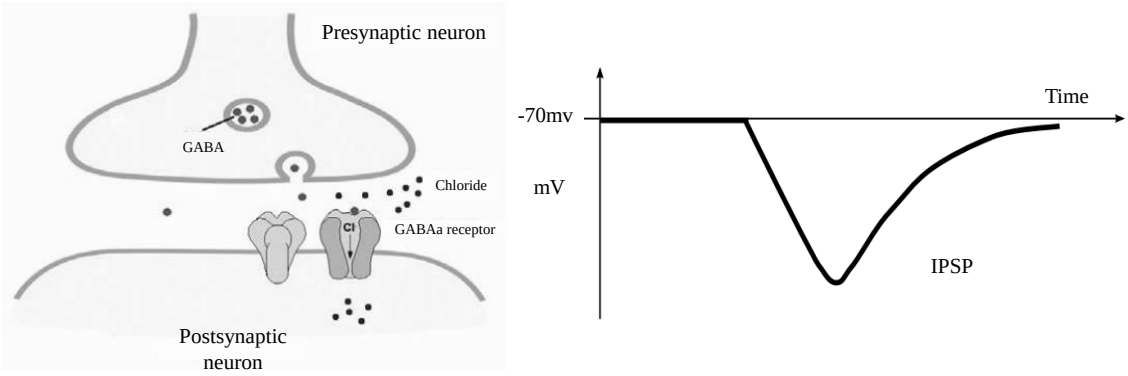

Figure 4.4 – Schematic of $GABAa$ receptors imbedded in the cell membrane (left) - Trace of an IPSP (right). $GABA$ molecules are released from the presynaptic neuron in the synaptic cleft. A molecule binds to $GABAa$ receptor which allows the entry of Cl^- in the cell generating a hyperpolarisation of the membrane potential (right) - The trace of an IPSP shows the hyperpolarization of the membrane from its resting potential - Adapted from [Giovannini (2017)]

the generation of action potentials and hence lead to inhibition of the postsynaptic neuron (see FIGURE 4.4) [Bear et al. (2016), Giovannini (2017), Neuroscientifically Challenged (2018)].

4.4.3 Synaptic plasticity

Synaptic plasticity refers to the capacity of synapses to modify their strength, hence it modifies the ability of neurons to communicate. This mechanism is crucial for the transfer of information between neurons and for memory consolidation.

Synaptic plasticity duration varies in time. A modification of the synaptic strength occurring over periods of seconds to minutes refers to short-term plasticity. A modification of the synaptic strength occurring over periods of times from hours, days or even more is called long-term plasticity. This type of plasticity is particularly of interest for the regulation of neuronal networks and memory consolidation

underlying long-term memory formation. An increase of long-term synaptic strength is called long-term potentiation (LTP) and a reduction of strength is called long term depression (LTD). [Hebb (1949)] said that learning was promoted by the enhancement of existing synaptic connections between neurons and also the establishment of new connections by stating that:

> *"When an axon in cell A is near enough to excite cell B and repeatedly and persistently takes part in firing it, some growth process or metabolic change takes place in one or both cells such that A's efficacy in firing B is increased."* [Hebb (1949)]

This statement could be reformulated by *Neurons that fire together wire together* [Hebb (1949)] which defines Hebbian potentiation. The counterparts of this mechanism could be formulated by *Neurons that fire out of sync lose their link* [Hebb (1949)] meaning that there is a reduction of the excitability between neurons [Heidelberger et al. (2014), Bear et al. (2016)]. Enhancement and decrease of communication between neurons could also be referred to as synaptic upscaling and synaptic downscaling respectively. The understanding of the different forms and the molecular principles underlying the mechanism behind LTP and LTD is not required in the context of this thesis as the model further developed does not apply synaptic plasticity mechanisms.

Chapter 5

Sleep-Wake cycle

The environment in which the human lives is rhythmically changing and the human being needs to adapt to these variations in order to survive. This is why the brain has adapted by developing rhythmic control systems, the most noteworthy of which is the sleep-wake cycle [Bear et al. (2016)].

5.1 What is sleep? Why is sleep needed?

Sleep is the state of the brain marked by a reduction of the brain responsiveness to external activity inducing an abolition of reactions to external stimuli combined with a loss of consciousness. It is a behaviour that recurs periodically. Its recurrence is controlled by homeostatic and circadian regulation. These two systems ensure that human beings are able to remain cognitively active for at least 16 hours at a time. The circadian rhythm is synchronized by light-dark cycles, it promotes wakefulness during the day and sleep during the night and is controlled by the suprachiasmatic nucleus in the thalamus which has the role of the biological clock. The clock helps the body to keep its rhythm even when the light-dark cycle is disrupted [G. Vandewalle (2019)]. Multiple physiological processes vary with this rhythm like body temperature, hormone levels etc. [Bear et al. (2016)]. Homeostatic regulation acts as the keeper of the internal balance of the body. Sleep is important for the energy balance of the body, thermoregulation, cell tissue reparation, hormonal regulation. Sleep function is essential for the brain. Indeed, it is primordial for cerebrospinal fluid detoxification, restoration of brain system functions and most importantly, it plays a role in memory consolidation and synaptic plasticity [Rasch and Born (2013), G. Vandewalle (2019)].

5.2 Sleep stages

Sleep is defined by a characteristic electrical activity of the brain.

It is marked by a cyclic occurrence of different stages identified by the different electrical activity of the cortex recorded by the EEG (see FIGURE 5.1).

There are two main distinguishable stages [Bear et al. (2016)]:

- Non-rapid eye movement (Non-REM) sleep stages 1-2-3-4 originates from neocortical, thalamic and hippocampal regions and constitutes 80 % of the offline period. Non-REM sleep is marked by high amplitude, low frequency, synchronous EEG patterns, disconnection and prevalence of parasympathetic system. During a nocturnal event, an individual encounters the following non-REM sleep stages [Bear et al. (2016)]:
  - An individual falls asleep and enters non-REM sleep stage 1 which is characterized by a rhythm between 8-13Hz called the alpha rhythm. It is a stage only lasting few minutes and which is very light.
  - Then, the individual enters a slightly deeper stage of sleep, stage 2 which lasts 5 to 15 minutes and is characterized by a particular activity called spindles which are represented by waxing and waning oscillations of 11-16Hz. Even though sleep spindles are best noticeable

in non-REM sleep stage 2, they also occur throughout all non-REM stages except stage 1. Non-REM sleep stage 2 is also characterized by K-complexes which have a slow activity and a sharp high amplitude [Fernandez and Lüthi (2020)].

– Then, the individual enters slow wave sleep (SWS) which corresponds to the deepest sleep stages of non-REM sleep stage 3 and 4, stage 4 being the deepest stage of sleep. SWS is characterized by slow and large amplitude oscillations being the delta rhythm with a frequency of less than 4 Hz and even less than 2 Hz for stage 4. The brain spends 15-20 minutes in this stage then goes back to lighter stages then REM sleep.

- REM sleep stages compose 15-20 % of the disconnected period. REM sleep outlines a low amplitude, high frequency, asynchronous EEG activity and preeminence of the sympathetic system and dreaming. The structures of the brain involved differ from the structures involved in the non REM sleep activity. This activity originates from the pontine nuclei, the amygdala and the temporo-parieto-occipital junction [Langille (2019)]. REM sleep is characterized by beta rhythms (15-30 Hz) and gamma rhythms (30-90 Hz). It has the same electrical activity as when the brain is in the waking state but differ in muscle atony and rapid jerky eye movements. It is the stage during which dreams occur. The waking state is also characterized by alpha rhythm (8-13 Hz) [Bear et al. (2016)].

Sleep can be divided into two parts due to circadian rhythm and homeostatic regulation (see FIGURE 5.1). Non-REM sleep prevails in the *early sleep* and REM sleep is almost absent and is predominant during the *late sleep* [Rasch and Born (2013)]. As night advances, stage 4 disappears. The patterns of oscillations and the sleep cycle are seen in FIGURE 5.1.

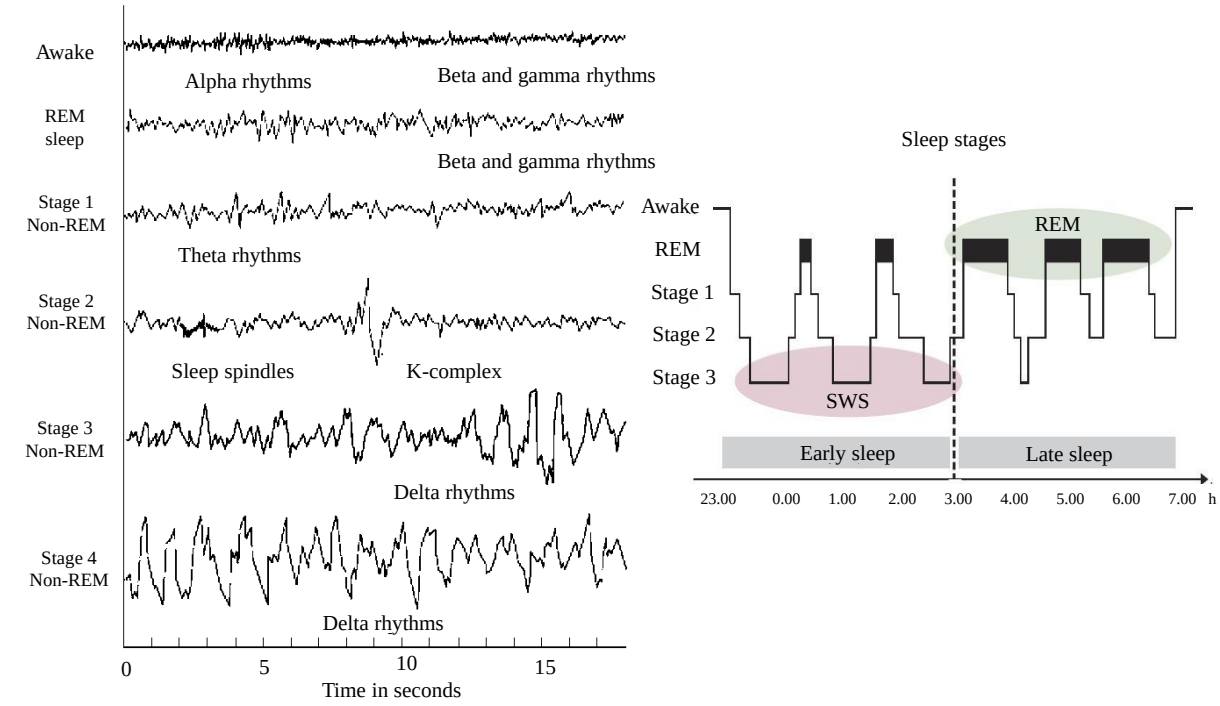

Figure 5.1 – EEG rhythms (left) - Sleep stages (right). -EEG electrical rhythms given for each stages of sleep and for wakefulness as a function of time. Names of the different rhythms are provided (left) - Cyclic occurence of the sleep stages. Sleep cycle is divided into two parts: early sleep during which slow wave sleep (SWS) is predominant and late sleep during which REM sleep is predominant. Stage 4 diminished as the cycle advances (right). - Adapted from [Chegg Study (2017) (left), Rasch and Born (2013) (right)]

5.3 Sleep signatures

Sleep synchronous oscillations occur during slow wave sleep and are characterized by local field potential recordings (LFP's). These are the neocortical slow oscillations, the thalamocortical spindles and the hippocampal sharp wave ripples and are shown in FIGURE 5.2. These LFP's rhythms enable the reactivation and the consolidation of memory representation in the neocortex [Rasch and Born (2013)]. Furthermore, LFP's arise from specific cellular signatures underlying their rhythm. These are exogenous and endogenous cells' bursting activity which are detailed later.

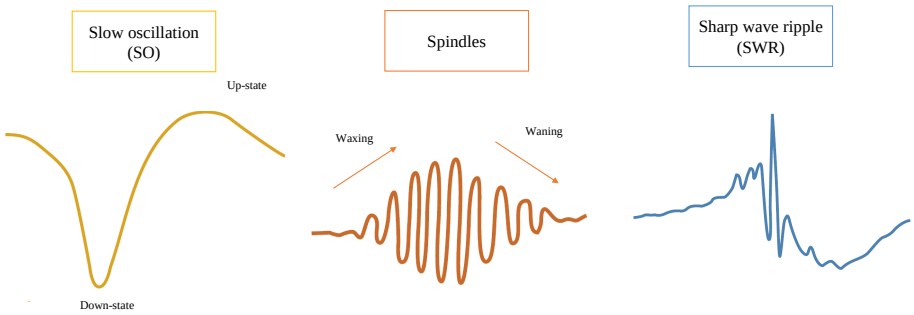

Figure 5.2 – Local field potentials traces occuring during slow wave sleep. The yellow trace corresponds to a neocortical slow oscillation characterized by an alternance of up-state and down-state, the orange trace corresponds to the spindle activity generated in the thalamus characterized by waxing and waning oscillations and the blue trace is the sharp wave ripple generated in the hippocampus. - Adapted from [Rasch and Born (2013)]

5.3.1 Origin of brain rhythmicity during sleep

Sleep in general and more specifically slow wave sleep is characterized by a synchrony of rhythms resulting from the coupling of recurrent excitation (positive feedback) and inhibition (negative feedback) between different types of neurons within a brain structure and in between brain structures. This internally generated oscillatory pattern are essential for sleep function to disconnect the brain from the external environment [Langille (2019), McCormick et al. (2015)]. The particular properties of the LFP's rhythms come from the type of neurons implicated depending on the brain structures and the synchronization between them according to the strength of their synaptic connectivity [McCormick et al. (2015)]. There are two ways for a network of neurons to produce synchronous oscillations [Bear et al. (2016)]:

- Neurons may take the rhythm of a neuron having an autorhythmic property (acting as a central clock), *i.e.* endogenous activity.
- They may mutually excite or inhibit one another which occurs via synaptic connections, *i.e.* exogenous activity.

A simple circuit generating synchronous activity is the following oscillator consisting of one excitatory and one inhibitory neuron connected in a feedback loop as seen in FIGURE 5.3.

As long as the excitatory neuron is excited by a stimulus, the activity will oscillate between the two neurons in a rhythmic way. The inhibitory interneurons present in the different structures of the brain are essential for the stability of the network through feedback interaction [Buzsaki (2006)]. Indeed, recurrent excitation between excitatory neurons leads to further increasing excitation and instability of the system. If an excitatory input excites one excitatory neuron, a chain of excitatory reaction is created generating the whole network of excitatory neurons to be excited. Inhibition is therefore primordial for keeping balance in the system and synchronizing the activity of the neurons of the

network, their activity increasing and decreasing together. The synaptic connection strength between excitatory and inhibitory neurons affect the firing pattern of both types of neurons. [McCormick et al. (2015)]

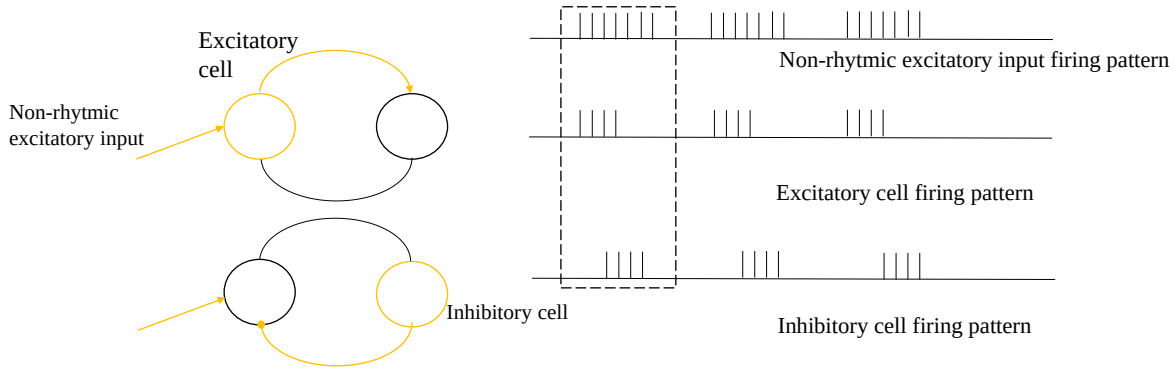

Figure 5.3 – Two-neuron oscillator. An excitatory input constantly fires without being specifically discharging rhythmically and excites an excitatory neuron. In turn, the excitatory neuron excites the inhibitory neuron which inhibits the excitatory neuron and this activity keeps on going back and forth generating a synchronous rhythm. Arrows indicate the excitatory projection. Dot arrowhead indicates an inhibitory projection. Yellow lines indicate that a neuron is discharging. The firing pattern for each type of cell is represented, one cycle being in the dashed box. - Adapted from [Bear et al. (2016)]

5.3.2 Spindles

Sleep spindles are an EEG signature for non-REM sleep stage 2 with 2-8 spindles/min but are also present in deeper non REM sleep stages with 1-6 spindles/min during stage 3. These sleep hallmarks consist of waxing and waning field potentials of 11-16Hz [Fernandez and Lüthi (2020)] arranged in a sequence happening once every 3 to 10s for a period of 1 to 3 sec [Steriade et al. (1993)] (see orange trace in FIGURE 5.2. They are generated in the thalamus in an autonomous way and result from the synaptic interaction between the inhibitory neurons of the reticular thalamic nucleus (TRN) and the thalamocortical cell (TC)of the thalamic relay nuclei [Steriade et al. (1993)]. Cortical feedback from cortical pyramidal cells is also involved in the synchronization and spatial coherence of spindles in the thalamus [Astori et al. (2013)].

Cellular mechanism of endogenous burst discharge

A burst is a discharge pattern consisting of periods of 2 to more than 10 action potentials of frequencies up to hundreds of Hz [Fernandez and Lüthi (2020)] followed by a period of silence. A burst resulting from the coaction of intrinsic membrane currents is called an **endogenous burst** or **intrisinc burst**. The discharge pattern of bursts procures vigorous rhythmicity for the generation of sleep spindles. The TRN acts as the principal pacemaker for the generation of sleep spindles in the thalamus [Astori et al. (2013)] and its bursting activity occurs simultaneously with the beginning of spindles [Astori et al. (2013) Fernandez and Lüthi (2020)]. The ion channels at the origin of the bursting activity in thalamic cells are the low-threshold T-type calcium channel (I_t), the hyperpolarization-activated cation current (I_h) and the traditional interaction between the sodium and potassium currents. The generation of a burst in thalamocortical cells is the following [McCormick and Bal (1997)]:

- I_h is active at hyperpolarized potentials and brings the membrane potential to -65mV leading to the activation of I_t which occurs much faster than its inactivation allowing an entry of positively charged calcium ions in the cell and inducing calcium spikes.

- This entry of calcium depolarizes the membrane upon membrane threshold at -55mV. At threshold, the dynamics of the potassium and sodium currents as described in the APPENDIX A.1 generates a burst *i.e.* a train of action potentials.

- After 100-200 ms, I_t inactivates and the membrane becomes repolarized. I_h becomes deactivated and induces a further reduction of the depolarization generating a hyperpolarization overshoot.

- This hyperpolarization activates I_h again and I_t is deinactivated. The activation of I_h due to hyperpolarization depolarizes the membrane and the cycle restarts.

Neurons from the TRN also generate burst in an alike manner [McCormick and Bal (1997)].

Interaction between TRN and TC at the origin of sleep spindles

The interaction between the inhibitory neurons of the TRN and the excitatory thalamocortical neurons are critical for the generation of sleep spindles and occurs in the subsequent manner:

- The burst discharge autonomously generated in the TRN inhibits several TC cells through particular synaptic contacts. When neurons of the TRN burst, they express vesicles $GABA$ transporters accumulating in the synaptic cleft which open $GABAa$ and $GABAb$ receptors expressed by TC neurons. The opening of $GABAa$ receptors induces an entry of negatively charged Cl^- as seen in SUBSECTION 4.4.2 and generates an IPSP in the TC neurons. TC neurons also express $GABAb$ receptors that play a modulatory role in the inhibition.

- TC neurons present rebound burst activity outcoming from the removal of inactivation of I_t due to several IPSPs. The calcium spike induced in TC cells flows through low-threshold calcium channels. The burst induced in TC neurons differ from the autonomous burst generated in the TRN neurons, they have a shorter duration, are more stereotyped and happen over a more confined scope of membrane voltage [Fernandez and Lüthi (2020), Steriade et al. (1993)].

- The TC cells axons project to inhibitory neurons of the TRN closed to the one from which it is inhibited in an open-loop manner. When bursting, TC neurons express glutamate and activate $AMPA$ and $NMDA$ receptors of the TRN neuron hence hyperpolarizing the inhibitory neurons and restarting the loop.

- TC neurons axons also project on cortical pyramidal cells where they generate EPSPs through $AMPA$ and $NMDA$ synaptic receptors.

Therefore, the sleep spindle can be measured by EEG on the scalp of the brain. The waxing phase of the sleep spindle as measured by the EEG originates from the generation of IPSPs in TC cells that are not sufficient to generate rebound bursting in these cells. In the central phase, IPSPs are sufficient to induce rebound bursting which generates EPSPs in cortical neurons and TRN. The waning phase arises from the desynchronization of thalamic and cortical discharge [Astori et al. (2013)]. This loop between inhibitory and excitatory neurons provide rhythmicity to the occurrence of sleep spindles.

5.3.3 Slow oscillations

The slow oscillations (SO's) are generated in the neocortical cells and have a frequency of $<$1Hz. They are influenced and distributed in the thalamus [McCormick et al. (2015)]. During non-REM sleep, the cortex is excited by the thalamus with a more temporarily and spatially coherent activity pattern than would typically be experienced in the conscious state [Steriade et al. (1993)]. Therefore, the rhythms arising from the thalamus guide the rhythms of the cortex which disappear if the thalamus is disconnected from the neocortex [Bear et al. (2016), McCormick et al. (2015), Rasch and Born (2013)]. The cortical rhythms also come from a collective interaction between inhibitory and excitatory neurons [Bear et al. (2016), McCormick et al. (2015)]. The slow oscillations arise from a transition of down-state resulting from membrane hyperpolarization combined with a period of neuronal quiescence and up-state generated by the membrane depolarization associated with a series of action potentials [Rasch and Born

(2013)] (see FIGURE 5.2). The switch from the down-state to the up-state originates from an excitatory input that excites multiple neurons of the excitatory cortical networks recurrently through $AMPA$ and $NMDA$ synaptic receptors. This phenomenon depolarizes the membrane. The excitation also excites cortical inhibitory cells which are mostly fast-spiking interneurons that dampen and stabilize the recurrent excitation via GABAergic synaptic receptors [McCormick et al. (2015)]. Therefore, the up-state stems from the interaction between recurrent excitation and recurrent local inhibition [McCormick et al. (2015)]. The synchronization of excitatory and inhibitory neurons during the up-state is weakened by refractory mechanisms such as synaptic depression, the activation of Ca^{2+} and Na^{+} dependent K^{+} conductances, spike frequency adaptation and this induces a transition to the down-state [Rasch and Born (2013), McCormick et al. (2015)]. The cortical slow oscillations are involved in the generation and synchronization of 50-70 % of spindles via corticothalamic feedback. SO's are more frequent during stage 3 than stage 2 during which they are named K-complex [Fernandez and Lüthi (2020)]. SO's helps in the temporal and spatial organization of spindles by recurrently exciting TRN neurons by corticothalamic connections [Astori et al. (2013), Fernandez and Lüthi (2020)]. Synchronized oscillatory pattern arises from the interaction of neural networks between brain structures.

Cellular mechanism of exogenous burst discharge in the neocortex

Bursting activity in the neocortex is exogenous and not endogenous as in the thalamus as hypothesized in this thesis. Indeed, the bursting activity in the neocortex results from synaptic interaction with the thalamus and not from an interplay of intrinsic currents [Bear et al. (2016), McCormick et al. (2015), Steriade et al. (1993)]. A cell discharging in **exogenous bursting activity** results from the synaptic interaction of this cell with others. In spite of that, [Izhikevich (2007)] states that there are multiple classes of neurons in the neocortex including the fast-spiking interneurons, the regular spiking neurons and the intrinsically bursting neurons. The regular spiking neurons are the most abundant type in the neocortex and the bursting cells are mostly found in layer V. [Franceschetti et al. (1995)] mentions the presence of endogenous bursting neurons in layer V of neocortical neurons which are due to I_{NaP} currents and not calcium type currents. He also indicates that regular spiking neurons are more prominent than intrinsically bursting neurons [Franceschetti et al. (1995)]. [Williams and Stuarty (1999)] says that there are regular firing and bursting cells in layer V. They tend to prove that endogenous bursting occurred thanks to calcium channel by using nickel antagonist. Moreover, lacking evidence from the literature compared to the proliferating literature on endogenous bursting in the thalamus, leads to the hypothesis that bursting activity in the neocortex is exogenous. In reality, exogenous bursts are transient tonic activity at high frequency.

5.3.4 Sharp wave ripples

A third local field potential rhythm hallmarking SWS and essential for memory consolidation is the hippocampal sharp wave ripple (SWR's) (see FIGURE 5.2). SWR's are characterized by high-frequency discharge pattern of 100-300 Hz of 40-120 ms duration emerging from the CA1 region of the hippocampus [Rasch and Born (2013)]. This activity originates from the CA3 region and stems from the synchronous population bursts firing from the neurons of the CA3-CA1 region, subiculum and deep layers of the entorhinal cortex [Buzsáki (1996)]. This particular rhythm arises from the reduction of subcortical afferents (cholinergic or non-cholinergic inputs from the neocortex) to the hippocampus and occurs in the subsequent way [Buzsáki (1986), Buzsáki (1989), Buzsáki (1996), Buzsáki (1998)]:

- The reduction from subcortical afferents generates a diminution of the inhibition on the recurrent synchronizing mechanisms occurring in the CA3 recurrent collateral system. Hence, the CA3 neurons can excite each other thanks to their extensive recurrent collaterals inducing population bursting activity in the CA3 neurons.

- Through the Schaffer collaterals, the bursting activity of CA3 neurons largely depolarizes CA1 neurons and their target interneurons. Fast discharge of interneurons can regulate the firing mode of CA1 pyramidal cells by generating coherent intracellular oscillations in the CA1 excitatory cells known as the SWR's.

There is a cortical control of this hippocampal rhythm. SO's synchronize the discharge activity of hippocampal neurons. The SWR's activity in the hippocampus comes from a top-down cortical activation and there is a temporal connection between the ripples and the spindles happening in the thalamus and neocortex [Navarrete et al. (2020), Rasch and Born (2008)]. SWR's are therefore the result of neocortical control, activation-inhibition neurons interaction, and the increase in neuronal excitation resulting from a decrease of cholinergic inputs and recurrent collaterals of the CA3 region [Astori et al. (2013), Rasch and Born (2013)].

Origin of the bursting activity in CA3 pyramidal cells, endogenous or exogenous?

CA3 neurons discharge in bursts and are responsible for the generation of population bursting activity due to their recurrent collaterals. According to [Migliore et al. (1995)], the burst discharge of CA3 pyramidal neurons can be spontaneous or induced by short pulses of injected currents. Moreover, they conducted simulations showing that the bursting activity of these neurons does not rely on Ca^{2+} dependent channels. [Buzsáki (1986)] also states that a manner for the CA3 pyramidal neurons to generate bursting activity can be endogenous resulting from currents interaction. They mention that the excitation of the neurons of the CA3 region can alternatively originate from mossy fibres and from the perforant path. They cite [Hablitz and Johnston (1981)] to motivate the theory of endogenous bursting of CA3 pyramidal neurons. Indeed, [Hablitz and Johnston (1981)] lead experiments showing that CA3 pyramidal neurons fulfil the criteria underlying endogenous bursting but state in their discussion that the bursting pattern of CA3 pyramidal cells might result from synaptic interactions among neurons rather than arising from particular membrane properties. The distinction between endogenous bursting and exogenous bursting is rather challenging to determine in CA3 pyramidal neurons [Hablitz and Johnston (1981)]. The hypothesis followed in this project concerning the initial burst discharge in a CA3 pyramidal neuron considers an exogenous type of burst directed by cortical activity and resulting from enhanced excitation among pyramidal neurons in the CA3 region resulting from the disinhibition occurring during slow wave sleep. [Rasch and Born (2013), Navarrete et al. (2020), Hablitz and Johnston (1981), Buzsáki (1986), Migliore et al. (1995), Chamberlin et al. (1990)]. This hypothesis was also motivated by the article of [Chamberlin et al. (1990)] who lead experiments on CA3 slices bathed in high potassium concentrations. They demonstrated that with enough cellular excitability and with reduction of inhibition as occurs in high potassium concentrations -thus as during slow wave sleep- endogenous bursting is not primordial for the generation of population bursting in the hippocampus. The exogenous bursting would be generated from EPSPs arising from mossy fibres or from excitatory collaterals and from the particularity of the CA3 region to have recurrent excitatory interactions.

5.4 Wake-sleep switch

Modes of discharge

Thalamic, neocortical and hippocampal neurons can exhibit two distinctive modes of firing: tonic and bursting (see FIGURE 6.2). Tonic consists of a train of action potentials occurring during wakefulness at frequencies varying between neuron types [Zagha and McCormick (2014)]. Neurons are kept at depolarized potential during tonic activity which prevents the presence of the hyperpolarized down-state happening during SWS [Zagha and McCormick (2014)]. Excitation happening asynchronously results in a low amplitude, irregular EEG signal during activated states. Bursting, previously described, occurs during sleep and is linked to the synchronous activity displayed by EEG represented by a larger surface signal [Bear et al. (2016)]. Bursting is endogenous in thalamic cells and considered exogenous for neocortical and hippocampal cells (except for subicular cells as explained later). These two different modes participate to relay function in different ways. The tonic mode is well known and enables the transfer of information to the neocortex in an accurate manner. Indeed, depending on the strength of the input, the rate of the firing changes linearly meaning that the information is relayed with high fidelity by fast sodium spikes during wakefulness. [Weyand et al. (2001)]. Bursting mode are rhythmic during sleep and actively participate in SWS activity generation and play an important role in synaptic

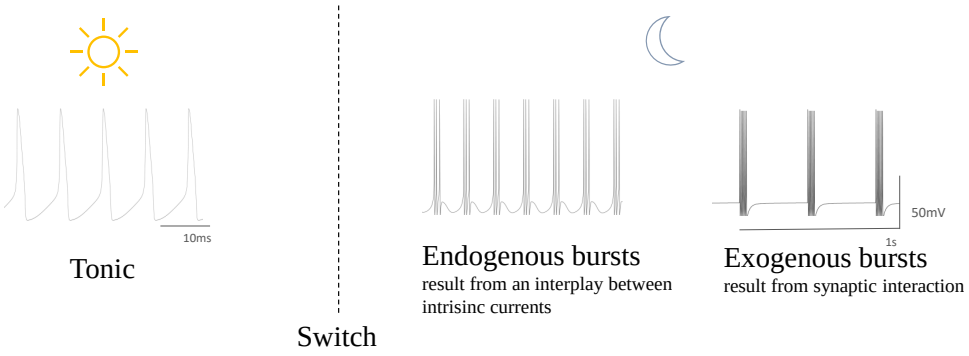

Figure 5.4 – Wake-sleep switch. During wakefulness (sun), neurons discharge in a tonic mode (left). During sleep (moon) (right), neurons can display two distinct modes of firing: endogenous bursting resulting from an interplay between intrisinc ionic currents and exogenous bursting resulting from synaptic interactions.

communication between regions as bursts constitute high-frequency input of short duration [Sherman (2001)].

Neuromodulators action on the anatomical structure of the brain

The transition between wakefulness and sleep comes from the afferent activating system in the brain stem and hypothalamus [Sherman (2001), Hasselmo (2006), Zagha and McCormick (2014), [McCormick and Bal (1997)]. Neuromodulators originating from these brain areas and essential for this transition are the acetylcholine (ACh), norepinephrine (NE), histamine (HA), serotonin (5-HT) and glutamate. The release of these neurotransmitters from their corresponding regions binds to specific receptors. This binding results in a transition of the thalamus, neocortex and hippocampus state from sleep to wakefulness due to depolarization of neurons membrane potential of these regions. According to [Zagha and McCormick (2014)], the activation of these receptors generates a reduction in K^+ conductances bringing the membrane potential closer to threshold and also enhance excitability by raising membrane resistance [McCormick and Bal (1997)]. In thalamic neurons, an increase in depolarization induces a decrease of the hyperpolarization thereby inactivating I_t, thus the neurons switch from bursting to tonic mode [Zagha and McCormick (2014)]) ([Sherman (2001)] . By this mechanism, the thalamus acts as a switch between sleep and wakefulness blocking incoming inputs to the brain. According to [Hasselmo (2006)] and [Steriade et al. (1993)], depolarization in hippocampal and neocortical pyramidal cells by the presence of high ACh enhance persistent spiking in these cells. [Hasselmo (2006)] reveals that during wakefulness, acetylcholine increases the influence of ascending input to the neocortex and enhance the afferent input transmission in mossy fibres and perforant path but does not enhance recurrent excitation within CA3 and CA1 region where it reduces excitatory feedback. This promotes encoding. Low ACh results in a removal of presynaptic inhibition which induces strong excitatory feedback compared to a weaker input influence which enhances consolidation.

5.4.1 Interconnection between the structures during the sleep-wake switch

Based on [Buzsáki (1996), Kunec et al. (2005), Giovannini (2017)], there is a dominance of neuronal ensembles activity in specific zones of the hippocampal formation according to the sleep-wake switch. During wakefulness, the information is relayed by the thalamus to the neocortex. The information is then transmitted to the hippocampal formation. Layer II and III of the entorhinal cortex and the dentate gyrus are preponderantly active. The representation of the event is encoded in the CA3 region. During sleep, the memory representation is replayed in the recurrent connection between neurons of the CA3 region and the CA3-CA1, subiculum, deep layers of the entorhinal cortex are predominantly active and are responsible for the population bursting activity in the hippocampus and for memory consolidation in the neocortex.

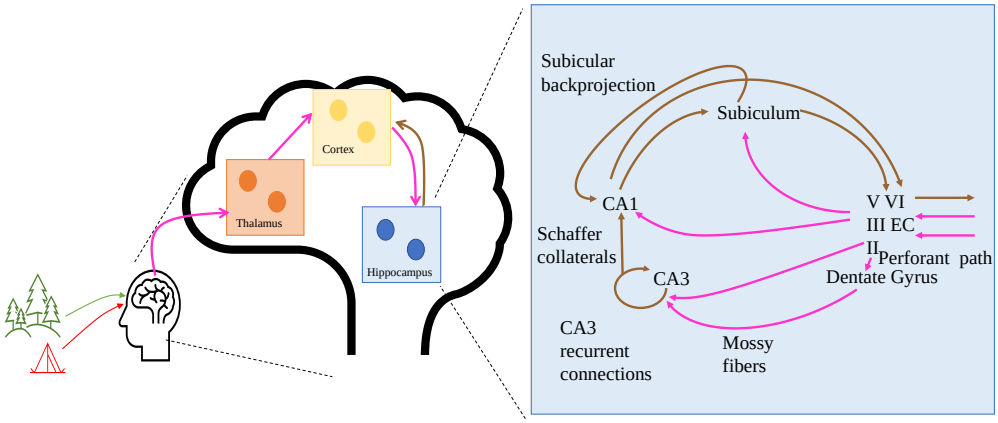

Figure 5.5 – Brain regions interconnection during the sleep-wake switch - During wakefulness, layer II and III of the EC and the dentate gyrus are predominantly active regions while CA3 recurrent connections, CA1 region, the subiculum and deep layers of the EC are mostly active during sleep. Pink arrows correspond to the dominant pathway during wakefulness and brown arrows correspond to the dominant pathway during sleep. - Adapted from [Xu et al. (2016)]

Chapter 6

Active systems consolidation theory

This thesis aims at reproducing the neuronal activity displayed during the encoding phase of the information during wakefulness and the synchronous neuronal pattern occurring during the consolidation phase throughout SWS. The processes of encoding and consolidation of the information discussed hereafter are defined by the *Active systems consolidation theory* established by Jan Born's laboratory [Klinzing et al. (2019a), Feld and Born (2017), Feld and Born (2020)].

6.1 The theory

Active systems consolidation theory determines the establishment of hippocampus-dependent declarative memory. During wakefulness, the representation of an experience flows through the neocortex to the initial store, the hippocampus. The hippocampus encodes the temporal and spatial features of an event by binding them into a unique episodic memory [Navarrete et al. (2020)] in CA3 pyramidal cells [Buzsáki (1998)]. The encoding of the information in the hippocampus happens after a one-shot occurrence and is subjected to disappearance suggesting that the hippocampus acts as a short-term store of the representation. During succeeding SWS, the connections between CA3 pyramidal cells that have been potentiated during wakefulness are reactivated [Buzsáki (1998)]. Reactivation consists in a re-appearance of neuronal ensemble patterns that were occurring during prior wakefulness. SWS diminishes the inhibition from hippocampal efferent path to the neocortex thus enabling that repeated reactivations in the hippocampus leads to a synchronous coactivation of neocortical neuronal ensembles resulting in consolidation of memory in the neocortex. The neocortex behaves as a long-term store supporting a reorganization of the representation in a more gist-like and abstracted representation due to the superposition of hippocampal patterns during reactivation. The reorganization of connections between neurons occurring during SWS arises from a synaptic rescaling promoted by sleep. The synaptic homeostasis hypothesis (SHY) followed by [Tononi and Cirelli (2014)] explains a promotion of synaptic upscaling during wakefulness in the neocortex and hippocampus and a synaptic downscaling of the connections in these regions during sleep to avoid high demands in energy and space. Following the active systems consolidation theory, SWS can increase synaptic upscaling rather than synaptic downscaling. Thus, consolidation of memory during SWS is enhanced by synaptic upscaling of connections supporting memory representations and the constitution of new synapses rather than synaptic downscaling as proposed by [Tononi and Cirelli (2014)].

6.2 Systems oscillations underlying memory consolidation

The coupling of LFP's (see FIGURE 6.1) coordinates the communication between the thalamus, the neocortex and the hippocampus and sets the clock for the reactivation of hippocampal neuronal ensembles which affects synaptic plasticity in neocortical networks. SO's, spindles and SWR's show a synchronization between their depolarization phase inducing the simultaneous firing in the corresponding regions which enhances synaptic plasticity among these networks. [Klinzing et al. (2019a)] suggests a triple coupling of the LFP's in a cortical-hippocampal-cortical cycle. The top-down process arises from the neocortical SO's up-state *i.e.* depolarization, which drives the generation of spindles.

Conversely, SO's down-state *i.e.* hyperpolarization abolish the generation of spindles and SWR's. In turn, excitable furrows of spindles conduct the generation of high-frequency SWR's. Spindles phase-locked to SO's and SWR's define the timing for the reactivation of hippocampal networks and enable the synchronization between SO's and SWR's for the transmission of the reactivation. Thus thalamic spindles are considered to act as a timer for the generation of all LFP's sleep rhythms. Bottom-up, the spindles can also transfer back to neocortical ensembles, the coupling of both rhythm is believed to strengthen synaptic plasticity in cortical neurons. SWR's can also feedback to cortical networks and immediately generate SO's. This coupled dialogue between the rhythms allows the transmission of the reactivation and a reinforcement of the synaptic connections within these regions.

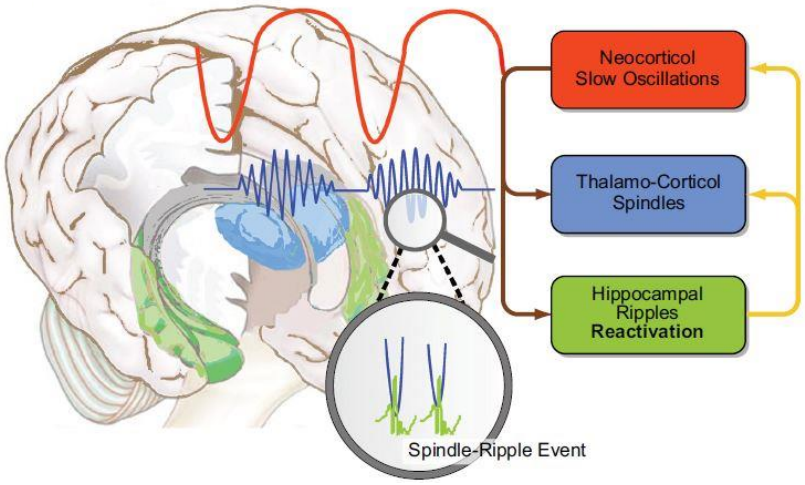

Figure 6.1 – Active systems consolidation theory model. Nesting of the neocortical slow oscillations, thalamo-cortical spindles and hippocampal sharp wave ripples enable the consolidation of the preencoded reprentation in the short time storage (hippocampus) into the long term storage (neocortex) - Adapted from [Rasch and Born (2013)]

6.3 The story

To illustrate the active systems consolidation theory, [Feld and Born (2020)] takes Jane's story as an example. An individual sees Jane at the beach in her red new car. The neuron coding for Jane spikes, and spike as well for the three other items independently in the neocortex. These episodic features flow cortical sensory regions to the hippocampus which connects and associates these items into one episodic representation of the event. During the succeeding night, the coupling of the three oscillations reactivates this association in the initial stores which lead to the establishment of reinforced connections of the four items in the long term store neocortex as a gist-like and unique representation of the event. The subsequent day, when the individual sees Jane, he associates her directly with the beach and the red car. In the context of this thesis, the preceding story is replaced by the story of the individual camping in the forest in his red tent as described in SECTION 3.4. The story is depicted in FIGURE 6.2.

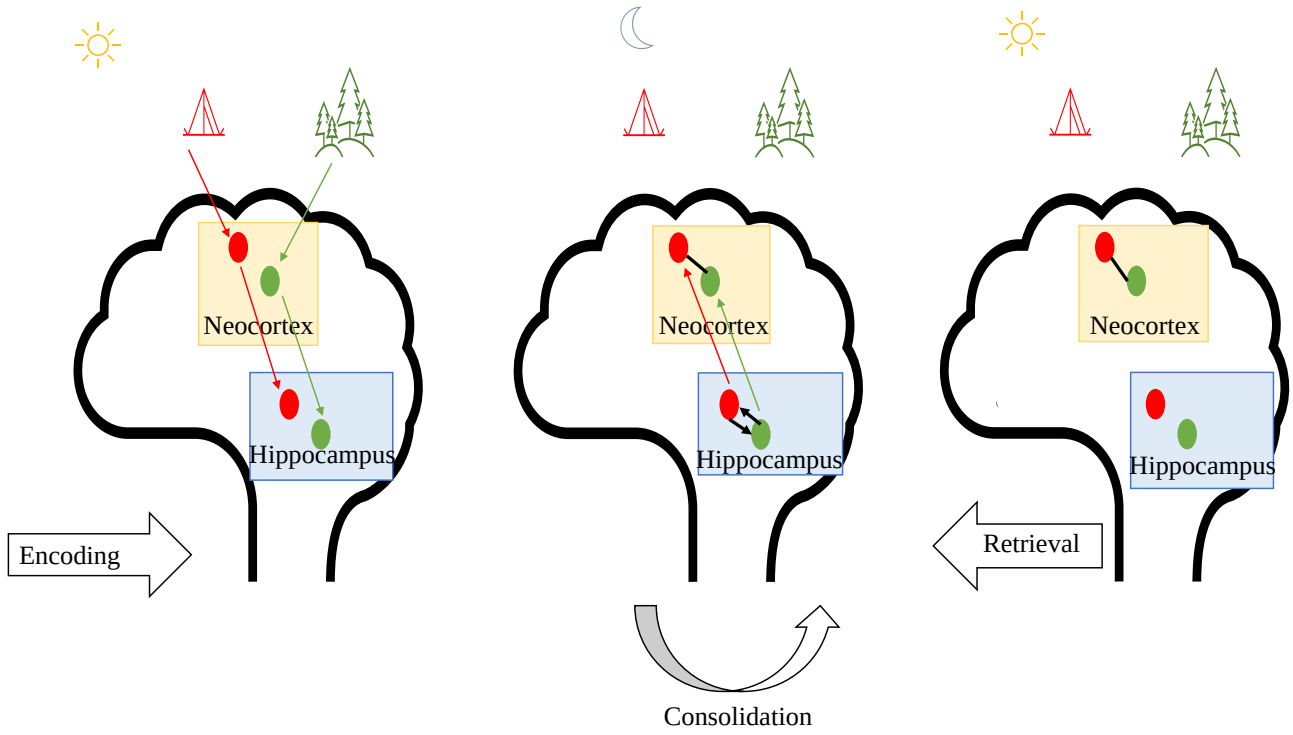

Figure 6.2 – The three stages of the active systems consolidation theory. During wakefulness (sun), an individual experiences the event of camping in the forest. The features of the representation, the red tent and the trees, are encoded in the neocortex (yellow) and flows to the hippocampus (blue). The neurons coding for the trees are represented in green and the neurons coding for the tent are represented in red. The subsequent night (moon), the pattern of activity is reactivated in the hippocampus (black arrows). The items are consolidated (black line) and integrated in the neocortex acting as a long-term storage. The following day, the consolidated representation of the experience can be retrieved without the involvment of the hippocampus. Inspired from [Feld and Born (2020)]

Part II

State of the art

Chapter 7

Neurophysiology of the thalamocortical system

This CHAPTER and the following CHAPTER 8 aim at providing intrinsic membrane properties of the main types of excitatory and inhibitory neurons involved in the thalamic, neocortical and hippocampal systems *i.e.* ionic currents and synaptic receptors, by investigating models found in the literature. The objective is also to provide an idea of the discharge frequency rate which depends on the state of the brain *i.e.* asleep or awake. In the present thesis, a convention concerning the name of the currents and the corresponding abbreviations are provided for the ease of the reading. The eight first ionic currents that are listed are those that are used in the *generic model* (see APPENDIX B) applied for the modeling in this thesis. It is important to notice that some models give diverse names for the same ionic current. The list is the following and also includes additional ionic currents presented in the models of the literature.

1. I_{Na}: A transient sodium current/A fast sodium current/A voltage-dependent sodium current
2. $I_{K,d}$: A delayed-rectifier potassium current/A fast delayed-rectifier potassium current
3. I_A: A A-type potassium current
4. I_T: A T-type calcium current/A low-threshold calcium current
5. I_L: A L-type calcium current
6. I_H: A H-current/A hyperpolarization-activated, mixed cation current.
7. $I_{K,Ca}$: A calcium-activated potassium current/A slow Ca^{2+}-dependent K^+ current/An afterhyperpolarization (AHP) calcium dependent potassium current/ A long duration Ca^{2+} dependent AHP K^+ current
8. I_{leak}: A leakage current
9. I_{NaP}: A persistent sodium current
10. I_{HVA}: A high threshold calcium current
11. I_M: A slow voltage dependent non-inactivating potassium current
12. I_{leak_K}: A potassium leak current
13. I_{Naleak}: A sodium leakage current
14. I_{Clleak}: A chlorine leakage current
15. I_{Kd_s}: A slow delayed-rectifier potassium current (which is another component of the delayed-rectifier current which is not considered for the modeling part of this thesis, only the fast delayed-rectifier current is considered (2.)

16. I_N: A N-type calcium current
17. $I_K(C)$: A short-term duration voltage and calcium dependent potassium current
18. I_{Ca}: A calcium current
19. I_R: A high voltage dependent calcium current
20. $I_{m_{AHP}}$: A medium fast AHP current

In the following SECTIONS and in the next CHAPTER, the different ionic currents are provided for the neurons of the different brain regions *i.e.* thalamus, neocortex, entorhinal cortex, dentate gyrus, CA3, CA1 and subiculum according to models found in the literature. Ionic conductances values presented in the models are given as an indicative basis to have a notion of their order of magnitude. This is done in order to realise the modeling of the circuit developed in PART III. Indeed, the modeling requires to respect ratios between ionic conductances but not their proper numerical value. Ionic currents names, synaptic conductances values and conductance-based equations given in the models subsequently presented are provided in the APPENDIX C.

7.1 Thalamus

7.1.1 Thalamic reticular cell

Thalamic reticular cells (RE) are GABAergic neurons constituting together the thalamic reticular nucleus [McCormick and Bal (1997)].

Ionic currents

[Destexhe et al. (1996)] establish a network model of thalamocortical and reticular cells which kinetics is described by the Hodgkin and Huxley equations. These cells are considered to be single-compartmental cells. Their model is fitted on experimental data to obtain the burst discharge in TC and TRN cells. At the network level, the goal is to replicate the spindle activity by interconnecting TC and reticular cells through synaptic receptors. The reticular cell in the network model is characterized by I_{Na}, $I_{K,d}$, I_T and I_{leak} and their corresponding ionic conductance values are given in TABLE 7.1.

[McCormick and Huguenard (1992)], based on voltage-clamp recordings, examine the ionic contributions involved in the intrinsic bursting capacity of thalamic neurons. Those currents are I_T, I_h, I_A and I_{K2} which is a slowly inactivating transient potassium current The currents are modeled according to Hodgkin and Huxley equations. The currents involved in TC cell model are: I_{Na}, I_{NaP}, $I_{K,d}$, I_L, I_A, $I_{K,Ca}$, I_T, I_{Naleak} and I_{Kleak}. They express two types of potassium current $I_{K_{2,a}}$ and $I_{K_{2,b}}$ which are regrouped in the column $I_{K,d}$ and two types of A-type potassium current I_A and I_{A_2} which are regrouped in the column I_A in TABLES 7.1 and 7.2.

[Drion et al. (2018)] develop a conductance-based model and will to investigate the tunability and the robust control of brain states based on phase plane and currents time-scales analysis. The currents used are I_{Na}, $I_{K,d}$, I_T, $I_{K,Ca}$, I_h and I_{leak}. Values of the maximal conductances corresponding to the ionic currents mentioned in the latter models are presented in TABLE 7.1.

Synaptic receptors

Both [Drion et al. (2018)] and [Destexhe et al. (1996)] model the interconnection between TC and reticular cells in their network model with $AMPA$, $GABAa$ and $GABAb$ receptors. The different synaptic receptors present in reticular cells are displayed in TABLE 7.5.

Firing mode

The firing rate of reticular neurons is given by [Drion et al. (2018) (figure 3A)]. The frequency rate of tonic discharge during wakefulness is given between 10 and 60Hz and the frequency rate of endogenous burst discharge during sleep is between 100 and 130 Hz (consists in 2 to 10 action potentials per burst [Fernandez and Lüthi (2020)]).

Articles	Ionic conductances values								
	g_{Na}	$g_{K,d}$	g_A	g_T	g_L	g_H	$g_{K,Ca}$	g_{leak} g_{Naleak} g_{Kleak}	g_{NaP}
[Destexhe et al. (1996)]	0.4	0.08	-	0.006	-	-	-	5e-5 - -	-
[McCormick and Huguenard (1992)]	12	38e-3 ($g_{K_{2a}}$) 26e-3 ($g_{K_{2b}}$)	20e-3 (g_A) 15e-3 (g_{A_2})	-	0.8	-	1	- 1.65e-3 7e-3	7e-3
[Drion et al. (2018)]	170	40	-	0.55	-	0.01	4	0.055 - -	-

Table 7.1 – Ionic conductances values in the models of [Destexhe et al. (1996), Drion et al. (2018), McCormick and Huguenard (1992)]. The conductances values are expressed in $[\frac{mS}{cm^2}]$ for [Drion et al. (2018)], in $[\frac{S}{cm^2}]$ for [Destexhe et al. (1996)] and in mS for [McCormick and Huguenard (1992)]. The first eight columns gather the conductances that are used in the *generic model* except for g_{Naleak} and g_{Kleak}

7.1.2 Thalomocortical cell

Thalamocortical cells (TC) are excitatory relay neurons as mentionned previously.

Ionic currents

[Destexhe et al. (1998)] compare his model of a TC neuron with experimental recordings in vitro to observe I_T density in dendrites and its implications in bursting behaviour. They develop a model of a TC cell based on recordings and computational modeling. The conductances of the model are modeled with Hodgkin and Huxley equations. The currents are I_{Na}, $I_{K,d}$, I_T and I_{leak}.

[Drion et al. (2018)] and [McCormick and Huguenard (1992)] models also accounts for TC cells.

Ionic conductances values for these models are given in TABLE 7.2

Articles	Ionic conductances values								
	g_{Na}	$g_{K,d}$	g_A	g_T	g_L	g_H	$g_{K,Ca}$	g_{leak} g_{Naleak} g_{Kleak}	g_{NaP}
[Destexhe et al. (1998)]	100	100	-	3.3	-	-	-	5e-2 - -	-
[McCormick and Huguenard (1992)]	12	38e-3 ($g_{K_{2,a}}$) 26e-3 ($g_{K_{2,a}}$)	20e-3 (g_{K_A}) 15e-3 (g_{A_2})	-	0.8	-	1	- 2.65e-3 7e-3	7e-3
[Drion et al. (2018)]	170	40	-	0.55	-	0.01	4	0.055 - -	-

Table 7.2 – Ionic conductances values in the models of [Destexhe et al. (1996), Drion et al. (2018), McCormick and Huguenard (1992)]. The conductances values are expressed in $[\frac{mS}{cm^2}]$ for [Drion et al. (2018)], in $[\frac{mS}{cm^2}]$ for [Destexhe et al. (1998)] and in $[mS]$ for [McCormick and Huguenard (1992)]. The first eight columns gather the conductances that are used in the *generic model* except for g_{Naleak} and g_{Kleak}

Maximal conductances values in TABLES 7.1 and 7.2 are given in [Jacquerie and Drion (2021)].

Synaptic receptors

The type of synpatic receptors present in TC cells are found in TABLE 7.5.

Firing rate

The burst discharge of TC cells during sleep lasts for a shorter period than reticular cells [Fernandez and Lüthi (2020)] and consists of fewer action potentials than reticular neurons. The frequency range of tonic firing is considered the same as the reticular neurons in this thesis.

7.2 Neocortex

7.2.1 Excitatory cell

Neocortical excitatory neurons are spiny neurons that can be classified in two categories according to their dendritic morphologies and the location of their soma [Costa and Müller (2015), Jones (2016)]:

- Stellate cells are solely situated in layer IV of the cortical column and mainly project to nearby locations. They possess dendrites of equivalent lengths.
- Pyramidal cells (PY) are present in all cortical layers except in the pia matter. They can join different cortical areas or send their projections to subcortical regions but they can also project to closer areas. Thus, they are the main excitatory input and output cells of the neocortex [Costa and Müller (2015)]. In addition, all the literature concerning the neocortex mentioned in this thesis refers to pyramidal cells as neocortical excitatory neurons.

Ionic currents

Three models and a review of models from the literature established thalamocortical circuit models and are presented in this thesis.

[Bazhenov et al. (2002)] provides a model of the thalamocortical system in which network activity corresponds to the one occurring during SWS and wakefulness. Pyramidal cells are modeled as two-compartment neurons (axosomatic and dendritic compartments) in which channels are defined by Hodgkin and Huxley dynamics. The currents involved for the dendritic and axosomatic compartments are the following: I_{Na}, $I_{K,d}$, I_{NaP}, I_{leak}, I_{leak_K}, I_{HVA}, I_M and I_{KCa}. The respective ionic conductances are given in TABLE 7.3.

A second comparable model is the model presented by [Wei et al. (2016)] which consists of investigating the SO's interaction with synaptic plasticity to transfer the hippocampal neuronal pattern into a stable cortical representation. [Wei et al. (2016)]'s neocortical model is the same as the one developed by [Bazhenov et al. (2002)] *i.e.* involving the same currents see TABLE 7.3.

[Hill and Tononi (2005)] constructs a thalamocortical circuit to examine the machinery behind the start, continuation and cessation of SO's as well as its synchronous rhythm through the thalamocortical system in order to understand the mechanism underlying the transition between wakefulness and sleep. The model consists of representing two visual areas and the connection to their corresponding thalamic nuclei. Neurons of the neocortical and thalamic regions are modeled as a one-compartment neuron with the Hodgkin and Huxley equations and the following currents are involved: I_{NaP}, I_{DK} (a Na^+ or $Ca2+$ activated K^+), I_T was not included in the model for neocortical neurons even though they mention that some neocortical neurons contain this current. They also modeled an I_h current for thalamic cells and for the intrinsically bursting neocortical neurons of layer V and VI which only consists of 30 % of cells in these layers. The corresponding ionic conductances values are provided in TABLE 7.3. Moreover, this thesis considers an exogenous type of burst as mentioned in SUBSECTION 5.3.3. Similarly, a low-threshold calcium current was not included for neocortical neurons. Moreover, sodium leak and potassium leak currents are added to the model. The maximal conductances for g_{NaP}, g_{DK} and g_{NaL} are varied to model the removal of acetylcholine inducing a transition from an active to an inactive state of the brain.

The article of [Pospischil et al. (2008)] reviews Hodgkin and Huxley type of models of thalamic and neocortical neurons distinguishing them into four types: the fast-spiking neurons, the regular spiking neurons, the intrinsically bursting neurons and the low-threshold spiking neurons. For this SECTION, the conductance values of regular spiking cells are relevant. Data from in vitro and in vivo

Articles	Ionic conductances values in $\frac{mS}{cm^2}$										
	g_{Na}	$g_{K,d}$	g_A	g_T	g_L	g_H	$g_{K,Ca}$	g_{leak} g_{Naleak} g_{Kleak}	g_{NaP}	g_{HVA}	g_M
B (soma)	3000	200	-	-	-	-	-	-	-	-	-
B (dendrite)	1.5	-	-	-	-	-	0.03	0.033 - 0-0.0025	0.07	0.01	0.01
W (soma)	3000	200	-	-	-	-	-	-	-	-	-
W (dendrite)	0.8	-	-	-	-	-	0.03	- - 0.03	-	0.02	0.02
H	-	0.5-1.25	-	-	-	-	0.5-1.25	- 0.02 1-1.85	0.5-1.25	-	-
P	50	4.8	-	-	-	-	-	1.90	-	-	0.13

Table 7.3 – Ionic conductances values in the models of [Bazhenov et al. (2002) (B), Wei et al. (2016) (W), Hill and Tononi (2005) (H), Pospischil et al. (2008) (P)]. The first eight columns gather the conductances that are used in the *generic model* except for g_{Naleak} and g_{Kleak}. The leak conductance is given by [Pospischil et al. (2008)] in nS.

preparation were collected to acquire rather generic models. The different models are described by the following currents: I_{Na}, I_{Kd}, I_M, I_L and I_T and I_{leak}. I_L and I_T induce bursting activity for intrinsically bursting neurons which is not relevant in the scope of this thesis. For 13 regular spiking neocortical neurons of the rat somatosensory cortex, they obtain the mean values for the maximal ionic conductances of the previous currents present in TABLE 7.3.

The models of [Bazhenov et al. (2002), Wei et al. (2016) Hill and Tononi (2005)] are well suited for the scope of this project as they explore the features behind SWS by developing a thalamocortical circuit. [Wei et al. (2016)] and [Bazhenov et al. (2002)] establish a two compartment model while [Hill and Tononi (2005)] and [Pospischil et al. (2008)] advance a one compartment model. All model are based on the Hodgkin and Huxley equation and employ the traditional sodium, potassium currents and a M-current (except for [Hill and Tononi (2005)]) in their models. [Bazhenov et al. (2002)] and [Wei et al. (2016)] also insert a Ca^{2+} dependent K^+ current. It is important to notice that [Hill and Tononi (2005)] refers to the included potassium current as a Na^+ or Ca^{2+} activated K^+ current which suggest also that a Ca^{2+} dependent K^+ current can be added to the thalamocortical model. Furthermore, the suggestion of a T-type current in [Pospischil et al. (2008)] and [Hill and Tononi (2005)] is also mentionned but for a bursting type of neuron in one case and in the other case, the purpose of this current combined with a I_h current is not mentionned but is considered as negligeable.

Synaptic receptors

The synaptic receptors are given in TABLE 7.5.

Firing mode

During wakefulness, neocortical pyramidal neurons are in tonic mode and receive IPSPs induced by cortical interneurons spiking at 40 Hz [Llinas et al. (1991)]. These IPSPs produce rhythmic firing in neocortical pyramidal neurons spiking at 40Hz. This 40Hz activity projects back to the thalamus which would in turn activate the cortex in a loop like manner. [Ferster (1988)] has demonstrated electrophysiologically the presence of IPSPs at 40 Hz in the primary visual cortex. During sleep, neocortical cells discharge in bursts of few action potentials that are exogenous as considered in this thesis. During sleep, the bursting activity is considered to be exogenous in the neocortical pyramidal cells as explained in 5.3.3.

7.2.2 Interneuron

The main types of interneurons in the neocortex are the parvalbumin positive (PV+) neurons which produce a perisomatic inhibition and the somatostatin positive (SOM+) cells which produces a dendritic inhibition [Zagha and McCormick (2014), Niethard et al. (2017)]. Each type of interneurons constitute respectively 40 % and 30 % of all the neocortical interneurons. PV+ being the most abundant type of interneurons in the neocortex, they are used in the model presented in this thesis. PV+ are fast-spiking interneurons implied in the LFP's which action is eased by the presence of acetylcholine and noradrenaline. fast-spiking neurons discharge at a high frequency that can possibly attain 1kHz [Descalzo et al. (2005)].

Ionic currents

Ionic currents and their respective conductance values for fast-spiking PV+ interneurons change slightly according to the models described for the neocortical pyramidal cells in TABLE 7.4. In [Pospischil et al. (2008)], the conductance values for the fast-spiking inhibitory cells are acquired for 14 fast-spiking cells in the rat somatosensory cortex. In [Bazhenov et al. (2002), Wei et al. (2016)], the interneuron does not present a I_{NaP} current and the value of g_M barely changes. [Hill and Tononi (2005)] does not argue for any changes between excitatory pyramidal neurons and interneurons of their model.

Articles	Ionic conductances values in $\frac{mS}{cm^2}$										
	g_{Na}	$g_{K,d}$	g_A	g_T	g_L	g_H	$g_{K,Ca}$	g_{leak} g_{Naleak} g_{Kleak}	g_{NaP}	g_{HVA}	g_M
B (soma)	3000	200	-	-	-	-	-	-	-	-	-
B (dendrite)	1.5	-	-	-	-	-	0.03	0.033 - 0-0.0025	-	0.01	0.01
W (soma)	3000	200	-	-	-	-	-	-	15	-	-
W (dendrite)	0.8	-	-	-	-	-	0.03	- - 0.03	2.5	0.02	0.03
H	-		-	-	-	-	0.5-1.25	- 0.2 1-1.85	0.5-1.25	-	-
P	46	5.1	-	-	-	-	-	8.21	-	-	0.07

Table 7.4 – Ionic conductances values in the models of [Bazhenov et al. (2002) (B), Wei et al. (2016) (W), Hill and Tononi (2005) (H), Pospischil et al. (2008) (P)]. The first eight columns gather the conductances that are used in the *generic model* except for g_{Naleak} and g_{Kleak}. The leak conductance given by [Pospischil et al. (2008)] is given in nS.

Synaptic receptors

The synaptic receptors for the neocortical inhibitory interneurons are given in TABLE 7.5.

Firing mode

[Llinas et al. (1991)] perform intracellular recordings to investigate the intracellular properties of layer VI interneurons of the guinea pig frontal cortex. They divide the interneurons into two classes: neurons with a wide frequency range from 10 to 45 Hz and neurons with a narrower frequency rate from 35 to 50Hz. [Golomb et al. (2007)] states that fast-spiking interneurons in the neocortex show a non-delayed frequency discharge ranging from 27.4 Hz to 100 Hz varying with the applied current intensity. The goal of their article is to study the variability between the delay of discharge of fast-spiking interneurons to

a step of current. One type shows no delay of response while another type of fast-spiking interneurons exhibits a delayed response. Fast-spiking interneurons are in tonic mode at high frequencies [Descalzo et al. (2005), Povysheva et al. (2013)] during sleep and wakefulness and their pattern of activity is influenced by synaptic inputs.

7.3 Synaptic receptors

The synaptic receptors enabling the communication between the cells of the thalamocortical system are displayed in the ensuing table and are based on [Bazhenov et al. (2002), Hill and Tononi (2005), Wei et al. (2016), Destexhe et al. (1996), Drion et al. (2018)] and also on [Fernandez and Lüthi (2020)] that synthesizes the properties of sleep spindles. The conductance values of the corresponding synaptic receptors are given in the table in APPENDIX C.8.

Pre-cell	Post-cell			
	TC	RE	PY	IN
PY	$AMPA$ (H)(F)	$AMPA$ (H)(F) $NMDA$ (F)	$AMPA$ (W)(B)(H) $NMDA$ (W)(B)(H)	$AMPA$ (W)(B)(H) $NMDA$ (W)(B)(H)
IN	-	-	$GABAa$ (W) (B) (H) $GABAb$ (H)	-
TC	-	$AMPA$ (W)(H)(F) (D)(De) $NMDA$ (F)	$AMPA$ (B)	$AMPA$ (H)
RE	$GABAa$ (B)(W)(H)(F) (D)(De) $GABAb$ (B)(H)(F) (D)(De)	-	-	-

Table 7.5 – Synaptic receptors enabling the communication between a pre-cell (neocortical pyramidal cell PY, neocortical parvalbumin positive interneuron IN, thalamocortical cell and reticular cells RE) and a post cell. The synaptic receptors are given by the article [Bazhenov et al. (2002) (B), Hill and Tononi (2005) (H), Wei et al. (2016) (W), Fernandez and Lüthi (2020) (F), Drion et al. (2018) (D), Destexhe et al. (1996) (De)]

Chapter 8

Neurophysiology of the hippocampus

8.1 Entorhinal cortex

8.1.1 Excitatory cell

There are three main important layers present in the entorhinal cortex (EC) involved in the transmission of information in and out of the hippocampal formation:

1. Layer II composed of stellate neurons constituting 65 % of all cell types existing in this layer [Chrobak et al. (2000), Dickson et al. (2000), Alonso and Klink (1993)].
2. Layer III is composed mostly of pyramidal neurons [Chrobak et al. (2000)].
3. Layer V consists mainly in pyramidal cells [Dickson et al. (2000)].

Ionic currents

1. The role of the stellate cells network in EC layer II in generating the theta rhythm is highlighted by [Acker et al. (2003)]. They want to examine the dynamics of the slow ionic currents for a single cell and a small network of cells that enable a cell to fire at rates similar to this of theta rhythm. They provide a model of two paired cells which dynamics is described by the traditional Hodgkin and Huxley equations with the sodium and potassium current, I_{Na} and $I_{K,d}$ generating an action potential but they also add slow ionic currents allowing subthreshold oscillations and consistent with theta rhythm. Those slow ionic currents are I_{NaP} and I_h. The values of the maximal ionic conductances for the ionic currents are given in the TABLE 8.1. [Rotstein et al. (2006)] uses the same currents and conductance-based model to elucidate the mechanism behind the subthreshold oscillations occurring in EC layer II stellate cells at the origin of synchronized oscillations and that are believed to be generated by the interaction between I_h and I_{NaP}. There are evidence in the litterature showing the involvment of an interaction between I_h adn I_Nap in EC layer II stellate cells but their interaction is still not well understood [Acker et al. (2003), Magistretti et al. (1999), Dickson et al. (2000), Rotstein et al. (2006)]. It is important to mention that models providing electrophysiological properties are more numerous for layer II stellate cells and are more challenging to find for layer III and V pyramidal cells.

Article	Ionic conductances values in $\frac{mS}{cm^2}$								
	g_{Na}	$g_{K,d}$	g_A	g_T	g_L	g_H	$g_{K,Ca}$	g_{leak}	g_{NaP}
[Acker et al. (2003)]	52	11	-	-	-	1.5	-	0.5	0.5

Table 8.1 – Ionic conductances values used in the model of [Acker et al. (2003)] for EC layer II stellate cells. The eight first columns correspond to the ionic conductances used in the *generic model*.

2. In their article, [Chrobak et al. (2000)] states that for layer III pyramidal cells, their physiology is closer to neocortical neurons and are thus assumed to have the same conductances as neocortical pyramidal neurons as neocortical pyramidal cells previously presented.

3. According to [Hamam et al. (2000)], it has been suggested that layer V pyramidal neurons of the EC approach the layer V pyramidal cells of the neocortex as literature concerning the electrophysiology of this cell type is sparse [Hamam et al. (2000)]. This thesis also assumes that layer V EC cells and layer V neocortical cells have a similar electrophysiology. [Dickson et al. (2000), Hamam et al. (2000)] propose that layer V EC pyramidal cells are subjected to subthreshold oscillations due to persistent sodium currents but not to I_h as layer II stellate cells.

Synaptic receptors

[Jones (1994)] examines the electrophysiological and morphological properties of EC layer II stellate cells by doing slice experiments on the brain of the rat. They found that layer II stellate cells interacted synaptically through $AMPA$, $NMDA$, $GABAa$ and $GABAb$ receptors.

Firing mode

The excitatory cells of the EC display two modes of discharge according to the brain state:

- During wakefulness, the different cell types discharge in a tonic mode with different frequencies:
    1. The stellate cells of layer II discharge in tonic mode at a frequency of 5-15Hz [Rotstein et al. (2006)].
    2. Pyramidal cells of layer V discharge with a frequency of 5-15 Hz a well and are believed to have the same pattern of activity as layer II stellate cells [Dickson et al. (2000)].
    3. No evidence on the frequency of discharge of layer III pyramidal neurons and are therefore assume in this thesis to have the same discharge frequency as neocortical neurons (40Hz as seen in SUBSECTION 7.2.1).
    4. Pyramidal cells of layer V discharge with a frequency of 5-15 Hz a well and are believed to have the same pattern of activity as layer II stellate cells [Dickson et al. (2000)].
- During sleep, neurons are believed to discharge in exogenous bursting:
    1. Cells of the EC region present a bursting activity within a frequency range of 125-500Hz [Bant et al. (2020)] mostly motivated for layer II stellate cells. [Bant et al. (2020)] declares that there is a gradient in bursting frequency from ventral to dorsal locations and that this gradient is explained by a change in non-inactivating sodium conductances (persistent and resurgent sodium according to [Bant et al. (2020)]) and suggest that burst could arise from the interaction between ionic conductances and the temporal dynamics of synaptic inputs. Therefore, in this thesis, the bursting activity of layer II stellate cells is believed to be exogenous.
    2. No information was found about the bursting frequency rate of layer III cells and are assumed to be exogenous bursting in this thesis.
    3. In their article, [Hamam et al. (2000)] also state that layer V pyramidal neurons do not present intrinsic bursting linked to Ca^{2+} conductances and are believed to follow the same activity pattern as layer II stellate cells [Dickson et al. (2000)].

8.1.2 Interneuron

[Chrobak et al. (2000)] suggests that the local interneuron present in layer two of the entorhinal cortex is the basket cell (BC) interneuron.

Ionic currents

No model was found on the fast-spiking basket interneurons in particular for the entorhinal cortex. Therefore, as being part of the PV+ interneuron family [Povysheva et al. (2013)], the currents and conductances values that are considered are those of the neocortical PV+ interneurons presented in SUBSECTION 7.2.2.

Synaptic receptors

[Jones and Bühl (1993)] obtained their data by performing intracellular recordings for four years on layer II fast-spiking cells and detected $AMPA$ and $NMDA$ receptors in layer II basket cells as well as $GABAa$ and $GABAb$ receptors. For layer III and layer V stellate cells, the same receptors as the one included in neocortical pyramidal cells are assumed.

Firing mode

As being fast-spiking interneurons, they discharge in tonic mode with periods of transient tonic activity due to local synaptic inputs coming from the excitatory cells to which they are connected. [Chrobak et al. (2000)] cites [Jones and Bühl (1993)] to motivate that the spiking frequency of basket cells are lower than 200 Hz. They observed cells firing continuously at those rates following injected current pulses. [Jones (1994)] also observed from intracellular recordings that fast-spiking interneurons discharge at frequencies greater than 150 Hz.

8.2 Dentate gyrus

8.2.1 Excitatory cell

The most important type of excitatory cell in the dentate gyrus (DG) is the granule cell. The granule cell has spiny dendrites with a cone tree shape. There are very abundant in the dentate gyrus (1.000.000 in the rat dentate gyrus) and are highly congested [Amaral et al. (2007)].

Ionic currents

[Santhakumar et al. (2005)] want to investigate the role of another type of excitatory cell present in the hilar region of the dentate gyrus mentioned later in SUBSECTION 9.2.2. They want to understand their involvement in hyperexcitability linked to post-trauma. They realize a dentate network model including four types of cells: the granule cells, the basket cells, the mossy cells and the hilar perforant-path associated cells. They were modeled as a multicompartment cell which inherent properties are established by experimental data. The current they used to model the behaviour of granule cell are: I_{Na}, $I_{K,d}$, I_{Kd_s}, I_A, I_L, I_N, I_T, $I_{K(C)}$, $I_{K,Ca}$ and I_{leak} [Santhakumar et al. (2005), Cutsuridis and Poirazi (2015)]. The table hereunder comprises the generic currents used in the present thesis and other currents provided in the model of [Cutsuridis and Poirazi (2015)]:

Article	Ionic conductances values in $\frac{mS}{cm^2}$										
	g_{Na}	$g_{K,d}$	g_A	g_T	g_L	g_H	$g_{K,Ca}$	g_{leak}	g_{Kd_s}	$g_{K(C)}$	g_N
[Santhakumar et al. (2005)]	120	16	12	0.037	5	-	6	0.004	1	0.6	2

Table 8.2 – Ionic conductance values used in the model of [Santhakumar et al. (2005). The first eight ionic conductances are the ones applied in the *generic model*

Synaptic receptors

[Santhakumar et al. (2005)] provides synaptic receptors conductances based on experimental data. They suggest that granule cells possess $AMPA$ receptors as well as $GABAa$ receptors presented in the following table:

Pre-cell	Post-cell
	Granule cell
Perforant path projection	$AMPA$
Granule cell	$AMPA$
Basket cell	$GABAa$

Table 8.3 – Synaptic receptors used in the model of [Santhakumar et al. (2005)] for the granule cells of the dentate gyrus. (Respective conductances values are provided in the APPENDIX C.9)

Firing mode

During wakefulness, granule cells discharge in tonic mode from 5Hz to 30Hz according to the current applied [Santhakumar et al. (2005) (figure 1E)].

During sleep, granule cell exhibits an exogenous type of bursting consisting of 10 action potentials in a burst episode as [Fricke and Prince (1984)] showed. [Fricke and Prince (1984)] says that little is known about DG granule cells and tries to investigate the synaptic response of granule cells to its inputs and the membrane properties using current-clamp techniques. The granule cells are bathed in a normal Ringer solution (physiological solution made of sodium chloride, potassium and calcium) and showed that only 3 out of 55 granule cells showed intrinsic bursting, they conclude that intrinsic burst discharge cannot arise in DG granule cells. In normal conditions, they show the experimental curve representing a bursting induced in the cell consisting of approximately 10 action potentials [Fricke and Prince (1984) (figure 9.1)].

8.2.2 Interneuron

The basket cell is the most examined type on interneuron in the dentate gyrus [Amaral et al. (2007)]

Ionic currents

The currents used to model basket cells membrane properties are also taken from [Cutsuridis and Poirazi (2015)] and [Santhakumar et al. (2005)] and are the following: : I_{Na}, $I_{K,d}$, I_A, I_L, I_N, $I_{K(C)}$, $I_{K,Ca}$ and I_{leak}. The maximum ionic conductances values for each current including the currents from the generic model of the somatic compartment given in $\frac{mS}{cm^2}$ are presented in the following table:

Article	Ionic conductances values in $\frac{mS}{cm^2}$									
	g_{Na}	$g_{K,d}$	g_A	g_T	g_L	g_H	$g_{K,Ca}$	g_{leak}	$g_{K(C)}$	g_N
[Santhakumar et al. (2005)]	120	13	0.15	-	5	-	0.002	0.004	0.2	0.8

Table 8.4 – Ionic conductance values used in the model of [Santhakumar et al. (2005). The first eight ionic conductances are the ones applied in the *generic model*

Synaptic receptors

[Santhakumar et al. (2005)] provides synaptic receptors based on experimental data. They suggest that granule cell possess $AMPA$ receptors with which projections from the perforant path and granule cells communicate (see TABLE 8.5) as well as $GABAa$ receptors (the latter is not considered in the scope of this thesis)

Pre-cell	Post-cell
	Basket cell
Perforant path projection	$AMPA$
Granule cell	$AMPA$

Table 8.5 – Synaptic receptors used in the model of [Santhakumar et al. (2005)] for the basket cell of the dentate gyrus. (Respective conductances values are provided in the APPENDIX C.9)

Firing mode

The firing mode of a basket cell, as being part of the family of the fast-spiking PV+ interneurons [Povysheva et al. (2013)] is tonic but can have a transient tonic activity due to the synaptic entry of the excitatory cell to which they are synaptically connected. Its spiking activity goes from 15-140 Hz according to [Santhakumar et al. (2005) (figure 1F)]. Moreover, [Bartos et al. (2001)] develop a model of DG interneuron network and sowed a frequency of approximately 100 Hz when a pair of interneurons were coupled [Bartos et al. (2001) (figure 6a)].

8.3 CA3 region

8.3.1 Excitatory cell

The principal type of excitatory glutamatergic cell in the CA3 region is the pyramidal cell possessing approximately 40 large dendrites each connected to a single mossy fibre bouton [Cutsuridis et al. (2019)].

Ionic currents

[Traub et al. (1991)] develops a 19-compartment model of the CA3 pyramidal cell of a pig and tries to reproduce at best the behaviour of these cells by integrating voltage-clamp data of the different currents involved and by fitting experiments for the distribution of densities of the corresponding channels. The ionic currents involved are I_A, $I_{K,Ca}$, I_{Na}, $I_{K,d}$, $I_{K(C)}$, I_{Ca} and I_{leak} The conductance-based equation describing the behaviour of the 19-compartment model, as well as the conductance values for the soma, are given in the Appendix C.13.

[Migliore et al. (1995)] highlights the presence of bursting and non-bursting CA3 pyramidal neurons and wants to understand what distinguish both types in terms of channel densities and distributions as well as in term of calcium concentrations. They used data from six different CA3 neurons with a varying number of compartments from different laboratories to conduct their simulations. They modeled the different conductances based on Hodgkin and Huxley equations. The currents introduced in the model for all types of CA3 pyramidal neurons are the following: I_{Na}, $I_{K,d}$, I_A, ,I_M, $I_{CaN,L,T}$, $g_{K(C)}$ and $I_{K,Ca}$. I_{Na}, $g_{K,d}$, I_A, I_M values differ from bursting and non bursting cell but as mentioned in subsection 5.3.4, the hypothesis that is made in this thesis suggests that CA3 pyramidal cells are non bursting. Thus, only values of non bursting cells are presented here concerning I_{Na}, $g_{K,d}$, I_A, I_M. The values are taken from the rat CA3 pyramidal cell. Values of the ionic conductances for this model are given in the appendix C.14.

The following table includes the conductance values for the model of [Traub et al. (1991)] and [Migliore et al. (1995)].

Articles	Ionic conductances in $\frac{mS}{cm^2}$											
	g_{Na}	$g_{K,d}$	g_A	g_T	g_L	g_H	$g_{K,Ca}$	g_{leak}	g_{K_C}	g_{Ca}	g_{K_M}	g_N
Traub	30	15	0.5	-	-	-	0.8	0.1	10	4	-	-
Migliore	15	30	1.5	0.25	2.5	-	0.4	-	0.8	-	0.1	2.5

Table 8.6 – Ionic conductances values used in the model of [Traub et al. (1991)] and Migliore et al. (1995). The first eight ionic conductances are the ones of the *generic model*

The Ca^{2+}-activated K^+ conductance, $g_{K_{AHP}}$, is assumed to be the $g_{K,Ca}$ in the previous table.

Synaptic receptors

[Traub et al. (1991)] highlights the presence of $NMDA$ and $AMPA$ receptors on CA3 pyramidal cells. [Migliore et al. (1995)] also suggest the presence of $NMDA$ receptors. They also mention the presence of $GABAa$ and $GABAb$ receptors. Values for the synaptic conductances are given in the appendix C.10.

Firing mode

The discharge mode of CA3 pyramidal cells is tonic firing during active states. [Migliore et al. (1995)] provides an experimental trace of the CA3 neuron discharging in tonic mode [Migliore et al. (1995) (figure 6)]. The spikes occur at a frequency of approximately 40Hz. During sleep, the neurons discharge in burst mode as hypothesized an exogenous mode of firing is considered in this thesis as explained in SUBSUBSECTION 5.3.4. [Traub et al. (1991)] shows the experimental trace of a spontaneous bursting neuron bursting at approximately 100Hz [Traub et al. (1991) (figure 4)].

8.3.2 Interneuron

[Gulyás et al. (2010)] states that fast-spiking basket cells' are mainly involved in perisomatic inhibition in the CA3 region. [Cutsuridis et al. (2019)] also mention the presence of BC in the CA3 recurrent circuitry.

Ionic currents

[Wang and Buzsáki (1996)] investigate if hippocampal inhibitory networks are at the origin of inducing an oscillatory rhythm to hippocampal pyramidal neurons. They develop a one-compartment model of a hippocampal interneuron in which I_{Na}, $I_{K,d}$ and I_{leak} are involved.

[Cutsuridis and Poirazi (2015)] apply a biophysical representation of granule cells, CA3 and CA1 pyramidal cell as basket cells to develop a model investigating the temporal delays present in the hippocampal regions.

[Cutsuridis and Poirazi (2015)] cite the article of [Santhakumar et al. (2005)] which provides the ionic currents and the corresponding ionic conductances values for basket cells given in TABLE 8.7. These currents are I_{Na}, $I_{K,d}$, I_A, I_L, $I_{K,Ca}$, I_{leak} and I_N. The ionic conductances values presented in these three models are given in TABLE 8.7.

Articles	Ionic conductances values in $\frac{mS}{cm^2}$								
	g_{Na}	$g_{K,d}$	g_A	g_T	g_L	g_H	$g_{K,Ca}$	g_{leak}	g_N
[Wang and Buzsáki (1996)]	35	9	-	-	-	-	-	0.1	-
[Santhakumar et al. (2005)]	120	13	0.15	-	5	-	0.002	0.004	0.8

Table 8.7 – Ionic conductance values for the CA3 interneuron in the model of [Wang and Buzsáki (1996)] and [Santhakumar et al. (2005)]. The eight first conductances are the ones applied in the *generic model*

Synaptic receptors

The synaptic receptors present in CA3 interneurons are $AMPA$ and $GABAa$ [Stanley et al. (2013) (table 3)].

Firing mode

[Gulyás et al. (2010)] and [Wang and Buzsáki (1996)] also indicate a tonic firing frequency range from 0-400Hz increasing with the applied current.

8.4 CA1

8.4.1 Excitatory cell

The CA1 region of the hippocampus is composed of pyramidal cells [Cutsuridis et al. (2019)].

Ionic currents

The goal of [Pongracz et al. (1992)] article is to explore the interplay between $NMDA$ receptors mediated conductances and dendritic conductances by leading simulations of a multicompartmental CA1 pyramidal neuron model with a heterogeneous distribution of various ionic conductances. The model dynamics of their CA1 neuron model is described by a modified Hodgkin and Huxley equation and involve the subsequent currents: I_{Na}, $I_{K,d}$, $I_{K,Ca}$, I_C and $I_K(C)$. which corresponding ionic conductances for the soma are given in TABLE 8.8.

[Traub et al. (1991)] also establish a conductance-based model of a 19-compartment neuron involving the currents: I_A, $I_{K,Ca}$, I_{Na}, $I_{K,d}$, $I_{K(C)}$, I_{Ca} and I_{leak} which conductance values are provided in the TABLE 8.8.

[Bianchi et al. (2012)] presents a rigorous morphological reconstructed model of a CA1 neuron and reduces this model to a single compartmental neuron model. The objective is to compare both models to examine which ionic conductance values and properties are needed to replicate the experimental results. The soma conductance values are considered here as the reduction to a single compartment model is performed by suppressing all the other compartments of the morphological model in the article. They also the somatic conductances to fit qualitatively the morphological model. The currents in the soma are: I_{Na}, $I_{K,d}$, I_L, I_T, I_R, I_M, I_{leak} and a I_mAHP. The conductance values are found in the TABLE 8.8.

Articles	Ionic conductances values $\frac{mS}{cm^2}$												
	g_{Na}	$g_{K,d}$	g_A	g_T	g_L	g_H	$g_{K,Ca}$	g_{leak}	g_{Ca}	g_C	g_M	g_mAHP	g_R
[Pongracz et al. (1992)]	50	50	-	-	-	-	1	-	0.2	1	-	-	-
[Traub et al. (1991)]	30	25	5	-	-	-	0.8	0.1	4	10	-	-	-
[Bianchi et al. (2012)]	22	5	-	-	0.1	-	-	✓	-	-	0.9	1	0.05

Table 8.8 – Ionic conductances values for the CA1 pyramidal cells in the models of [Pongracz et al. (1992), Traub et al. (1991), Bianchi et al. (2012)]. ✓indicates the presence of the conductance in the model without mentioning any value. The eight first ionic conductances are the one applied in the *generic model*

Synaptic receptors

[Pongracz et al. (1992)] indicate that the synaptic receptors present in the model are $AMPA$, $NMDA$, $GABAa$ and $GABAb$ and give values for the corresponding conductances in the APPENDIX C.

Firing mode

[Jarsky et al. (2008)] demonstrate using patch-clamp recordings that there are 16 % of CA1 pyramidal neurons that show intrinsic bursting activity that may be generated by the presence of high-threshold calcium currents [Jung et al. (2001), Metz et al. (2005)] which channels activate at much more depolarized voltages than T-type channels. It appears that there is a gradient of bursting neurons which is higher in distal regions. It is assumed in this thesis that CA1 pyramidal cells display an exogeneous bursting activity. Staff also states that the discharge mode of CA1 and subicular neurons are different. A CA1 neuron discharge in tonic mode in response to an applied somatic current while the subicular neurons generate bursts of action potentials. [Golding et al. (2001)] lead intracellular recording to investigate the course of action potential in CA1 pyramidal apical dendrites. When injecting a depolarizing current, the pyramidal cell discharge in tonic mode of 10-20 Hz. This frequency range is also corroborated by [Scorza et al. (2011)] and [Milior et al. (2016)].

8.4.2 Interneuron

Ionic currents

[Shuman et al. (2020)] suggest that epilepsy may kill interneurons and therefore alter the synchrony of neuronal circuit that these neurons provide. They study the role of interneurons death in spatial

coding using a CA1 network model including different types of interneurons which ionic currents and corresponding conductances values are given in TABLE 8.9.

Articles	Ionic conductances values in $\frac{mS}{cm^2}$								
	g_{Na}	$g_{K,d}$	g_A	g_T	g_L	g_H	$g_{K,Ca}$	g_{leak}	g_N
[Shuman et al. (2020)]	✓	✓	✓	-	✓	-	✓	✓	✓
[Santhakumar et al. (2005)]	120	13	0.15	-	5	-	0.002	0.004	0.8

Table 8.9 – Ionic conductances values for the CA1 interneuron in the model of [Shuman et al. (2020), Santhakumar et al. (2005)]. ✓indicates the presence of the conductance in the model without mentioning any value. The eight first ionic conductances are the ones applied in the *generic model*

Synaptic receptors

The synaptic receptors used in the model of [Shuman et al. (2020)] for basket cells are the $AMPA$ and $GABAa$ receptors.

Firing mode

The firing frequency range of basket cells is from 25-300Hz [Buhl et al. (1994)]. They want to compare the physiological properties of two types of gabaergic cells in the CA1 region including the basket cells by leading intracellular recordings.

8.5 Subiculum

8.5.1 Excitatory cell

The main cell layer of the subiculum contains pyramidal neurons [O'Mara (2005)].

Ionic currents

The model of [Buchin et al. (2016)] explores the cellular mechanism behind the generation of epileptic activities. According to them, it is due to a change in chloride homeostasis and changes in potassium concentrations resulting from an absence of the KCC2 cotransporter (potassium chloride cotransporter 2) to regulate chlorine and potassium equilibrium. They studied an alteration of this cotransporter in a model of subicular pyramidal cells and interneurons. They modeled the regular spiking pyramidal cells and fast-spiking interneurons as two-compartment cells (somatic and dendritic).

[Joksimovic et al. (2017)] highlights the presence of T-type calcium channel and is further explained in this SUBSECTION.

[Buchin et al. (2016)] based his model on the model of [Krishnan and Bazhenov (2011)] which provide conductance values that are missing. [Krishnan and Bazhenov (2011)] model has the purpose of understanding the ending of seizure established with a cortical network model. Ionic conductances values are given in TABLE 8.10.

Synaptic receptors

[Buchin et al. (2016)] provides the type of synaptic receptors between the pyramidal cells and the fast-spiking interneurons present in his model which are found in the following table:

Articles	Ionic conductances values in $\frac{mS}{cm^2}$									
	g_{Na}	$g_{K,d}$	g_A	g_T	g_L	g_H	$g_{K,Ca}$	g_{Naleak} g_{Clleak} g_{Kleak}	g_{NaP}	g_M
[Buchin et al. (2016)]	3450	200	-	-	✓	-	✓	✓ ✓ ✓	✓	✓
[Krishnan and Bazhenov (2011)]	3450	200	-	-	0.0165	0.1	2.5	0.02 0.01 0.044	3.5	0.01
[Joksimovic et al. (2017)]				✓						

Table 8.10 – Ionic conductances values for the subicular pyramidal neurons in the model of [Buchin et al. (2016)] and [Krishnan and Bazhenov (2011)]. ✓indicates the presence of the conductance in the model that does not mention the value. The first eight conductances are the ones applied in the *generic model*

Pre cell	Post cell	
	PY	IN
PY	$AMPA$ $NMDA$	$AMPA$
IN	$GABAa$	$GABAa$

Table 8.11 – Synaptic conductances values used in the model of [Buchin et al. (2016)]

Firing mode

[Jarsky et al. (2008)] states that there are 68% of the subicular neurons that burst intrinsically. This property is also highlighted by [Joksimovic et al. (2017)]. Indeed, the goal of his research on rats is to investigate the involvement of T-type calcium channels in the intrinsic bursting of subicular neurons through a pharmacological approach. By blocking T-type calcium channels, subicular neurons switch from a bursting mode to a tonic firing mode. The tonic firing trace has a frequency of approximately 15Hz. [Taube (1993)] highlights from intracellular recordings in the rat that there is two categories of subicular neurons, the regular spiking and the intrinsically bursting neurons. Out of 91 neurons, 28 are regular spiking and 63 are characterized by an endogenous bursting activity. [Taube (1993)] mentions that the burst consist in 2-5 action potentials. [Joksimovic et al. (2017)] says that a burst consists of two action potentials at a high frequency of hundreds of Hz.

8.5.2 Interneuron

The interneurons are fast-spiking interneurons [O'Mara (2005)] and consist in less than 20% of the subicular neurons [Joksimovic et al. (2017)].

Ionic currents

The model of [Buchin et al. (2016)] and [Krishnan and Bazhenov (2011)] both provide the voltage-gated sodium current and the delayed rectifier potassium currents as being involved in the fast-spiking interneuron dynamic which ionic conductances values are given in TABLE 8.12. [Joksimovic et al. (2017)] also mentions the presence of a T-type channel in the interneurons of the subiculum.

Synaptic receptors

The synaptic receptors are found in TABLE 8.11.

Articles	Ionic conductances values in $\frac{mS}{cm^2}$							
	g_{Na}	$g_{K,d}$	g_A	g_T	g_L	g_H	$g_{K,Ca}$	g_{Naleak} g_{Clleak} g_{Kleak}
[Krishnan and Bazhenov (2011)]	3800	200	-	-	-	-	-	0.02 0.01 0.035
[Joksimovic et al. (2017)]	-	-	-	✓	-	-	-	-

Table 8.12 – Ionic conductances values used in the model of Krishnan and Bazhenov (2011). The first ionic conductances are the ones applied in the *generic model*

Firing mode

[Joksimovic et al. (2017)] also study the presence of T-type calcium channels in gabaergic interneurons of the subiculum. They established four categories of interneurons and almost half of the tested interneurons studies in six rats are fast-spiking with rebound firing and that some of them present spiking induced by hyperpolarization which is due to T-type calcium current. Interneuron display some T-type current which amplitude is smaller than for the pyramidal neurons [Joksimovic et al. (2017) (figure 4)]. The fast-spiking activity has a frequency of approximately 90Hz.

Chapter 9

Building of the model architecture based on the literature

A simplified model architecture is built in the context of this thesis to represent the connections between the three brain regions involved in memory consolidation *i.e.* the thalamus, the neocortex and the hippocampus. The model also aims to represent the synchronization of the cellular activity in these regions during SWS. In this CHAPTER, the establishment of the model architecture is explained based on evidence found in the literature underlined in this CHAPTER and provided the synaptic receptors mentioned in CHAPTERS 7 and 8. The role of the different hippocampal regions in memory processing is also highlighted in this CHAPTER. The developed circuit is shown in FIGURES 9.1 and 9.2.

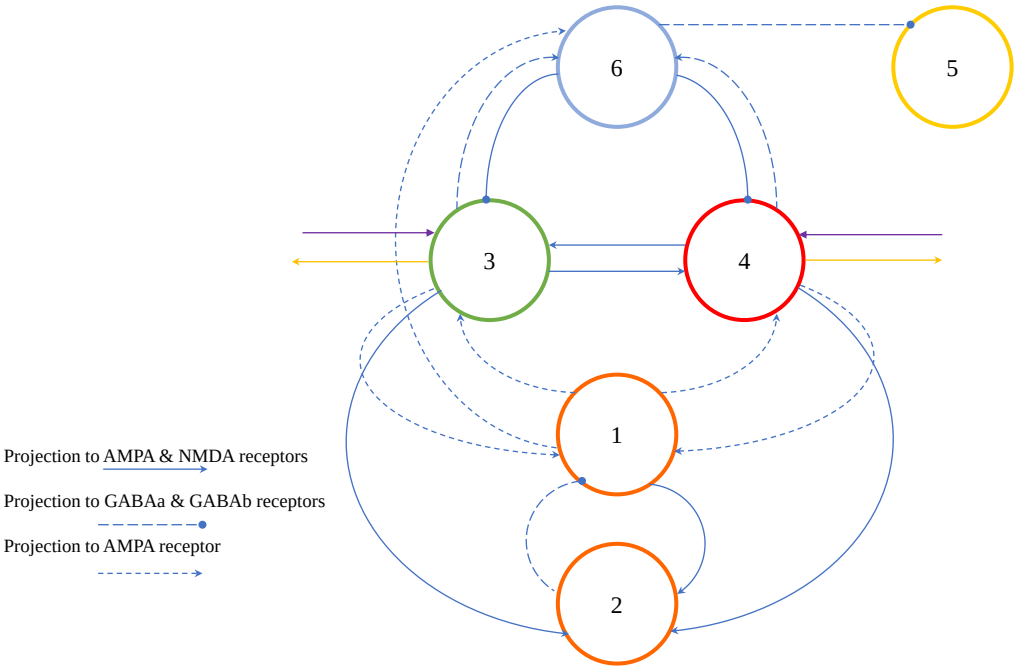

Figure 9.1 – Thalamocortical network. The network is composed of six cells from the thalamus and the neocortex. 1: TC cell (orange), 2: RE cell (orange), 3: neocortical pyramidal cell coding for the trees (green), 4: neocortical pyramidal cell coding for the tent (red), 5: neocortical pyramidal cell coding for the beach (yellow) and 6: parvalbumin positive fast-spiking interneuron (blue). The cells are interconnected via three different types of projections. Full line arrow: excitatory projection pointing to $AMPA$ and $NMDA$ receptors. Small dashed arrow: excitatory projection pointing to AMPA receptors. Dot arrowhead in big dashed line projects to $GABAa$ and $GABAb$ receptors. Yellow line indicate the projection of the neocortical pyramidal cell to the entorhinal cortex of the hippocampus, purple lines are projections from the entorhinal cortex layer V to the neocortical pyramidal cells which are not considered in the modeling

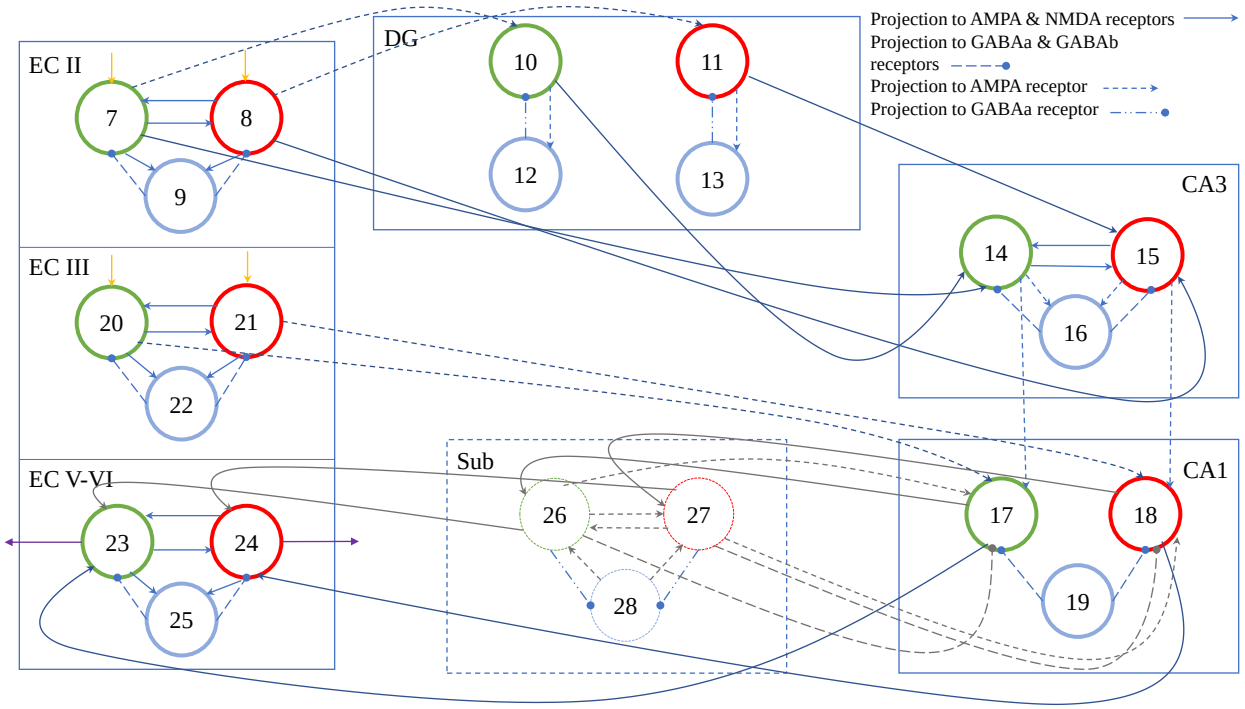

Figure 9.2 – Hippocampal network. The network is composed of 22 cells from the different regions of the hippocampus presented in each box. The subiculum is presented in a dashed box as it is not considered for the modeling. Green circles represent excitatory cells coding for the trees and red circles represent excitatory cells coding for the tent. Blue circles represent basket cells except the interneuron of the subiculum (28) which is just considered as being fast-spiking. Cells 7 and 8 are stellate cells of the EC layer II, cells 10 and 11 are granule cells of the dentate gyrus, cells 14 and 15 are pyramidal cells of the CA3 region, cells 17 and 18 are pyramidal cells of the CA1 region, cells 20 and 21 are pyramidal cells of the EC layer III, cells 23 and 24 are pyramidal cells of the EC layer V and cell 26 and 27 are pyramidal cells of the subiculum. The cells are interconnected via four different types of projections. Full line arrow in blue: excitatory projection pointing to AMPA and NMDA receptors. Small dashed arrow in blue: excitatory projection pointing to AMPA receptors. Dot arrow head in big dashed line in blue projects to GABAa and GABAb receptors and twodashed dot arrow head projects to GABAa repeptor. Grey lines correspond to connections with the subiculum which is not considered in the modeling. Yellow arrows are projection from the neocortical pyramidal cells (considered in the modeling), purple lines are projections from the entorhinal cortex layer V to the neocortical pyramidal cells which are not considered in the modeling

Cell type	number	color	abbreviation
Thalamocortical cell	1	orange	TC1
Reticular cell	2	orange	RE2
Pyramidal cell	3	green	C3
Pyramidal cell	4	red	C4
Pyramidal cell	5	yellow	C5
Parvalbumin interneuron	6	blue	PV7
EC layer II stellate cell	7	green	EC7
EC layer II stellate cell	8	red	EC8
EC layer II interneuron	9	blue	IN9
DG granule cell	10	green	DG10
DG granule cell	11	red	DG11
DG basket cell	12	blue	IN12
DG basket cell	13	blue	IN13
CA3 pyramidal cell	14	green	CA3-14
CA3 pyramidal cell	15	red	CA3-15
CA3 basket cell	16	blue	IN16
CA1 pyramidal cell	17	green	CA1-17
CA1 pyramidal cell	18	red	CA1-18
CA1 basket cell	19	blue	IN19
EC layer III pyramidal cell	20	green	EC20
EC layer III pyramidal cell	21	red	EC21
EC layer III interneuron	22	blue	IN22
EC layer V pyramidal cell	23	green	EC23
EC layer V pyramidal cell	24	red	EC24
EC layer V interneuron	25	blue	IN25
Subicular pyramidal cell	26	green	SUB26
Subicular pyramidal cell	27	red	SUB27
Subicular interneuron	28	blue	IN28

Table 9.1 – Recapitulative table representing the 28 cell types present in the circuits in FIGURES 9.1 and 9.2 with their corresponding numbers, colours and abbreviations found on the axis of the traces displayed in PART III

For the simplification of the model and the ease of the visualization, the thalamic region reveals two neurons (TC and RE), neocortical and hippocampal regions are composed of two excitatory neurons, one coding for the tent symbolized by the colour red and one coding for the trees symbolized by the colour green and one interneuron. It appears that there are far more excitatory neurons than inhibitory neurons in each region as synthesized by [Aussel et al. (2018)] for the hippocampal regions and as modeled by [Wei et al. (2016), Bazhenov et al. (2002), Hill and Tononi (2005), Olcese et al. (2010)]. The dentate gyrus is also composed of two excitatory neurons but also two interneurons as hypothesized in this model. This hypothesis is explained in SECTION 9.2.2. The principal types of neurons per region are considered and investigated in CHAPTERS 7 and 8. The subsequent table (TABLE 9.1) provides the abbreviations of the cell type (also present on the axis of the traces in PART III), the corresponding number of the cell in the circuit and the associated colour as represented in the above circuit and in the traces in PART III. The interconnections in the above architecture are found based on indications from the literature investigated within and between:

- the thalamocortical model
- the entorhinal cortex
- the DG-CA3 network
- the CA3-CA1 network
- the subiculum

9.1 Building of the thalamocortical model

The thalamocortical loop represented in FIGURE 9.1 is the following:

- As previously stated in SUBSECTION3.1.2, the LGN neuron receives external sensory inputs (green and red input). The stimulated LGN neuron projects to PGN neuron through $AMPA$ connections as seen in [Wei et al. (2016), Bazhenov et al. (2002)] and [Hill and Tononi (2005)] and also through NMDA connections [Fernandez and Lüthi (2020)]. It also projects to the neocortical pyramidal cells to transmit the external information received. One pyramidal neuron is coding for the tent (red) and the other is coding for the trees (green) in the presented model. A third pyramidal neuron coding for the colour yellow is not innervated by the LGN cell. This colour might symbolize the beach for example, which is not a feature that is part of the memory of camping that is encoded and then consolidated in this context. LGN cell connects to these neurons through $AMPA$ receptors as established in the model of [Bazhenov et al. (2002), Wei et al. (2016)] and [Hill and Tononi (2005)].

- The PGN neuron in turn inhibits the LGN cell through $GABAa$ and $GABAb$ receptors [Fernandez and Lüthi (2020), Hill and Tononi (2005), Wei et al. (2016), Bazhenov et al. (2002), Drion et al. (2018), Destexhe et al. (1996)].

- The neocortical pyramidal cells innervate each other through $AMPA$ and $NMDA$ receptors as in the model of [Bazhenov et al. (2002)] and [Hill and Tononi (2005)]. Despite excitating each other, they also excite the PV+ interneuron through $AMPA$ and $NMDA$ receptors a modeled by [Bazhenov et al. (2002)] and [Wei et al. (2016)]. The interneuron is also excited through $AMPA$ receptors by the LGN [Bazhenov et al. (2002), Wei et al. (2016), Fernandez and Lüthi (2020)].

- The interneuron in turn sends its inhibitory connections to the three pyramidal cells interacting through $GABAa$ [Bazhenov et al. (2002), Wei et al. (2016), Hill and Tononi (2005)] and $GABAb$ receptors [Hill and Tononi (2005)]. The pyramidal neuron coding for yellow only receives inhibition and is therefore not part of the encoded information.

- The excited pyramidal cells in turn feed back to the thalamic cells *i.e.* the LGN and PGN [Bazhenov et al. (2002), McCormick et al. (2015), Fernandez and Lüthi (2020), Hill and Tononi (2005)] through $AMPA$ [Bazhenov et al. (2002), Wei et al. (2016), Hill and Tononi (2005)] and through $AMPA$ and $NMDA$ receptors respectively [Fernandez and Lüthi (2020), Astori et al. (2013)].

9.2 Building of the hippocampal formation model

The activity of the two excited neocortical neurons reaches the hippocampal formation passing by the entorhinal cortex (EC) then looping in the hippocampal trisynaptic circuit then going out through the entorhinal cortex. The different regions have different purposes in memory processing and are judiciously connected to one another to achieve their function in this task as seen in FIGURE 9.2.

9.2.1 The entorhinal cortex

The entorhinal cortex receives two-thirds of its input from the perirhinal and parahippocampal cortices. These cortices are not included in the model for the sake of simplicity as they are not part of the "hippocampal formation". The entorhinal cortex acts as a relay of the information from the neocortex to the hippocampus but receives projection from other neocortical areas. It is an associative stage of the information before it enters the hippocampus, the associative function inducing a more gist-like representation of the event. Indeed, the EC possesses inherent associative connections intensifying the level of integration of the information.

The intrinsic associational coupling between EC neurons stems from layer II, V and VI. Neurons from each layer connect to neurons of the same layer (particularly in the case of superficial layer cells) and neurons of other layers [Lavenex and Amaral (2000)]. [Chrobak et al. (2000)] also mentions that deep layers project onto the superficial layers. For a simplistic purpose, only the associational connections between neurons from the same layer are considered in this model. Axons from neurons in layer II terminates in the dentate gyrus and the CA3 region while axons from neurons in layer III terminates in the CA1 region and the subiculum [Lavenex and Amaral (2000)]. The superficial layers constitute the input stream of the EC. The deep layer forms the output stream of the EC and receives input from the subiculum and the CA1 region as mentioned in SUBSECTION 3.3.1.

9.2.2 The DG-CA3 connection

The dentate gyrus receives inputs via the perforant path from EC layer II stellate cells coding for the trees and for the tent. The dentate gyrus is believed to be principally responsible for *pattern separation* in the hippocampus [Myers and Scharfman (2011)] as illustrated by an example in FIGURE 9.3. The CA3 region, due to its recurrent collaterals, is the main actor for auto-association in the hippocampus. This auto-associative network can store information patterns thanks to the synaptic plasticity between its cells. The number of different patterns that the CA3 network can store depends on the ability of the DG to perform pattern separation. The perforant path (containing the representation to be stored) innervates the DG and the CA3 network. The DG due to its strong connections with CA3 cells, induces robust EPSPs in those cells which allow an enhancement of the synaptic strength between those cells when receiving the pattern to be stored by the EC layer II. Mossy fibres are known as the teaching inputs of CA3 PY cells. The DG modifies overlapping input representation from the EC into nonoverlapping output representations which are essential for discerning resembling experiences and to store an experience in the CA3 network as a unique representation with almost no interference with other mnemonic representations which decrease the recall mistakes [Chen and Knierim (2018)]. The DG is able to perform pattern separation as it projects singular and sparse mossy fibres to CA3 cells. The sparsity comes from the smaller number of stellate cells of EC layer II that terminates in the larger portion of granules cells (in the rat there are 200.000 stellate cells that project to 1.000.000 granule cells) resulting in sparsely firing granule cells that have almost no overlap with each other. Moreover, the dentate gyrus is greatly inhibited. When granule cells are excited, they excite interneurons that inhibit in turn the granule cells and only the granule cells that are not inhibited are involved in the

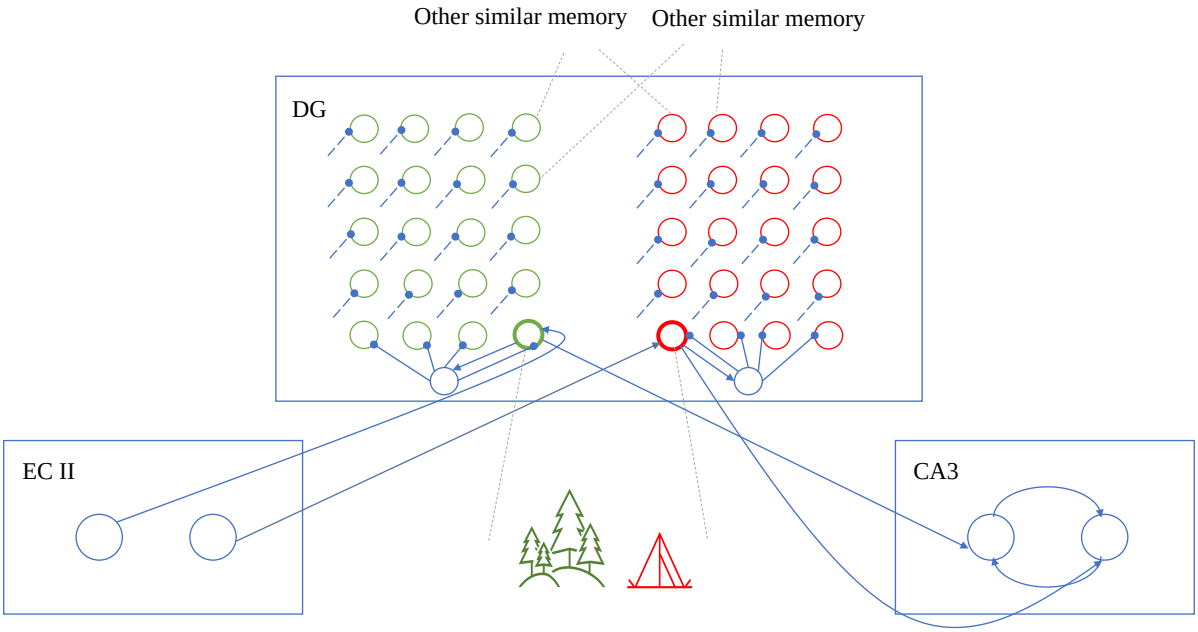

Figure 9.3 – *Pattern separation*: A sparse number of granule cells corresponding to the cells coding for the camping event spike. High inhibition in the dentate gyrus enables only the most excited cells to spike (bold font) and transmit the mnemonic representation to the recurrent collaterals of the CA3 region which store the representation. Other granule cells coding for another similar event for example another camping summer camp in a red tent and the forest do not spike as they are highly inhibited. One interneuron (blue) inhibits the other granule cells coding for the red tent and one interneuron inhibits the granule cells coding for the trees. The results is that a unique episodic memory is stored in the CA3 region. When the individual sees his red tent again, he remembers the particular camping event thanks to the dentate gyrus which enables pattern separation. Dashed dot arrows head represent the inhibition from the interneuron.

synaptic reinforcement of CA3 cells. Furthermore, the DG is also important for pattern completion *i.e.* operation of restoring a previously stored pattern completely from a portion of this pattern presented afterwards to the individual which occurs as a result of pattern separation as the winning cells that experienced synaptic reinforcement are more likely to be activated later by a portion of inputs of the same representation.

It is assumed in this thesis that the two excitatory granules cells represented in FIGURE 9.2 are the two "winning" cells of FIGURE 9.3 (in bold) and that one interneuron inhibits the cells coding for tent (red) and the other inhibits the cell coding for the trees (green) to corroborate the example of pattern separation in FIGURE 9.3. The excitatory cells are symmetrically connected as is explained in PART III. As the granule cells possess the same ionic and synaptic conductances values and receive the same inputs due to the symmetry in their connections, the two interneurons could be regrouped as one interneuron by dividing the excitatory synaptic connexion from the two granule cell by two.

An additional area that is not represented in the context of this thesis and which is sometimes present in biophysical and large-scale models of the dentate gyrus is the hilar region. Until 2009, there was no obvious relationship between pattern separation and the function of the hilar region. To keep the model simple, the hilar region is not represented here as is also the case in other simplified models. [Myers and Scharfman (2009), Myers and Scharfman (2011), Aimone et al. (2011)].

9.2.3 CA3-CA1 network

What distinguishes the CA1 network and the CA3 network is the nature of their recurrent connections. Indeed, as previously mentioned, the CA3 region is identified by a recurrent excitatory network and no

inhibition among the interneurons. Conversely, the CA1 network is characterized by heavy inhibitory connections with no excitation among the pyramidal cells. This lacking of associational connections in these regions distinguishes it from other parts of the hippocampal formation. Through Schaffer collaterals, CA3 pyramidal neurons innervate CA1 pyramidal cells and interneurons [Lavenex and Amaral (2000), Taxidis et al. (2012), Taxidis et al. (2013)]. During sleep, the connexions in the CA3 region involved in memory encoding are reactivated. Recurrent networks allow the needed excitation to sustain synaptic persistent firing [Giovannini (2017)] thus revealing the benefit of the CA3 region for consolidation [Klinzing et al. (2019a)]. Sharp waves ripples (SWR's) occur concurrently with this reactivation. Indeed the recurrent CA3 connections induce population bursts transmitted through Schaffer collaterals to the CA1 regions which glutamatergic neurons and gabaergic interneurons are depolarized, the latter bringing fasts rhythmic oscillations to the network and giving rise to fast ripple activity [Csicsvari et al. (2000)]. [Hunsaker et al. (2008)] realizes experiments that suggested that CA3 and CA1 play a role in episodic memory, CA1 being crucial for joining the spatial and temporal features of the representation and CA3 solely plays a role in the spatial processing being less essential for the processing than CA1.

9.2.4 The subiculum

[O'Mara et al. (2000)] suggests that the subiculum has a unique pivotal role in regulating the interaction between the hippocampal regions and cortical regions due to its connections to the entorhinal cortex and the CA1 region. It acts as an output synaptic relay to the neocortex. It translates the information held in the short-term store hippocampus to a more long-lasting type of memory in the neocortex, thus being involved in the memory consolidation process during sleep. Indeed, [O'Mara (2006)] demonstrates that the subicular projections experience modification of synaptic strength and that CA1-subiculum-entorhinal cortex projections display LTP triggered very quickly and persist for at least 3 hours. This could be due to its distinct functional and electrophysiological features from the rest of the hippocampal formation [Staff et al. (2000)]. There are two categories of pyramidal subicular neurons: neurons exhibiting an endogenous type of bursting activity and the other being regular spiking. There is a majority of intrinsically bursting neurons [O'Mara et al. (2000), Taube (1993)] as seen in SUBSUBSECTION 5.3.2. T-type calcium channels are involved in the bursting activity of subicular pyramidal and interneurons enhancing the excitability and synaptic plasticity of these neurons as was demonstrated by [Joksimovic et al. (2017)]. Accordingly, the accuracy of synaptic transmission is intensified by passing through the subiculum and thereby it has a beneficial impact on memory processing [Joksimovic et al. (2017)]. Despite the fact that the subiculum has amplifying input properties thanks to its bursting activity, it is lightly inhibited [O'Mara (2006)].

Additionally, the bursting capacity of subicular neurons confers a major role of the subiculum in epilepsy. In fact, epileptiform activity initiated in the superficial layers of the entorhinal cortex can be amplified by the subiculum and transmitted to the cortex [O'Mara et al. (2001)]. The subiculum is significantly involved in the generation of epilepsy [Stafstrom (2005), Knopp et al. (2005)]. This could be the reason why only models are concerned with epilepsy as the one presented in SECTION 9.2.4. Moreover, it is important to notify that the subicular complex is underinvestigated compared to the rest of the hippocampal formation, consequently, its role and mechanism underlying memory processing are not well understood and are still under investigations [O'Mara et al. (2001)]. This is why it is not considered as part of the circuit for the modeling of the network (represented in a dashed box and with grey connections in FIGURE 9.2).

[Xu et al. (2016)] encourages the evidence of strong subicular back projection to CA1 both inhibitory and excitatory which is sustained by various electrophysiological studies. They make suppositions on the role of such a back projection but it is still understudies. They suggest that the back projection may be involved in synchronous rhythms. [Staff et al. (2000)] indicates that bursting back propagation in the CA1 region may influence synaptic integration. [Sun et al. (2019)] highlights the fact that CA1-projecting subicular neurons (a category of subicular neurons constituting a passage between the visual cortex and the CA1 region) receive inputs from inhibitory subicular neurons in addition to excitatory CA1 inputs. This inhibitory feedback serves in the control of object location data treatment.

Summary

STATE-OF-ART					
Region	Mnemonic role	Cell type	Generic Currents	Synaptic receptors	Firing mode Wake/*sleep* *(burst = B)*
Thalamus	Wake: relay Switch wakefulness/sleep Sleep: generator of sleep rhythm	Reticular cell	Na, Kd, H, T, Kca, leak	AMPA NMDA	Tonic *Endogenous B*
		Thalamocortical cell	Na, Kd, H, T, Kca, leak	AMPA GABAa,b	Tonic *Endogenous B*
Neocortex	Information processing Long-term memory storage	Pyramidal cell	Na, Kd, KCa, leak	AMPA NMDA GABAa,b	Tonic *Exogenous B*
		Parvalbmin positive interneuron	Na, Kd, KCa, leak	AMPA NMDA	Tonic *Tonic*
Entorhinal cortex layer II	Input stream to the hippocampus Associative function	Stellate cell	Na, Kd, H, leak	AMPA NMDA GABAa,b	Tonic *Exogenous B*
		Parvalbmin positive interneuron	Na, Kd, KCa, leak	AMPA NMDA	Tonic *Tonic*
Entorhinal cortex layer III	Input stream to the hippocampus Associative function	Pyramidal cell	Na, Kd, Kca, leak	AMPA NMDA GABAa,b	Tonic *Exogenous B*
		Parvalbmin positive interneuron	Na, Kd, Kca, leak	AMPA NMDA	Tonic *Tonic*
Entorhinal cortex layer V	Output stream from the hippocampus Associative function	Pyramidal cell	Na, Kd, Kca, leak	AMPA NMDA GABAa,b	Tonic *Exogenous B*
		Parvalbmin positive interneuron	Na, Kd, Kca, leak	AMPA NMDA	Tonic *Tonic*
Dentate gyrus	Pattern separation = distinguishing similar memories	Granule cell	Na, Kd, A, T, L, KCa, leak	AMPA GABAa	Tonic *Exogenous B*
		Basket cell	Na, Kd, A, L, Kca, leak	AMPA	Tonic *Tonic*
CA3	Encodes the representation Reactivation Spatial processing	Pyramidal cell	Na, Kd, A, L, Kca, leak	AMPA NMDA GABAa,b	Tonic *Exogenous B*
		Basket cell	Na, Kd, A, L, Kca, leak	AMPA	Tonic *Tonic*
CA1	Temporal and spatial processing	Pyramidal cell	Na, Kd, H, T, Kca leak	AMPA NMDA GABAa,b	Tonic *Exogenous B*
		Basket cell	Na, Kd, H, T, Kca, leak	AMPA	Tonic *Tonic*
Subiculum	Pivotal role Increase synaptic reinforcement	Pyramidal cell	Na, Kd, H, T, L Kca, leak	AMPA NMDA GABAa	Tonic *Endogenous B*
		Fast-spiking interneuron	Na, Kd, leak	AMPA	Tonic *Tonic*

Part III

Anatomical brain areas modeling

Chapter 10

Modeling

10.1 Procedure

The modeling realized in this thesis applies the equations developed in a *generic conductance-based model* found in the APPENDIX B. This model enables the adaptation of the conductances values resulting in a possibility to reproduce the distinct electrical activity of various neurons. This is very beneficial for the aim of this project as the goal is to reproduce particular discharge activity of specific neurons explicitly described in PART II and to obtain the desired pattern of activity consisting in the transfer of the representation during wakefulness and the transfer of the bursting rhythmicity during sleep. The order of magnitude of ionic conductances of the neurons of each region is also examined in PART II in order to respect their respective activity by conserving the order of magnitude of these ionic conductances. The procedure followed to obtain the complete circuit presented in FIGURES 9.1 and 9.2 to find the desired transfer of activity between the 25 cells during wakefulness and sleep consists of four steps as presented in FIGURE 10.1:

- **Step 1: Individual neuron simulations** The different neurons are simulated individually *i.e* disconnected from the circuit by tuning the ionic conductances found in CHAPTERS 7 and 8 while respecting the ratios between them and by adapting the intensity of the applied current to adjust their frequency. This way, the experimental cell behaviour is respected and modeled.
- **Step 2: Subnetwork simulations** The entire circuit in FIGURES 9.1 and 9.2 are separated in subnetworks *i.e.* the thalamocortical circuit (cells 1-6), the EC layer II-DG circuit (cells 7-13), the CA3-CA1 circuit (cells 14-19) and are simulated. There are three categories of cells displaying distinct pattern of activity during sleep which are encountered in the model (see FIGURE 10.2):
  - The excitatory cells manifesting an exogenous bursting activity (neocortical and hippocampal cells except for subicular cells as stated in SUBSUBSECTIONS 5.3.3, 5.3.4 and in SECTIONS 7.2, 8.1, 8.2, 8.3 and 8.4) are artificially stimulated with steps of currents mimicking the synaptic inputs from other connected cells.
  - The intrinsically bursting cells (thalamic and subicular cells as highlighted in SECTIONS 5.3.2, 9.2.4 and 7.1) are hyperpolarized by the cellular mechanism highlighted in SECTION 5.3.2.
  - Fast-spiking interneurons are under the influence of local synaptic inputs and only appear to display a tonic mode of discharge.

  The goal of dividing the circuit into subcircuits is to tune the synaptic conductances values in order to obtain the transmission of the desired pattern of activity. The tuning of the synaptic conductances (which describe the communication between two cells) consists in finding a compromise between the values of inhibitory and excitatory synaptic conductances of a cell.
- **Step 3: Complete network** The subnetworks are connected together to obtain the fully connected model seen in FIGURES 9.1 and 9.2. In most cases, the ionic conductances values, synaptic values and the applied currents that were tuned in the preceding steps are reused.

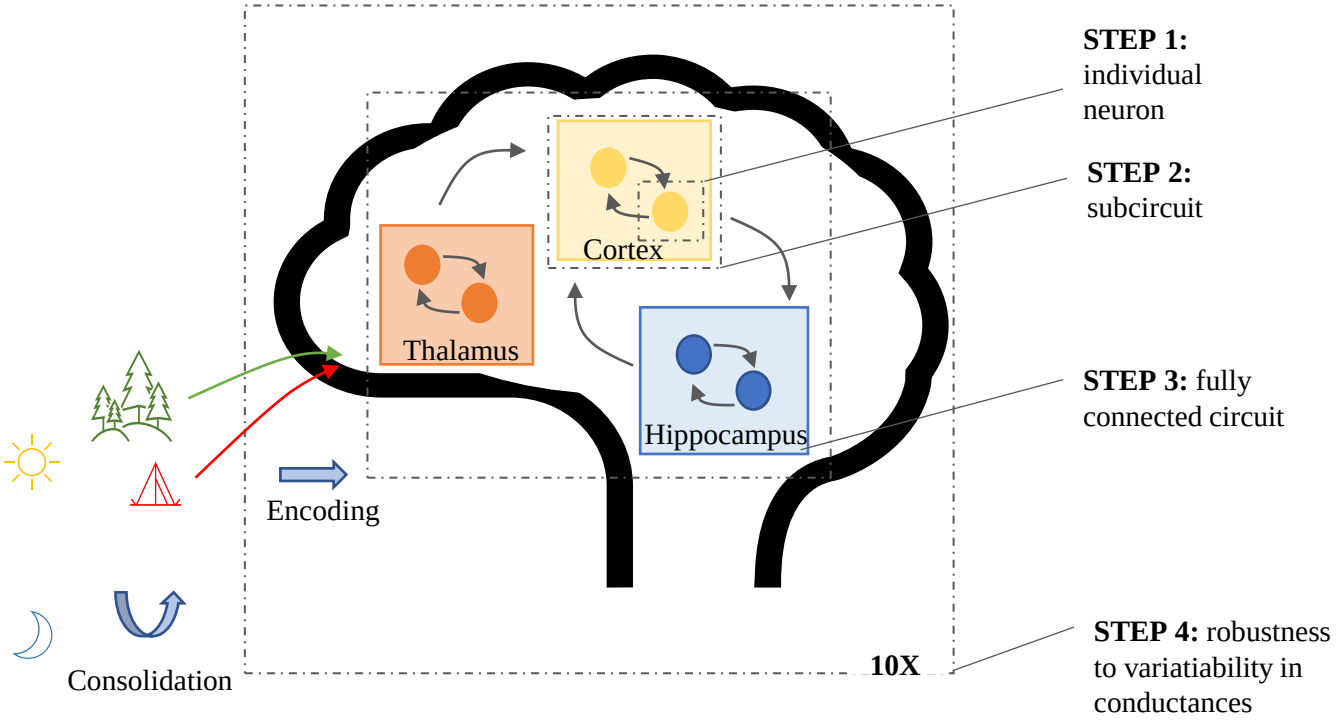

Figure 10.1 – Summary of the modeling procedure. -Step 1 consists in the modeling of a single neuron, step 2 is devoted to the modeling of subnetworks of neurons, step 3 consists in the modeling of the fully connected circuit and step 4 consists in testing the robustness of the fully connected network for ten different circuits. During wakefulness (sun), the features of the representation (tent in red and trees in green) are encoded and prone to decay. During sleep (moon), no input enters the brain. The features preliminarly encoded are consolidated in the neocortex.

- **Step 4: Testing the robustness** The robustness of the model is tested and dephasing in the bursting activity is introduced.

In each of the subsequent temporal traces, the transition from wakefulness to sleep occurs at 2000 ms. The traces are displayed starting from 400 ms because of the presence of a transitory period at the beginning of the simulations. These are due to the set-up of the differential equations formatted by initial conditions. This is the case for all the subsequent traces. The same colour convention as in FIGURES 9.1 and 9.2 is followed. The traces presented were simulated based on the type of ionic currents, the order of magnitudes of the ionic conductances, the type of synaptic receptors involved and the firing rate depending on the state (sleep or awake) presented in PART II in order to obtain the desired model representing the switch between tonic and wakefulness (at 2000 ms) of the interconnected model (see FIGURES 9.1 and 9.2).

Step 1: Individual neuron simulations

Neurons of each region taken individually are implemented by respecting the ratio between ionic conductances provided in CHAPTERS 7 and 8 for each cell. Their applied currents are tuned as well to obtain the frequencies in tonic mode shown in TABLE 10.1 which matches the theoretical frequencies presented in CHAPTERS 7 and 8. The different frequencies of the 25 cells in tonic mode are extracted and the recordings are given in APPENDIX C.21. When disconnected from other cells, the neocortical and hippocampal neurons and fast-spiking interneurons are assumed to display a tonic firing activity. Indeed, it is hypothesized in this thesis that they exhibit exogenous bursting induced by synaptic connections as explained in SUBSUBSECTIONS 5.3.3, 5.3.4 and in SECTIONS 8.1, 8.2 and 8.4. This is not

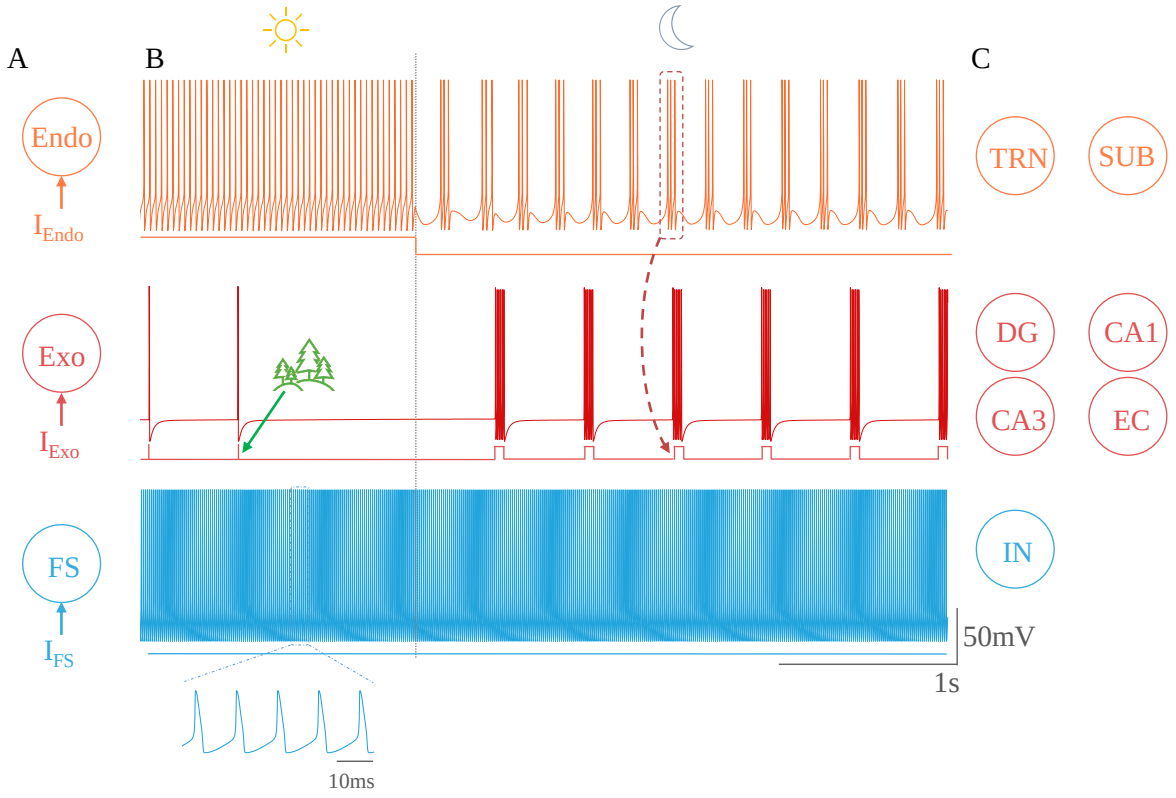

Figure 10.2 – Summary of the switch in firing activity depending on the type of cells A. Type of switch. B. Membrane voltage traces and the associated applied current. Sun (resp. moon) is associated to firing activity during wakefulness (resp. sleep). A-B (top) Endo. stands for endogenous bursting. The neuron switches from tonic to burst when the applied current is hyperpolarized. (middle) Exo stands for exogenous bursting. The neuron is silent during wakefulness except when it receives a current pulse to mimic the excitation from a visual input (represented by the vision of the trees). It generates one action potential. The bursting activity is caused by the influx of excitatory synaptic current due to the endogenous bursting (represented by the dashed red arrow). To mimic this input, the neuron receives a square pulse current. (bottom) FS stands for fast-spiking. The neuron is spiking regardless the brain state. The zoom shows the succession of action potentials. C. Type of neurons reproducing the given switch.

the case for the thalamic and subicular neurons as explained in SECTIONS 7.1 and 8.5 which exhibit endogenous bursts of 3 and 6 action potentials respectively which corroborate the values indicated in SECTIONS 7.1 and 8.5 (The traces of the endogenous burst are found in FIGURE 10.2 (orange trace) and in the APPENDIX C.21 respectively). The subiculum is modeled connected to the EC layer V but not in the fully connected model, thus information about its modeling and its tonic frequency are given in PROSPECTS 11.2. It is important to notice that in each region, the excitatory cells coding for the tent (red) and the trees (green) possess identical ionic conductance values, synaptic conductance values and applied currents, they are symmetrically connected. Therefore, only the frequencies of the disconnected cells coding for red are displayed as well as their traces in APPENDIX C.21.

Cells	Frequency in Hz	Cells	Frequency in Hz
TC1	70	CA3-15	40
RE2	50	IN16	90
C4	50	CA1-18	10
PV6	60	IN19	90
EC8	20	EC21	40
IN9	140	IN22	60
DG11	20	EC24	20
IN13	140	IN25	140

Table 10.1 – Frequencies given for each type of cells of the model (FIGURES 9.1 and 9.2) disconnected from the others. See APPENDIX C.21 for voltage traces.

Step 2: Subnetworks simulations

Once the tonic frequency of the different neurons is set and the ionic conductances tuned, there are connected together in the following subcircuits:

- **Subnetwork 1:** The thalamocortical network consisting of the cells 1 to 6 seen in FIGURE 9.1
- **Subnetwork 2:** The EC layer II connected to the dentate gyrus corresponding to the connexion of the cells 7 to 13 in FIGURE 9.2
- **Subnetwork 3:** The CA3-CA1 network including the cells 14 to 19 in FIGURE 9.2

The layer III and V of EC are not simulated in a subnetwork but are modeled individually (in **step 1**) and added in the fully connected model (in **step 3**).

Subnetwork 1: Thalamocortical network

The pattern of activity provided in FIGURE 10.3 translates the transmission of the stimulation across the thalamocortical network during wakefulness and sleep. During wakefulness, the goal is to see the communication between the cells coding for the tent and the cells coding for the trees. This way, a unique representation is encoded. During sleep, the aim is to reproduce the transmission of the bursting activity at the origin of the synchronized oscillations occurring during sleep. FIGURE 10.3 can be described in the following manner:

- From 400ms to 2000ms, the brain is in an activated state. Two spikes are artificially generated by injecting two current pulses in the TC neuron as explained in FIGURE 10.2. Indeed, the TC neuron is the relay of the information coming from the external world to the neocortex. The two spikes correspond to the visual stimulation of the TC neuron provoked by the sight of the red tent and the green trees. One stimulation occurs at 500ms (for the sight of the tent for example) and the second occurs at 1000ms (for the sight of the trees). The TC relay cell excites the RE neuron which in turn inhibit the TC cell. The activity is also relayed to the neocortical pyramidal neurons C3 and C4 coding for the trees (green) and for the tent (red). The communication between these cells is successfully reproduced as there are spiking simultaneously at 500 ms and 1000 ms. The inhibitory interneuron is also excited by the relay cell and by the excited pyramidal neurons and in turn, inhibits the pyramidal neurons that excited it. The inhibition from interneurons induces a silent mode in the excitatory cells to which they are connected. Only a sufficient excitation enables an action potential to occur and to be transmitted to other cells as the spikes implemented in the TC cell in 500 and 1000ms. Other pyramidal cells like C5, which are not excited by the TC cell, are also inhibited. C5 codes for a feature that does not take part in the event that is visualized, for example, the beach. The recurring excitation between C3 and C4 wins over the inhibition and the two action potentials in 500ms and 1000ms occur while C3 does not spike. The information is well transmitted to the neocortex.

- During sleep, a hyperpolarization current is applied at 2000ms to the RE cell that bursts intrinsically. The endogenous bursting of the RE cell induces the endogenous bursting of the TC excitatory cell which in turn burst intrinsically. The relay cell communicates its bursting activity to the neocortical pyramidal cells coding for the trees (green) and the tent (red). Indeed, those are the features that need to be consolidated in the neocortex during sleep. Therefore, C3 and C4 burst in an exogenous way as seen in FIGURE 10.2. The inhibitory interneuron is also excited by the neocortical cells and by the TC cell and presents a period of transient tonic activity due to the change of the input into a bursting activity.

The activity of the six thalamocortical cells presented here is obtained by tuning synaptic conductances values.

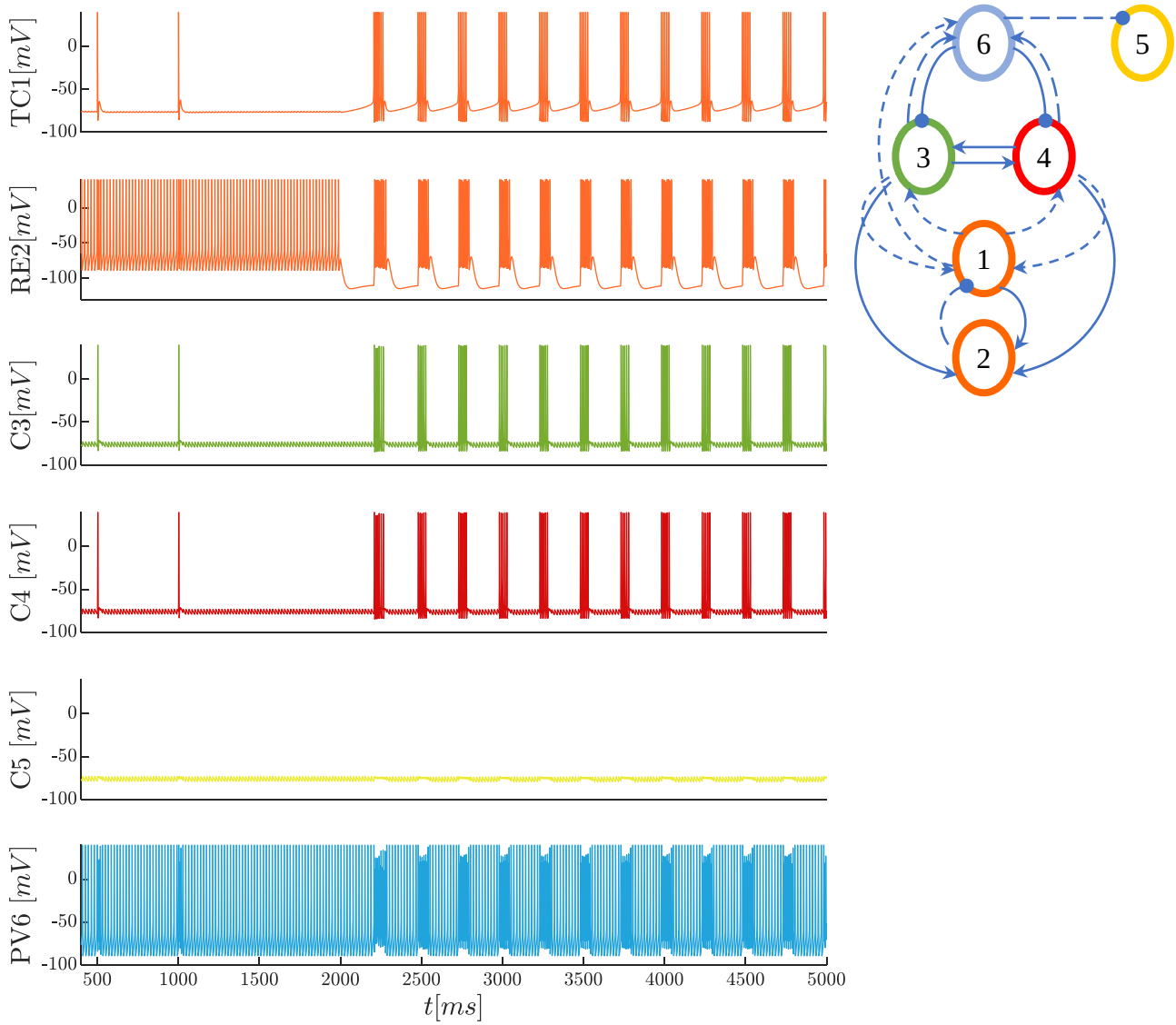

Figure 10.3 – **Subnetwork 1:** Thalamocortical network consisting of the thalamic cells: TC1 and TRN2 (orange), the neocortical pyramidal cells: C3 (green), C4 (red), C5 (yellow) and the parvalbumin cell, PV6 (blue). The membrane potentials of the cells evolve as a function of time displayed from 400ms to 5000ms with a switch to bursting mode at 2000ms. The circuit (top right) is the thalamocortical subnetwork.

Subnetwork 2: Entorhinal cortex layer II - Dentate gyrus network

In this SUBSECTION, the entorhinal cortex is disconnected from the neocortex. Artificial activity reproducing the spiking and the bursting activity are artificially implemented by current pulses to mimic the synaptic input of other cells as explained in SECTION 10.1 in order to visualize the transmission of the information from the EC layer II to the dentate gyrus and the transmission of the bursting activity. This enables to tune the synaptic conductances values suitable for the transfer of the activity.

- During wakefulness, the neocortex transmits the information to the stellate cells of EC layer II coding for the trees and the tent. Being disconnected from the neocortex, artificial spikes are generated in the stellate cells EC7 (at 500 ms) and EC8 (at 1000ms) coding for green and red respectively. Their communication is visible as both spikes are present in 500 ms and 1000 ms in the trace of the two cells. They excite the basket cell interneuron which in turn inhibits the exciting cell. The spikes are transmitted to the pyramidal cells of the dentate gyrus, DG10 and DG11. DG10 and DG11 excite the corresponding basket cell.
- During sleep (from 2000 ms), artificial bursts mimicking the ones coming from the neocortex are implemented as explained in FIGURE 10.2. Synaptic conductances values are tuned to obtain the transfer of the bursting activity to the other cell of the subcircuit.

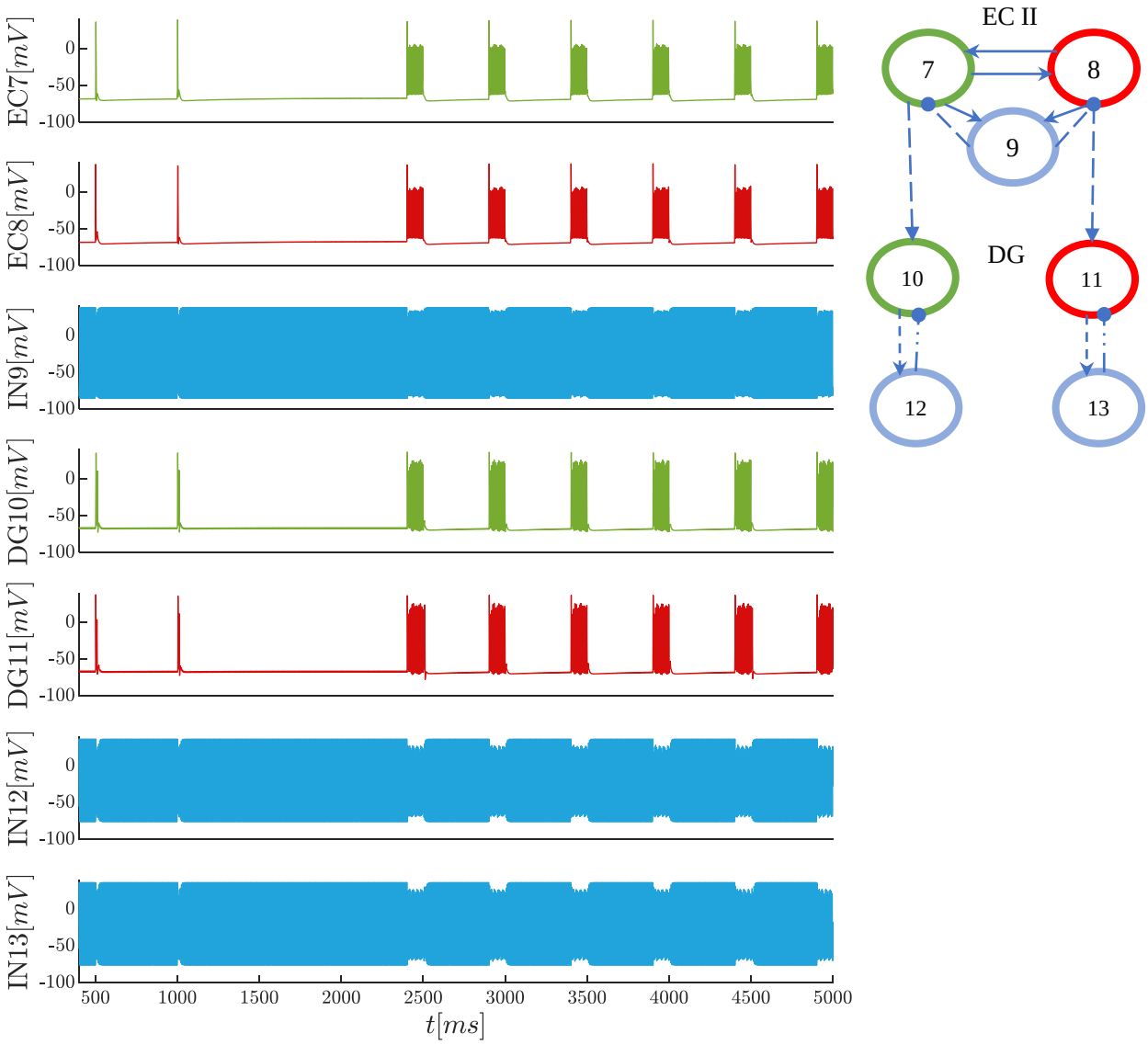

Figure 10.4 – **Subnetwork 2:** Entorhinal cortex layer II - Dentate gyrus network consisting of the stellate cells: EC7 (green) and EC8 (red), the basket cell (blue) IN9, the granule cells (green and red), DG10 and DG11 and their corresponding basket cells (blue) (IN12 and IN13). The membrane potentials of the cells evolve as a function of time displayed from 400ms to 5000ms with a switch to bursting mode at 2000ms. The circuit (top right) is the entorhinal cortex - dentate gyrus subnetwork.

Subnetwork 3: CA3-CA1 network

CA3 is disconnected from EC and DG. As in the previous SUBSECTION, artificial bursts and spikes are implemented in the pyramidal cells of the CA3 region to imitate the activity of external stimulation and to ensure the transmission of the activity in this subnetwork. The artificial activity is accurately transmitted to the CA1 region by tuning the ionic conductances and synaptic conductances values.

- During wakefulness (400ms-2000ms), one spike at 500ms is implemented in CA3-14 cell and is well transmitted to the CA3-15 cell and the CA1 excitatory cells. A spike at 1000 ms is implemented in CA3-15 cell and is also transmitted to the other excitatory cell of the subcircuits. The communication is therefore well established.
- The bursting activity during sleep implemented in the CA3-14 and CA3-15 cell is also passed to the other cells.

In the interneurons, the synaptic inputs from CA3-14 and CA3-15 cell are also visible.

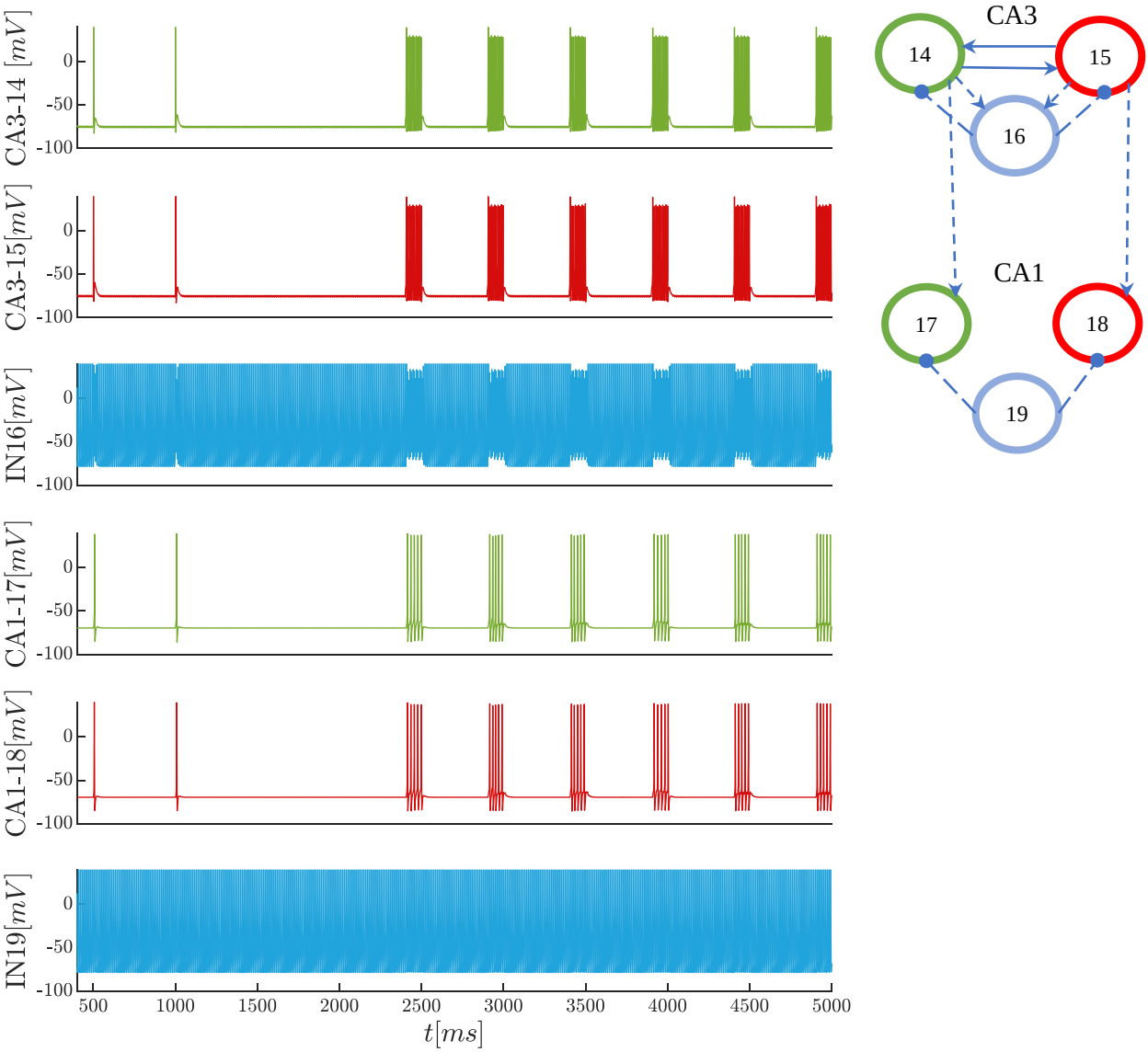

Figure 10.5 – CA3-CA1 network consisting of the CA3 pyramidal cells: CA3-14 (green) and CA3-15 (red), the basket cell IN16 (blue), CA1 pyramidal cell, CA1-17 and CA1-18 (green and red) and the corresponding basket cell (blue) IN19. The membrane potentials of the cells evolve as a function of time displayed from 400ms to 5000ms with a switch to bursting mode at 2000ms. The circuit (top right) is the CA3-CA1 subnetwork.

Step 3: Modeling of the complete circuit

The complete circuit modeling consists of adding the different subnetworks together and keeping the ionic conductances and synaptic conductances values as have been tuned for the subcircuits based on the ionic conductances values and the frequencies highlighted in CHAPTERS 7 and 8. The artificial bursting and spiking implemented in the stellate cells of the EC layer II and the pyramidal cells of the CA3 region are removed as they receive synaptic inputs when connected to ascending neurons in the fully connected circuit. The corresponding synaptic conductances have also to be tuned. The spikes transferred during active brain states are implemented in the thalamocortical cell TC1 as it has the role of relay of the information. The bursting activity transmitted to all the regions during sleep comes from the intrinsically bursting TRN cells. The pattern of activity is accurately and qualitatively transmitted from the thalamic cells to all the cells as can be seen in FIGURES 10.6, 10.7 and 10.8. Indeed, the transfer of the information is properly transmitted by TC during wakefulness. Indeed, both spikes are visible in 500 ms and 1000 ms in the excitatory cells (green and red) of each region. The rhythmic bursting activity during sleep is also suitably passed on from the RE cell.

In FIGURE 10.9, the net spikes during wakefulness are not clearly visible in the EC layer III and layer V cells. The entorhinal cortex layer III is directly stimulated by the pyramidal cells of the neocortex. The spikes are not appearing in 500 and 1000ms in the figure but EPSP's are visible at those times showing the communication between the neocortex and the EC layer III. A seen in the APPENDIX in FIGURE C.18, when a spike is implemented in 1500 ms in the EC3-20 and EC3-21 cells, a spike is transmitted and appears in the pyramidal cells of the entorhinal cortex layer III. This is due to the fact that even at a silent mode occurring during wakefulness, the voltage is not completely static. Indeed, the inhibition from the interneuron cells (IN9 for EC layer III and IN25 for EC layer V) is dynamic and induces small IPSP wavelets. Thus, when an artificial current is injected at the peak of a wavelet, an action potential might occur while at other timings, only EPSP is visible because the voltage is not sufficient to reach the action potential threshold. For those two regions, the value of the applied current had to be adapted to obtain the desired pattern of activity. The bursting activity is amplified as well as the transitory period as the EC layer V is the last stage of the loop. The EC layer III and V are not modeled in any of the previous subcircuits and the currents have to be modified from the ones that are used to model their frequency.

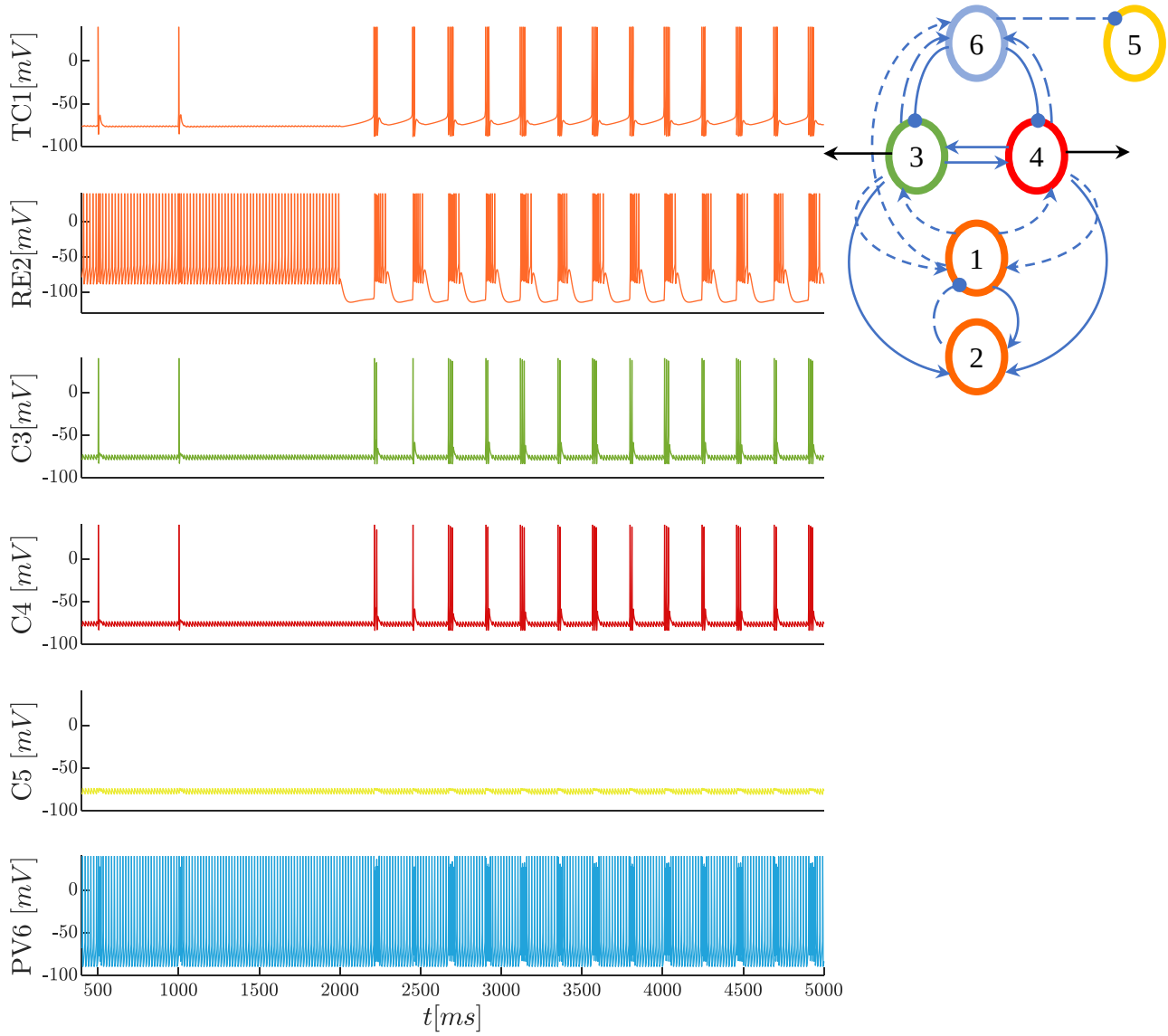

Figure 10.6 – **Fully connected circuit** consisting in the TC and RE cells of the thalamus (orange) the neocortical pyramidal cells: C3 (green) and C4 (red), C5 (yellow) and the PV+ interneuron PV6 (blue). The membrane potential of the cells evolves as a function of time displayed from 400ms to 5000ms with a switch to bursting mode at 2000ms. The circuit (top right) is the thalamocortical subnetwork with the black arrows representing the projection from the neocortex to the entorhinal cortex layer II indicating that the neocortex is connected to the rest of the circuit.

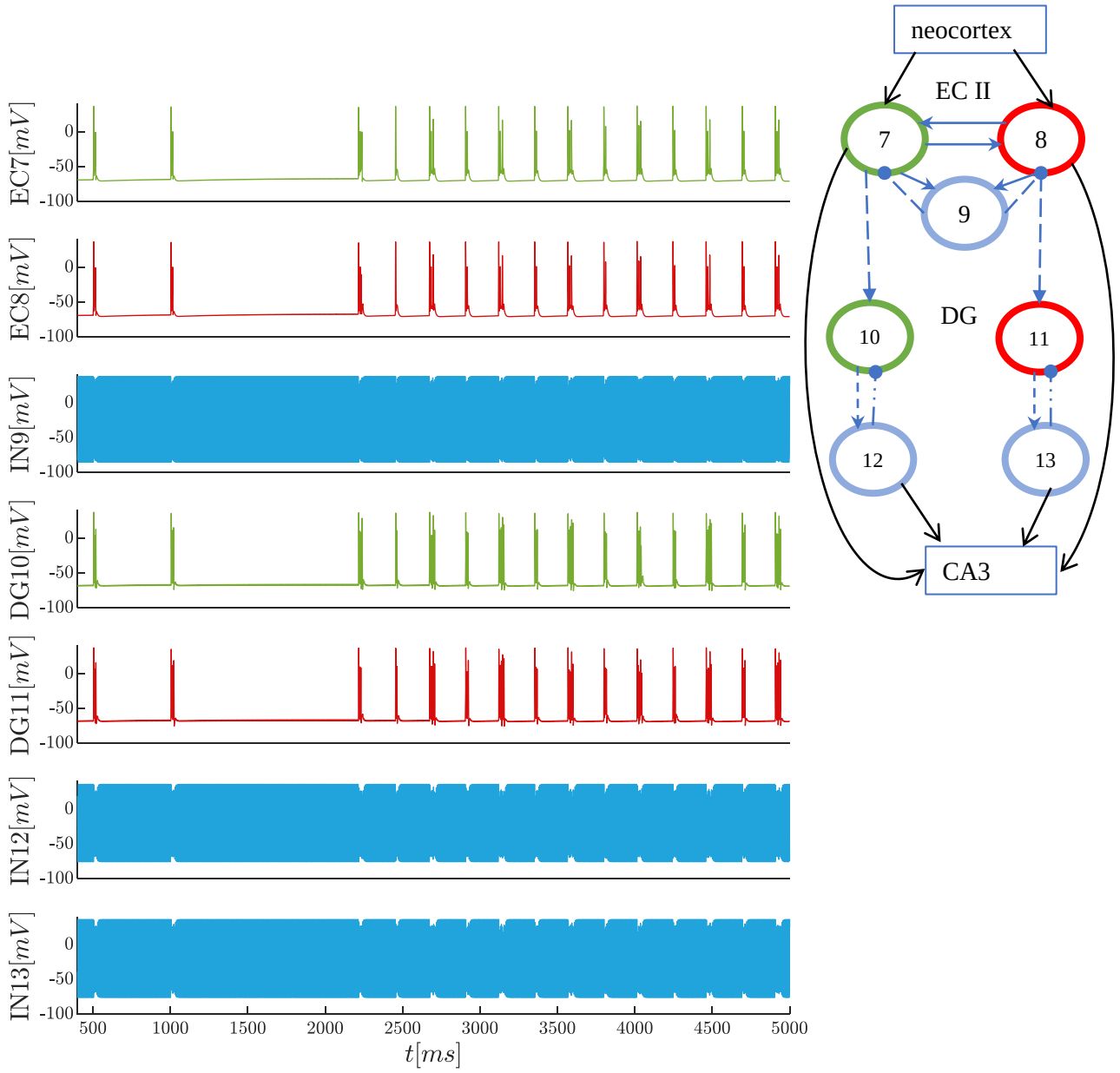

Figure 10.7 – **Fully connected circuit** consisting of the stellate cells EC7 (red) and EC8 (green), the basket cell (blue) IN9, the granule cells (green and red), DG10 and DG11 and their corresponding basket cells (blue) (IN12 and IN13). The membrane potentials of the cells evolve as a function of time displayed from 400ms to 5000ms with a switch to bursting mode at 2000ms. The circuit (top right) is the EC layer II - DG subnetwork with the black arrows representing the connections of the EC layer II with the neocortex and the CA3 region and the connections of the DG with the CA3 region.

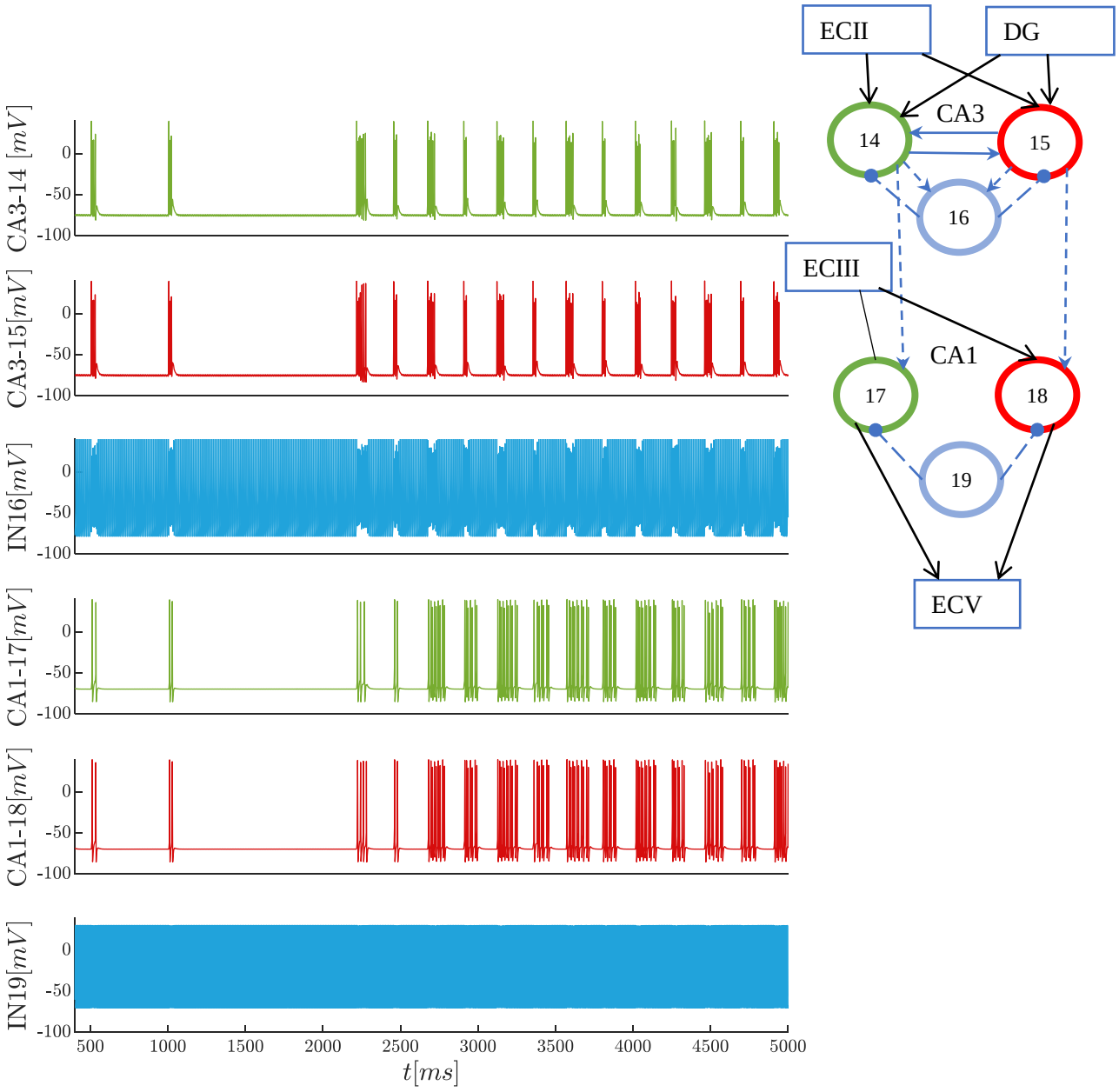

Figure 10.8 – **Fully connected circuit** consisting of the CA3 pyramidal cells: CA3-14 (green) and CA3-15 (red), the basket cell (blue), CA1 pyramidal cell, CA1-17 and CA1-18 (green and red) and the corresponding basket cell (blue) IN19. The cells evolve as a function of time displayed from 400ms to 5000ms with a switch to bursting mode at 2000ms. The circuit (top right) is the CA3-CA1 subnetwork with the black arrows representing the connections of the CA3 region with entorhinal cortex layer II and the connections of the CA1 region with the entorhinal cortex layer III and layer V indicating that this subnetwork is connected to the rest of the circuit.

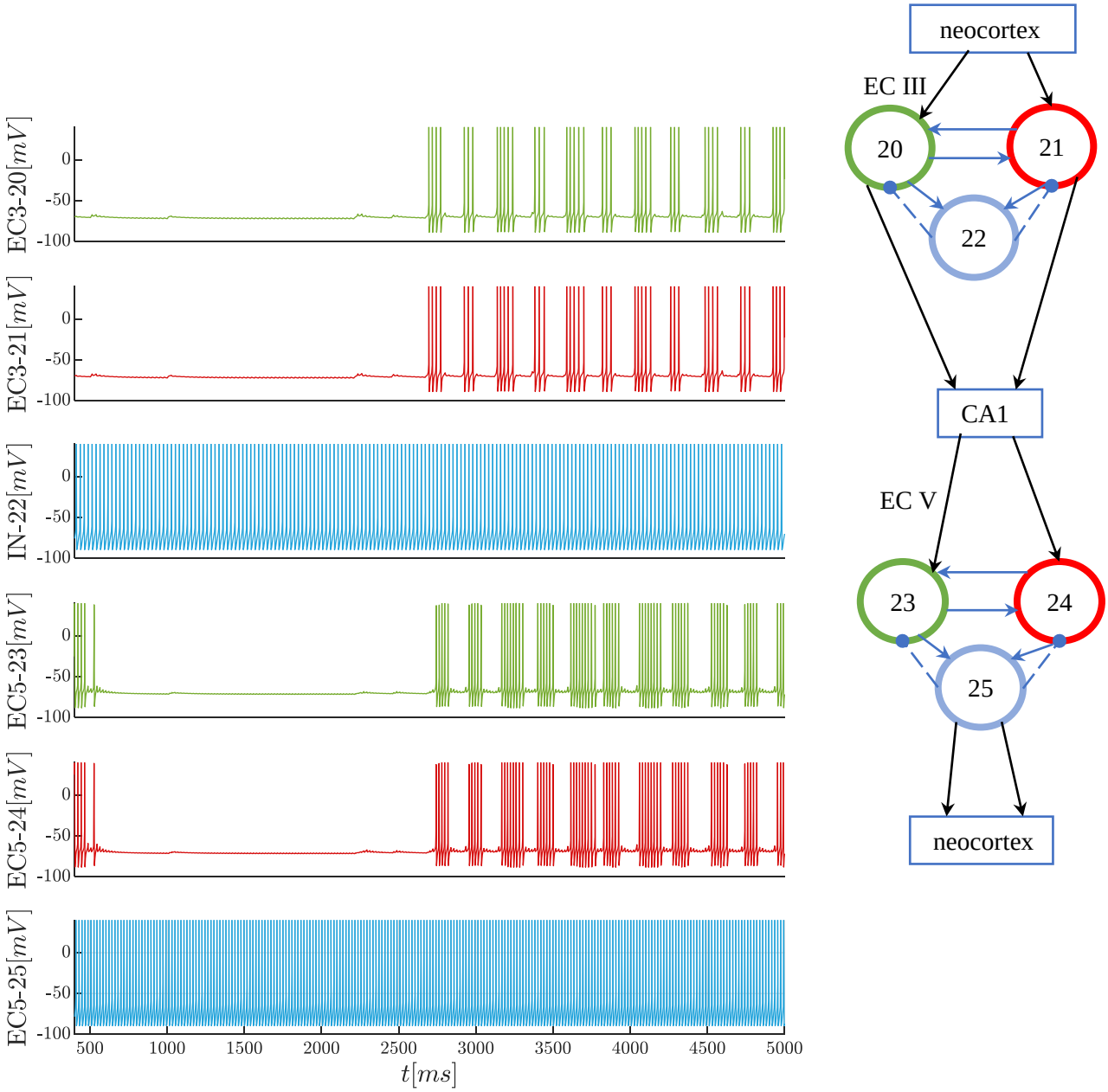

Figure 10.9 – **Fully connected circuit** consisting in the pyramidal cells of the entorhinal cortex layer III, EC20 and EC 21 (in green and red), the corresponding interneuron IN22 in blue, the pyramidal cells of the entorhinal cortex layer V EC23 and EC25 (in green and red) and the corresponding interneuron IN25 in blue. The cells evolve as a function of time displayed from 400ms to 5000ms with a switch to bursting mode at 2000ms. The circuit (top right) is the EC layer III and the EC layer V circuit and the black arrows are the connexions of the EC layer III with the neocortex and the CA1 region and the projection of EC layer V with the CA1 region and the neocortex indicating that the EC layer III and V are connected to the rest of the circuit.

Step 4: Model robustness

In the previous steps, the excitatory neurons coding for the trees (green) and for tent (red) in the same region and the thalamic cells were implemented with the same ionic conductances values. In a realistic world, two neurons do not have exactly the same number of ionic channels. To provide a more

physiological dimension to the project, variability is added to ionic conductances of every neuron of the circuit. The variability consists in incorporating variations of 10% on the eight ionic conductances of the *generic model* tuned in step 1 for the 25 cells present in FIGURES 9.1 and 9.2. This is tested for ten circuits and for each circuit the ionic conductances are changed by 10%. The model is robust if the pattern of activity remains unchanged compared to the model without variability *i.e.* there are some quantitative changes but no qualitative change. The traces without variability are shown in dark red and corresponds to the top trace and the four traces beneath represent four circuits with variability. The results are shown for TC1 cell and the C4 cell (FIGURE 10.10 left and right respectively), the CA1-18 cell and the EC24 cell (FIGURE 10.11 left and right respectively). The remaining traces for other cells are shown in the APPENDIX C.23. To better observe the impact of variability on the bursts parameters, zoomed voltages traces are available in APPENDIX C.23.2. It is also checked that the frequency of interneurons remains relatively unaltered by the 10% of variability. It appears that the frequency remains unchanged and the interneurons are robust to variability as shown in the voltage traces in APPENDIX C.23.3.

TC1, C4 and CA1-18 reproduce qualitatively the initial pattern without variability in dark red. EC24 does not replicate qualitatively the initial trace for 10 % of variability. Indeed, its rhythm is fragile when its nominal parameters are subjected to 10% variability. This is due to the fact that this cell is part of the last stage of the network i.e. the activity originating from the thalamus have been transmitted through different preliminary subnetworks (neocortex, EC layer II and III, DG, CA3) before being transferred to CA1 cells and finally to EC layer V cells. Through the stages, the activity is amplified and bursts of the EC layer V are amplified and are more sensitive to variability. It was decided to apply a variability of 5% on the ionic conductances of the EC24 in the model, it appears that the bursting rhythm is respected (see FIGURE 10.12). Therefore, the model is robust up to the entorhinal cortex layer V with 10 % of variability and is completely robust for 5 % variability. It can be concluded that the model developed in this thesis is relatively robust.

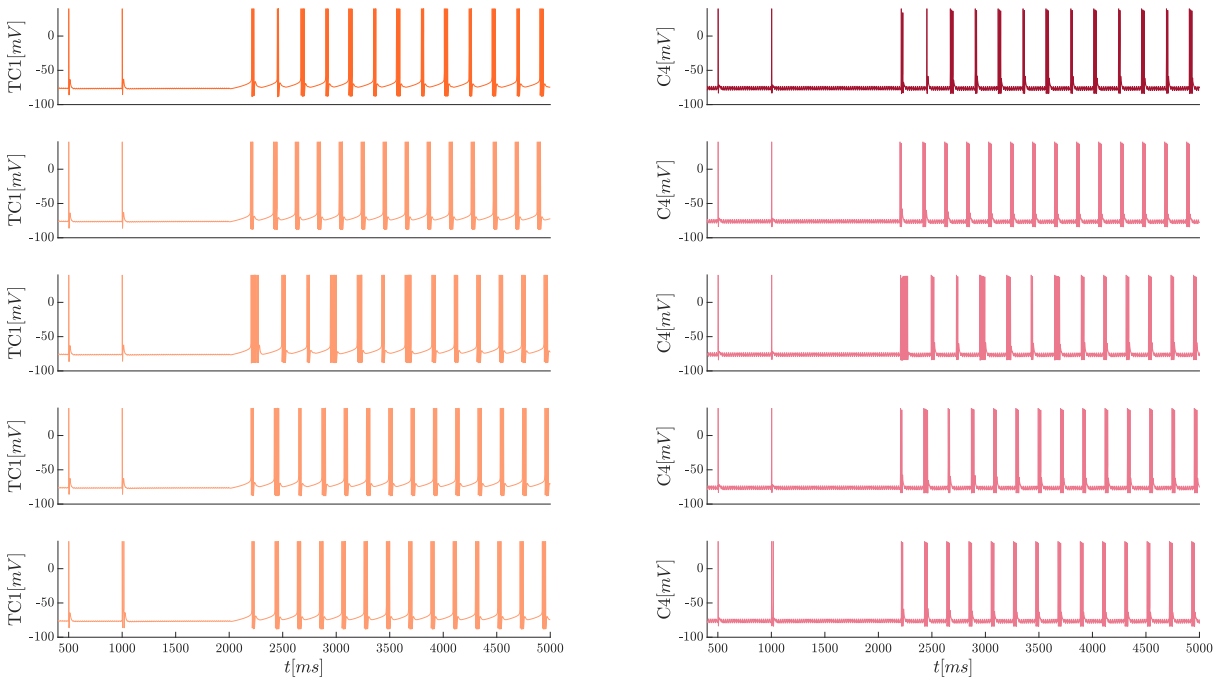

Figure 10.10 – Evolution of the membrane potential (in mV) of TC1 (left) and C4 (right) in the fully connected model according to time (in ms) with 10% of variability on their ionic conductances. The trace in dark orange is the trace without variability and traces in light orange corresponds to traces with variability.

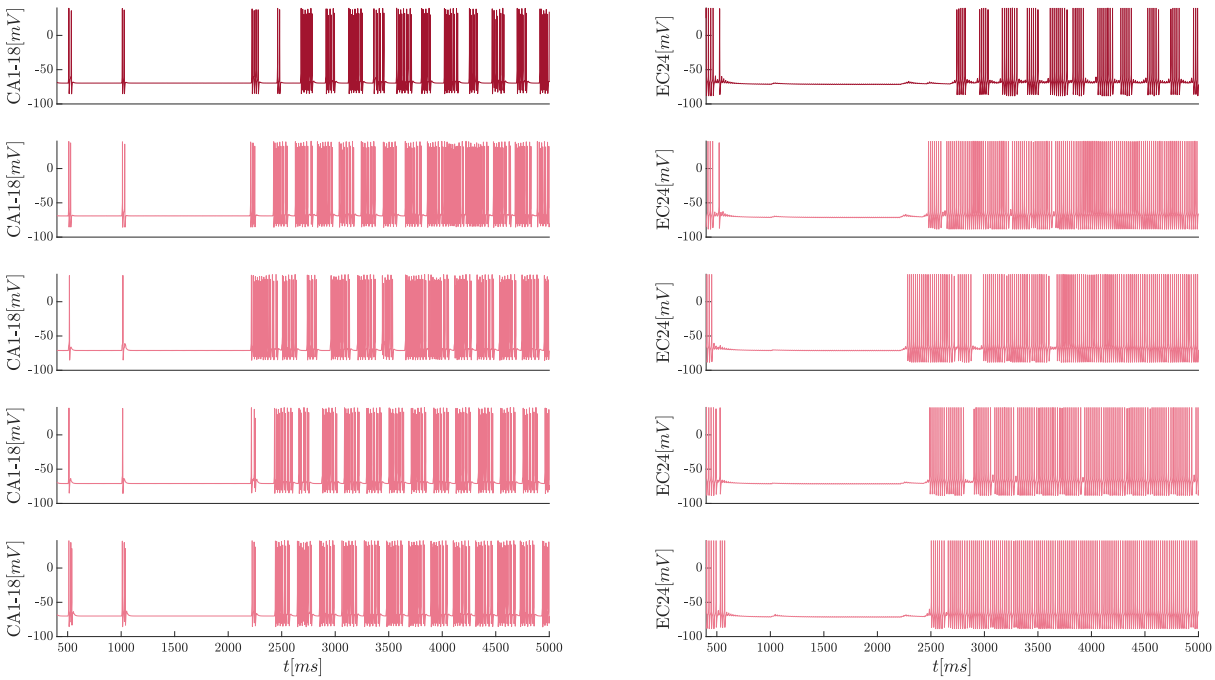

Figure 10.11 – Evolution of the membrane potential (in mV) of CA1-18 (left) and EC24 (right) in the fully connected model according to time (in ms) with 10% of variability on its ionic conductances. The trace in dark red is the trace without variability and traces in light red corresponds to traces with variability

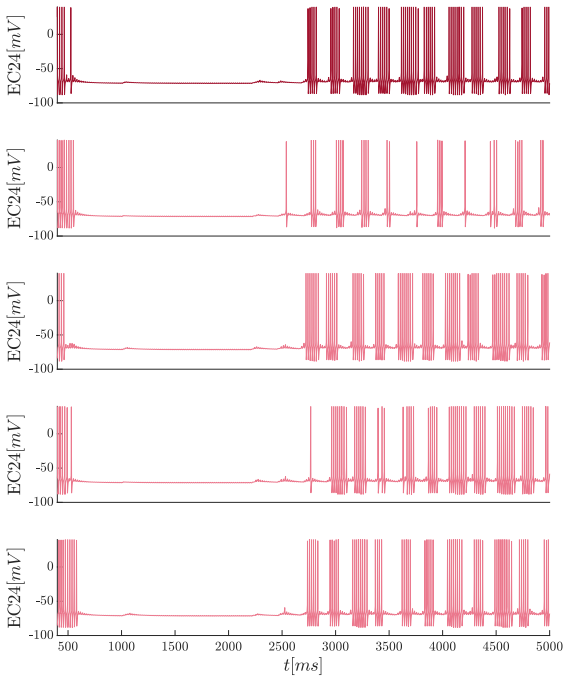

Figure 10.12 – Evolution of the membrane potential (in mV) of EC24 in the fully connected model according to time (in ms) with 5% of variability on their ionic conductances. The trace in dark red is the trace without variability and traces in light red corresponds to traces with variability

A spike is added in the activity pattern of TC1 to make sure that it does not induce a qualitative change in the pattern, that the bursting activity remains and that the bursting frequency is not globally altered. In FIGURE 10.13, a spike is implemented in between bursts at 2690 ms which generates a burst at this time. The bursting frequency remains unchanged. A spike is implemented in 2800 ms, in a burst, which does not alter the firing pattern qualitatively.

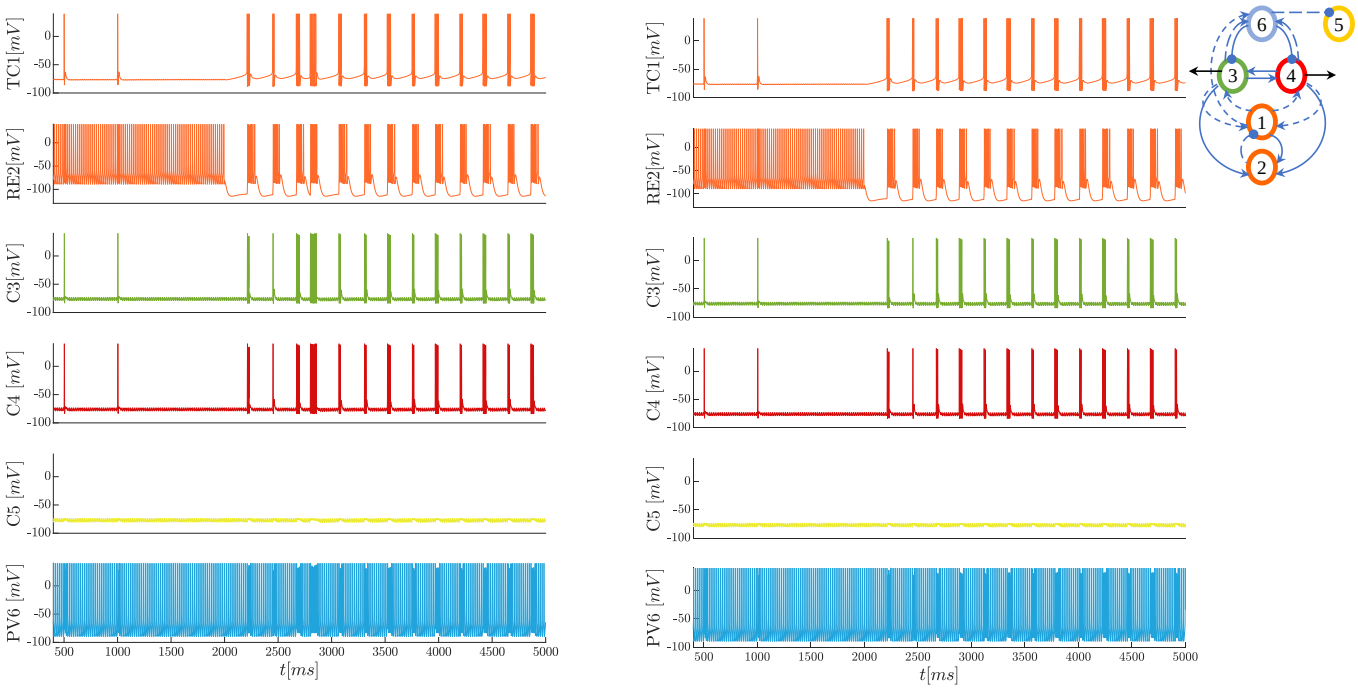

Figure 10.13 – Fully connected model consisting in the thalamocortical cells: the RE cell and TC cell (orange) and neocortical pyramidal cell (green, red and yellow) and the parvalbumin positive interneuron (blue). The membrane potential of the cells evolve as a function of time displayed from 400 ms to 5000 ms with a switch to bursting mode at 2000 ms. A spike is implement in 1690 ms (left) and in 2800 ms (right).

10.2 Modeling conclusion

The modeling of the fully connected model aiming at visualizing the transfer of the features tent and trees of the camping event during wakefulness and the transfer of bursting rhythmicity during sleep was realized by following subsequent steps:

- First, each neuron of every region were modeled individually by respecting the frequency range and the order of magnitude of the ionic conductances presented in CHAPTERS 7 and 8.
- Then, the different neurons were connected in subnetworks by mimicking the synaptic inputs generated by the activity of other regions by implementing current steps.
- Once the cells were successfully simulated in subnetworks, they were associated to reproduce the circuit in FIGURES 9.1 and 9.2by adjusting the synaptic conductances values.
- Finally, variability was introduced to prove that parameters choices are not fragile and that the model is robust in a more biological situation.

Part IV

Conclusion and perspectives

Chapter 11

Conclusion and perspectives

11.1 Conclusion

The work carried out during this thesis has shed light on the following points:

- ✓ How do the thalamus, the neocortex and the hippocampus interact?
  What is the journey of the external stimulation throughout these regions during sleep and wakefulness?
  CHAPTER 3 examines the global pathway joining the three organs. It studies the connections involved in the transfer of the information from the external world relayed by the thalamus to the neocortex then to the hippocampus during wakefulness. It also examines the pathway of the population activity generated by the reactivation occurring in the CA3 region back to the neocortex during sleep. The hippocampal loop is also anamyzed and the corresponding pathway of the transfer of information is pointed out.

- ✓ What is the specific role of these regions in memory consolidation? Their role in memory consolidation and encoding are highlighted in CHAPTER 3. The thalamus has the role of relay during wakefulness and acts as a switch for the generation of sleep spindles which is the main source for driving sleep rhythms and the underlying population rhythms in the neocortex and the hippocampus. The neocortex has the role of integrating and processing the information transferred by the thalamus during wakefulness. It is long term memory storage after consolidation of the representation generated by the hippocampus during sleep. The hippocampus is shown to gather different subregions, each having a distinct and important role in the encoding and in the consolidation of the information (CHAPTER 9). Those regions are namely:

  - the entorhinal cortex which is itself composed of definite layers having different roles in the mnemonic process and acts as a hub between the neocortex and the hippocampus
  - the dentate gyrus which is believed to play a role in pattern separation
  - the CA3 region which is the place of storage and reactivation of the representation due to its recurrent collaterals
  - the CA1 region which further processes the representation spatially and temporally
  - the subiculum which is still underinvestigated but plays a role in synaptic reinforcement

- ✓ What are the principal cells of each region and how to provide a simplified but faithful model?
  The brain being extremely complex and composed of billions of cells, it is very complicated to consider all the types of cells of each region to build a neuronal network. Therefore, solely the principal cells should be considered to try to provide a model as explicit as possible while avoiding the modeling of numerous and different cells provided in CHAPTERS 7 and 8. Inhibitory neurons for each region should also be considered as they are essential for the generation of rhythms as mentioned in CHAPTER 5.

- ✓ How do these cells discharge during wakefulness and subsequent sleep? The firing mode of the different cells investigated depends on the brain state. They fire in tonic mode during wakefulness

and in bursting mode during sleep. Bursting activity can be distinguished as being endogenous or exogenous. Thalamic cell and subicular cells are demonstrated to be intrinsically bursting cells while neocortical and other hippocampal cells are believed to discharge in exogenous bursting drived by the endogenous bursting cells through synaptic connections. Fast-spiking interneurons are also considered and discharge in tonic mode with high frequencies thereby being still in tonic mode during sleep (CHAPTERS 5, 7 and 8).

✓ What is the neurophysiology of each type of cell? CHAPTERS 7 and 8 provide a complete review on the neurophysiology of each cell types present in the thalamus, the neocortex and the hippocampus furnishing the order of magnitudes of the corresponding ionic conductances, the synaptic receptors enabling the communication between two cells and their firing rate. Each type of cell is modeled individually by respecting the neurophysiological data provided in the literature.

✓ What is the architecture of each region? The way the principal cells of the different regions are interconnected is studied based on findings from the literature. A complete circuit has been built in the most accurate way possible to respect these findings (CHAPTER 9).

✓ How do the principal neurons of each region interact during sleep and wakefulness and how can this interaction be modeled? The neurophysiological data found in CHAPTERS 7 and 8, the complete architecture of the circuit involving the three main actors taking part in memory consolidation in CHAPTER 9 and the general understanding of their role and anatomy as well as their electrical behaviour during wakefulness and sleep (CHAPTERS 3, 5, 7 and 8) enabled to develop a schematic, clarified and robust network. The latter was successfully modeled thanks to conductance-based modeling which ensures reliable modeling of the network. It appears that the model developed is robust to variability (PART III).

11.2 Prospects

11.2.1 Subiculum

The neurophysiology and the interconnections of the cells of the subiculum with the rest of the regions have been investigated in this thesis. An attempt at modeling the interaction between the subiculum and the entorhinal cortex layer V is performed. The subicular neurons exhibit an endogenous type of bursting as explained in SECTION 8.5. The amplitude of the T-type calcium current in subicular pyramidal cells is 100 pA and the amplitude of this ionic current in the subicular interneurons is 60 pA [Joksimovic et al. (2017) (figure 4)]. The ionic conductances values chosen for the excitatory neurons and interneuron respected the ratio between the amplitudes of the currents. With the same hyperpolarizing current applied to both type of cells, the interneuron does not burst. It is considered that only the pyramidal subicular cells burst intrinsically. The bursting activity is well transmitted to the EC layer V when interconnected as in FIGURE 11.1. The tonic frequency is also tuned to respect the one found in the literature. The ionic conductance of the I_A current is increased to obtain the lowest frequency which could not attain 15 Hz as predicted in the literature (in SECTION 8.5). The problem encountered while implementing this circuit is that no compromise is reached between the inhibition and the excitation. When the inhibition is increased to obtain the silent phase during wakefulness then the bursting activity disappears. The ionic and synaptic conductances should be further tuned to obtain the accurate transfer of the activity pattern during sleep and wakefulness. Finally, the subiculum should also be integrated into the complete circuit to complete the loop presented in this model for memory consolidation (see FIGURE 9.2).

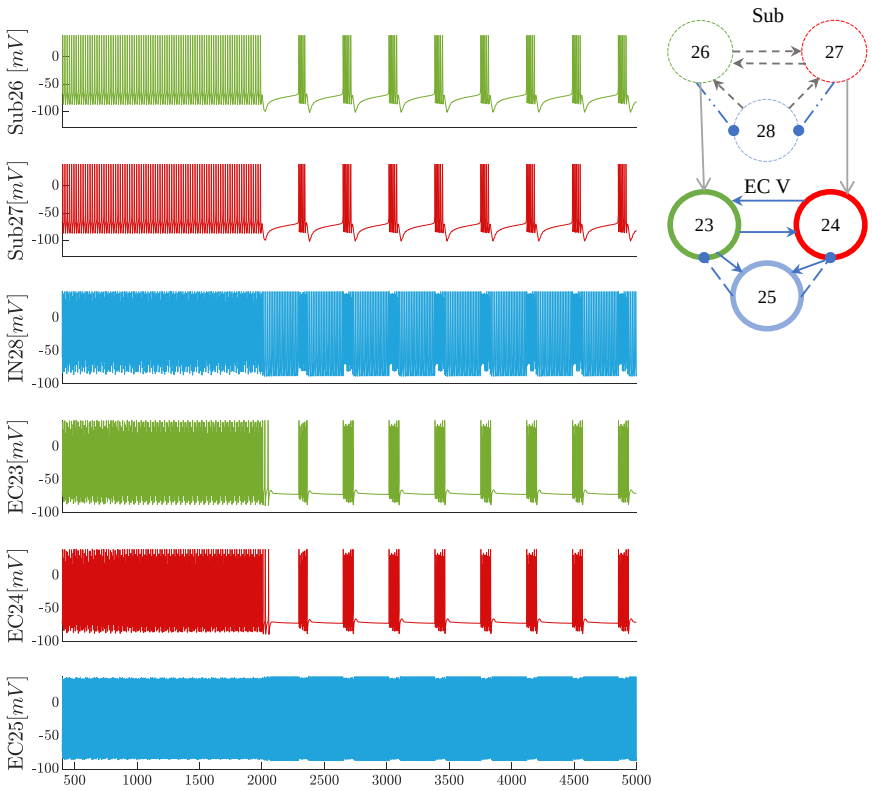

Figure 11.1 – Evolution of the potential (in mV) of the pyramidal cells (red/green) Sub26 and Sub27 and the interneuron (blue) Sub28 of the subiculum connected to the pyramidal cells of entorhinal cortex layer which potential (in mV) is also evolving as a function of time (in ms)

11.2.2 Robustness

Robustness was only tested on ten circuits to verify that the model is not fragile to parameters variations. An extension of this project would be to quantify more deeply the impact of variability with various bursts parameters such as intraburst frequencies, number of spikes per bursts on a bigger amount of circuits such as 10.000 circuits and not only ten.

11.2.3 Synaptic plasticity

The aim of this project is to reproduce the "Active systems consolidation theory" explained in CHAPTER 6. To that end, the physiological interconnections between the organs involved in memory consolidation as stated by the theory are developed. The pattern of activity encountered during wakefulness and sleep are well reproduced. During wakefulness, the information is correctly transmitted from the external world to the hippocampus for encoding. During sleep, the rhythmicity between the different regions is adequately reproduced as well. What is not considered in this thesis is the synaptic plasticity enabling the encoding of the representation in the hippocampus after one occurrence (subjected to decay) and the consolidation of memory during sleep in the neocortex. Indeed, synaptic weight is considered to be fixed while in reality, they are dynamic. For consolidation to occur, the "Active systems consolidation theory" states that during sleep, there is a reactivation of the neuronal populations involved in the encoding of the representation. The reactivation is accompanied by synaptic consolidation processes. As a matter of fact, as explained in SUBSECTION 4.4.3, recurrent excitations between cells (occurring during reactivation) increase the synaptic strength between these cells and enhances the memory representation in the neocortex. The "Active systems consolidation theory" believes in

an upscaling of the synaptic connections involved in the memory consolidation during sleep. As also mentioned in CHAPTER 6, there are different theories supporting the memory consolidation principle. The synaptic homeostatis hypothesis (SHY) on the other hand supports synaptic downscaling during sleep. Adding synaptic plasticity to the model would enable to analyze both theories with respect to memory consolidation.

Appendix A

Neurophysiology basis

A.1 Generation of the action potential

The information is conveyed through neurons in the form of an electrical signal called the action potential *i.e.* spike or neuron discharge. The understanding of the mechanism underlying the generation of membrane potential was developed by Hodgkin and Huxley. Thanks to the establishment of their voltage-clamp technique, they could study variations of membrane conductances and determined that the gating properties and dynamics of ionic channels were responsible for the generation of the action potential. bear. Sodium and delayed-rectifier potassium channels dynamics are at the origin of the action potential. Sodium channels possess a rapid activation gate and a slow inactivation gate. Potassium possesses only one inactivation gate with the same kinetics as sodium channels. The generation of an action potential occurs in the following manner (see FIGURE) [Drion (2013)]:

1. At resting potential (-65mV), the membrane is hyperpolarized being somewhat more permeable to potassium than sodium but their activation gates are closed and their inactivation gates are open. Gates being in these states, no ions can flow through the membrane.

2. Excitation of the membrane by an external stimulus opens the activation gate of sodium but leaves its inactivation gate and the activation gate of potassium unchanged due to their kinetics. This induces an influx of sodium in the cell, depolarizing the membrane to a suprathreshold value. If the threshold value is reached (-55mV), a huge amount of sodium ions enters the cell further depolarizing the membrane towards sodium reversal potential (+40mV).

3. After a very short period of time, the activation gate of potassium opens leading to an efflux of potassium outside the cell and the inactivation gate of sodium begins to close leading to a reduction of sodium entry in the cell. This results in the repolarisation of the membrane potential towards potassium reversal potential (-90mV) leading to a hyperpolarization phase.

4. The hyperpolarization induce the closing of potassium and sodium activation gate and the opening of sodium inactivation gate bringing the membrane potential to its resting value.

Appendix B

Generic model

The goal of the generic model is to reproduce different neuron types and their activity by adapting the ionic conductances. Here are the different ionic currents dynamic and the differential equation describing the membrane dynamic:

$$\begin{aligned} C\dot{V} = &- \bar{G}_{leak}\,(V - E_{\text{leak}}) - G_{Na}(V,t)\,(V - E_{Na}) - G_{K,d}\,(V - E_K) - G_A\,(V - E_K) \\ &- G_T\,(V - E_{Ca}) - G_L\,(V - E_{Ca}) - G_H(V,t)\,(V - E_H) - G_{K,Ca}\left(\left[Ca^{2+}\right]_{in}, t\right)(V - E_K) + I_{ext}(t) \end{aligned}$$

- Transient sodium current $G_{Na}(V,t)\,(V - E_{Na})$ transient sodium current that activates on a fast timescale and inactivates on a slower timescale. Its conductance is described as

$$G_{Na}(V,t) = \bar{G}_{Na} m_{Na}^3 h_{Na}$$

- Delayed-rectifier potassium current $G_{K,d}\,(V - E_K)$ otassium current that activates on a slow timescale and does not inactivate. Its conductance is described as

$$G_{K,d}(V,t) = \bar{G}_{K,d} m_{K,d}^4$$

- A-type potassium current $G_A\,(V - E_K)$ potassium current that activates on a fast timescale and inactivates on a slow timescale. Its conductance is described as

$$G_A(V,t) = \bar{G}_A m_A^3 h_A$$

- T-type calcium current $G_T\,(V - E_{Ca})$ low-threshold calcium current that activates on a slow timescale and inactivates on an ultraslow timescale. Its conductance is described as

$$G_T(V,t) = \bar{G}_T m_T^3 h_T$$

- L-type calcium current $G_L\,(V - E_{Ca})$ high-threshold calcium current that activates on a slow timescale and does not inactivate. Its conductance is described as

$$G_L(V,t) = \bar{G}_L m_L$$

- H-current $G_H(V,t)\,(V - E_H)$ tion current that is activated by hyperpolarization. It is permeable to both sodium and potassium ions, wich explains its specific reversal potential. Its conductance is described as

$$G_H(V,t) = \bar{G}_H m_H$$

- Calcium-activated potassium current $G_{K,Ca}\left(\left[Ca^{2+}\right]_{in}, t\right)(V - E_K)$ m current that is activated by a rise intrallular calcium concentration is calcium-gated rather than voltage-gated. Its conductance is described as

$$G_{K,Ca}(V,t) = \bar{G}_{K,Ca} \frac{\left[Ca^{2+}\right]_{in}^4}{(15.0 + \left[Ca^{2+}\right]_{in})^4}$$

Appendix C

Modeling details

C.1 [Destexhe et al. (1996)]

The membrane potential of the RE cells is given by the following equation:

$$C_m\dot{V} = -g_L\left(V - E_L\right) - I_{Ts} - I_{Na} - I_K - I_{AMPA} - I_{GABAa}$$

The equation follows the formalism of the conductance-base model equations present in SUBSECTION 4.2.3. I_{Na} and I_K are the sodium and potassium currents. The subscript L denotes the leakage current. I_T and I_{Ts} are low-threshold calcium currents, I_h is the hyperpolarization-activated cation current, I_{KL} is a leak potassium current. There are also synaptic currents I_{AMPA}, I_{GABAa} and I_{GABAb}.

C.2 [McCormick and Huguenard (1992)]

The membrane potential is described by

$$C_m\dot{V}_m = -\left(I_{Na} + I_{\mathrm{Nap}} + I_L + I_T + I_{CaT} + I_A + I_{K2} + I_{\mathrm{Kleak}} + I_{\mathrm{Naleak}}\right) + I_{\mathrm{app}}$$

where I_{Na} is a transient Na^+ current, I_{NaP} is a depolarisation-activated Na^+ current, I_L is a high-threshold Ca^{2+} current, I_{CaT} is a low-threshold Ca^{2+} current, I_A is a transient and depolarisation-activated K^+ current,I_{K2} is a slowly inactivating and depolarisation-activated K^+ current, I_{KL} K^+ leak current and I_{Naleak} is a Na^+ leak current.

C.3 [Drion et al. (2018)]

The conductance-based equation is given by:

$$C_m\dot{V}_m = -I_{Na} - I_K - I_{CaT} - I_{K,Ca} - I_H - I_{leak} + I_{app}$$

where I_{CaT} denotes the T-type calcium current.

C.4 [Destexhe et al. (1998)]

The conductance-based equation is given by:

$$C_m\dot{V}_m = -I_{Na} - I_K - I_{CaT} - I_{leak} + I_{app}$$

C.5 [Bazhenov et al. (2002), Wei et al. (2016)]

$$\begin{aligned} &C_{\mathrm{m}}\tfrac{dV_{\mathrm{D}}}{dt} = -g_{\mathrm{L}}\left(V_{\mathrm{D}} - E_{\mathrm{L}}\right) - g\left(V_{\mathrm{D}} - V_{\mathrm{S}}\right) - I_{\mathrm{D}}^{\mathrm{int}} - I^{\mathrm{syn}} \\ &g\left(V_{\mathrm{S}} - V_{\mathrm{D}}\right) = -I_{\mathrm{S}}^{\mathrm{int}} \end{aligned}$$

where the subscript D and S denote respectively the dendritic and the axosomatic compartment. The subscript L denotes the properties relative to a leakage current. g is the conductance between the dendritic and axosomatic compartments. I^{int} represents the summation of intrinsic currents for each compartment and I^{syn} describes the summation of synaptic currents. The remaining of the characters present in the equations refer to the characters presented in SUBSUBSECTION 4.2.3.

	g_{Na}	g_K	g_{NaP}	g_L	g_{KL}	g_{HVA}	g_{KCa}	g_{Km}
Axosomatic Bazhenov Wei	3000	200	0.07 15	-	-	-	-	-
Dendritic Bazhenov Wei	1.5 0.8	-	0.07 2.5	0.033	0-0.0025 0.003	0.01 0.02	0.3	0.01 0.01

Table C.1 – Ionic conductances values in $\frac{mS}{cm^2}$ used in the model of [Bazhenov et al. (2002)] for the axosomatic and the dendritic compartments

The currents involved are: I_{N_a} is a fast Na^+ current, I_K is a fast delayed rectifier potassium K^+ current, $I_{Na(p)}$ is a persistent sodium current, I_L is the leakage current, I_{KL} is the potassium leak current, I_{HVA} is g high-threshold Ca^{2+} current, I_{Km} is a slow voltage-dependent noninactivating K^+ current and I_{KCa} is a slow Ca^{2+} -dependent K^+ current

C.6 [Hill and Tononi (2005)]

Ionic conductances values in $\frac{mS}{cm^2}$	g_{NaP}	g_{DK}	g_{NaL}	g_{KL}
	0.5/1.25	0.5/1.25	0.2	1/1.85

Table C.2 – Ionic conductances values used in the model of [Hill and Tononi (2005)], the left value for g_{NaP}, g_{DK} and g_{KL} corresponds to the value during wakefulness and the right value is the value during sleep

C.7 [Pospischil et al. (2008)]

$$C_m \frac{\mathrm{d}V}{\mathrm{d}t} = -g_{\text{leak}}\ (V - E_{\text{leak}}\ ) - I_{\text{Na}} - I_{\text{Kd}} - I_M - I_T - I_L$$

where I_{Na^+} is a voltage-dependent Na^+ current, I_{Kd} is a delayed-rectifier K^+ current, I_M is a slow

Ionic conductances values	g_{leak}	g_{Na}	g_{Kd}	g_M
	1.90 nS	50 $\frac{mS}{cm^2}$	4.8 $\frac{mS}{cm^2}$	0.13 $\frac{mS}{cm^2}$

Table C.3 – Ionic conductances values reported in 13 regular spiking neurons of the rat somatosensory cortex

non-inactivating K^+ current for spike-frequency adaptation and I_L and I_T are a high-threshold and a low-threshold Ca^{2+} currents to induce bursting activity for intrinsically bursting neurons which is not relevant in the scope of this thesis. I_{leak} is a leak current.

C.8 Thalamocortical synaptic receptors

Values of the synaptic conductances involved in the thalamocortical circuit.

	Post-cell			
Pre-cell	TC	RE	PY	IN
PY	g_{AMPA} (H)(F)	g_{AMPA}(H) g_{AMPA}(F) g_{NMDA}(F)	g_{AMPA}=0.08µS (Wei) g_{NMDA}=0.006µS (Wei) g_{AMPA}=0.08-0.15µS (Bazhenov) g_{NMDA}=0.01µS (Bazhenov) g_{AMPA}(Hill) g_{NMDA}(Hill)	g_{AMPA}=0.08µS (W) g_{NMDA}=0.05µS (W) g_{AMPA}=0.05µS (B) g_{NMDA}=0.008µS (B) g_{AMPA}(H)
IN	-	-	g_{GABAa}=0.25µS (W) g_{GABAa}=0.05 µS (B) g_{GABAa}(H) g_{GABAb}(H)	-
TC	-	g_{AMPA}=0.35µS (W) g_{AMPA}(H)(F) g_{NMDA}(F)	g_{AMPA}=0.1 µS (B)	g_{AMPA}=0.1 µS (B)
RE	g_{GABAa}=0.0 µS (B) g_{GABAb}=0/04µS (B) $GABAa$=0.15µS (W) $GABAa$ (H) (F)(D)(De) $GABAb$(H) (F)(D)(De)	-	-	-

Table C.4 – Synaptic conductances values in the models of [Bazhenov et al. (2002) (B), Hill and Tononi (2005) (H), Wei et al. (2016) (W), Fernandez and Lüthi (2020) (F), Drion et al. (2018) (D), Destexhe et al. (1996) (De)]

C.9 Dentate gyrus synaptic receptors

Pre-cell	Post-cell
	Granule celll
Perforant path projection	g_{AMPA} = 20 nS
Granule cell	g_{AMPA} = 2 nS
Basket cell	g_{GABAa} = 1.6 nS

Table C.5 – Synaptic conductance values used in the model of [Santhakumar et al. (2005)] for the granule cells of the dentate gyrus

Pre-cell	Post-cell
	Basket cell
Perforant path projection	g_{AMPA} = 10 nS
Granule cell	g_{AMPA} = 4.7 nS

Table C.6 – Synaptic conductances values used in the model of [Santhakumar et al. (2005)] for the basket cell of the dentate gyrus

C.10 CA3 synaptic receptors

Synaptic receptors	$AMPA$	$NMDA$	$GABAa$	$GABAb$
	4 nS	3 nS	✓	✓

Table C.7 – Synaptic conductances values of CA3 pyramidal cells given by [Migliore et al. (1995)]. ✓indicates the presence of the synaptic receptors in CA3 pyramidal cell for which no value is given

C.11 [Acker et al. (2003)]

The conductance-based equation of the model of [Acker et al. (2003)] for stellate cells layer II is given by

$$\begin{aligned} & C\frac{dVm}{dt} \\ & = I_{\text{app}} - \left(g_{\text{Na}} m_{\text{Na}}^3 h_{\text{Na}} + g_{\text{Nap}} m_{\text{Nap}}\right)(Vm - V_{\text{Na}}) \\ & \quad - \left(g_{\text{k}} n^4 + g_{\text{Ks}} m_{\text{Ks}}\right)(V_{\text{m}} - V_{\text{K}}) \\ & \quad - g_{\text{h}}\left(0.65 m_{\text{hf}} + 0.35 m_{\text{hs}}\right)(Vm - V_{\text{h}}) \\ & \quad - g_{\text{L}}(Vm - V_{\text{L}}) - g_{\text{syn}} m_{\text{syn}}(Vm - V_{\text{syn}}) \end{aligned}$$

Article	Ionic conductances values				
	g_{Na}	g_K	g_{NaP}	g_h	g_{leak}
[Acker et al. (2003)]	52	11	0.5	1.5	0.5

Table C.8 – Ionic conductances values given in the model of [Acker et al. (2003)]

C.12 [Santhakumar et al. (2005)]

	Ionic conductances values									
	g_{Na}	g_{Kd_f}	g_{Kd_s}	I_A	g_L	$I_{K(C)}$	I_N	I_T	I_{AHP}	I_{leak}
Excitatory cell	120	16	6	12	5	0.6	2	0.037	1	0.004
Interneuron	120	13	-	0.15	5	0.2	0.8	-	0.002	0.000018

Table C.9 – Summary of the conductance values used in the model of Traub and Migliore

where the currents are :the sodium current, I_{Na}, a fast delayed rectifier K^+ current I_{Kd_f}, a slow delayed rectifier K^+ current I_{Kd_x}, an A-type K^+ current I_A, a L-type $I_{Ca^{2}+}$ current I_L, a N-type $I_{Ca^{2+}}$ current I_N, a T-type $I_{Ca^{2+}}$ current I_T, a calcium and voltage K^+ current I_{BK}, a small conductance AHP calcium dependent K^+ current I_{AHP} and a leak current I_{leak} .

C.13 [Traub et al. (1991)]

The cable equation modeling the 19-compartment model is the following:

$$C_k \frac{\mathrm{d}V_k}{\mathrm{dt}} = \gamma_{k-1,k}(V_{k-1} - V_k) + \gamma_{k+1,k}(V_{k+1} - V_k) - I_{\text{ionic},k}$$

where $\gamma_{k-1,k}$ is the conductance between compartment k and l, V_k is the transmembrane potential of the corresponding compartment and $I_{\text{ionic},k}$ represents the sum of the ionic currents and synaptic currents for a compartment k. The conductance densities presented in the article for the somatic compartment and for each type of currents is as follows:

Conductance $\frac{mS}{cm^2}$	$g_{K(A)}$	$g_{K(AHP)}$	g_{Na}	$g_{K(DR)}$	$g_{K(C)}$	g_{Ca}	g_L
	0.5	0.8	30	15	10	4	0.1

Table C.10 – Ionic conductance densities values used in the model of Traub for the somatic

The ionic currents are $I_{K(A)}$ an A-type transient K current, $I_{K(AHP)}$, a long duration Ca-dependent AHP K current, I_{Na}, a sodium current, $I_{K(DR)}$ a delayed rectifier K current, $I_{K(C)}$, a short-duration voltage- and Ca-dependent K current, I_{Ca} a calcium current and a leakage current I_L.

Conductance $\frac{mS}{cm^2}$	g_{Na}	$g_{K_{DR}}$	g_{K_A}	g_{K_M}	g_T	g_L	g_N	g_{K_C}	$g_{K_{AHP}}$
	15	30	1.5	0.1	0.25	2.5	2.5	0.8	0.4

Table C.11 – Ionic conductance densities values used in the model of Migliore

C.14 [Migliore et al. (1995)]

I_{Na}, a sodium current, $I_{K_{DR}}$, a delayed rectifier current, I_{K_A}, ,I_{K_M}, a noninactivating voltage-dependent K^+ conductance, $I_{CaN,L,T}$ are four types of calcium conductances, I_{K_C}, a voltage and Ca^{2+}-dependent K^+ conductance and $I_{K_{AHP}}$, a Ca^{2+}-activated K^+ conductance.

C.15 [Wang and Buzsáki (1996)]

The currents involved in the equation are a a sodium, a potassium and a leak current.

$$C_m \frac{dV}{dt} = -I_{\mathrm{Na}} - I_{\mathrm{K}} - I_{\mathrm{L}} - I_{\mathrm{syn}} + I_{\mathrm{app}}$$

C.16 [Buchin et al. (2016)]

$$C_m dV_d/dt = -I_d^{Int} - g_c^d \left(V_d - V_s\right) - I_d^{\mathrm{leak}} - I_d^{\mathrm{pump}}$$
$$g_c^d \left(V_d - V_s\right) = -I_s^{Int} - I_s^{\mathrm{leak}} - I_s^{pump}$$

in which the subrcript d and s denote respectively the dendritic and the somatic compartment. The somatic compartment contains a voltage-gated sodium current I_{Na}, a delayed-rectifier potassium current I_{K_ν} and leak currents, I_{leak_K}, $I_{leak_{Na}}$; the dendritic compartment contains a high-threshold calcium current I_{HVA}, a calcium-activated potassium current I_{KCa}, a calcium current I_{Ca}, a slowly activating potassium current, a voltage-gated current I_{Na}, a persistent sodium current I_{NaP} and leak currents I_{leak_K}, $I_{leak_{Na}}$ and $I_{leak_{Cl}}$.

Ionic conductances values in $\frac{mS}{cm^2}$	g_{Na}	g_{K_ν}	g_{HVA}	g_{KCa}	g_{Ca}	g_{NaP}	g_{leak}	I_{leak_K}	$I_{leak_{Na}}$	$I_{leak_{Cl}}$
Soma	3450	200	-	-	-	-	-	0.019	0.042	-
Dendrite	✓	-	✓	✓	✓	✓	✓	0.035	0.02	0.01

Table C.12 – Ionic conductances values given by [Buchin et al. (2016)]

C.17 [Krishnan and Bazhenov (2011)]

The conductance-based equation is the same but the currents involved in each compartment differ slightly. The somatic compartment consists in a voltage-gated sodium current I_{Na}, a delayed-rectifier potassium current I_{K_ν}, a persistent sodium current I_{NaP}, a sodium-activated potassium current I_{KNa}. The dendritic compartment has high-threshold calcium, I_{Ca}, calcium-activated potassium I_{KCa}, slowly activating potassium, I_{Km}, persistent sodium, I_{NaP}, hyperpolarization-activated depolarizing mixed cationic, I_h, voltage-gated sodium I_{Na}, and leak conductances.

Ionic conductances values $\frac{mS}{cm^2}$	g_{Na}	g_{K_ν}	g_{NaP}	g_{KNa}	g_{Ca}	g_h	g_{KCa}	I_{leak_K}	$I_{leak_{Na}}$	$I_{leak_{Cl}}$
Soma	3450	200	3.5	1.3	-	-	-	0.042	0.0198	-
Dendrite	3450	200	3.5	-	0.0165	0.1	2.5	0.044	0.02	0.01

Table C.13 – Ionic conductance values used in the model of [Krishnan and Bazhenov (2011)]

C.18 [Pongracz et al. (1992)]

The ionic conductances used in the model are a sodium current I_{Na}, a potassium current I_K, a calcium current I_{Ca}, a Ca^{2+}-mediated K^+ conductances $I_{K(Ca)}$ and I_cCa.

Ionic conductances values $\frac{mS}{cm^2}$	g_{Na}	g_{K_ν}	g_{Ca}	$g_{K(Ca)}$	$g_c Ca$
Soma	50	50	0.2	1	1
Dendrite	10	10	0.2	1	1

Table C.14 – Ionic conductances used in the model of [Pongracz et al. (1992)]

C.19 [Bianchi et al. (2012)]

The membrane behaviour is described by the following conductance-based equation:

$$\begin{aligned} C_m \frac{dV}{dt} = &- I_{NaT} - I_{K_{DR}} - I_{K_U} - I_{K_A} \\ &- I_{\mathrm{CaT}} - I_{\mathrm{CaR}} - I_{\mathrm{CaL}} - I_h \\ &- I_{\mathrm{sAHP}} - I_{\mathrm{mAHP}} - I_{\mathrm{leak}} + I_{\mathrm{inj}} \end{aligned}$$

where a leak current, a transient sodium (NaT) current, a delay-rectifier potassium (K_{DR}) current, an A-type potassium current (K_{A}), a M type potassium current (K_{M}), a mixed conductance hyperpolarization activated h-current, three types of voltage dependent calcium currents (namely LVA Ttype current, a HVA R-type current, a HVA L-type current), two types of calcium dependent potassium currents (a slow AHP current and a medium fast AHP current) are used.

C.20 [Shuman et al. (2020)]

The model doesn't provide any value but provides currents used for modeling CA1 interneurons which are a sodium current, a delayed-rectfier current, a leak channel and A-type K^+, L-type and N -type Ca^{2+} currents, and Ca^{2+} -dependent K^+ and Ca^{2+} dependent and voltage-dependent K^+ conductances.

C.21 Individual traces

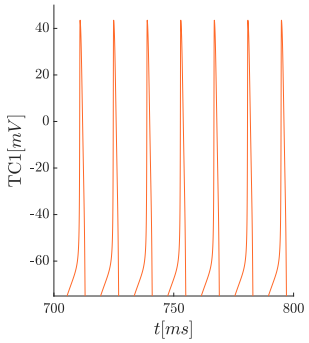

Figure C.1 – Zoom of the evolution of the membrane potential of TC1 between 700 ms and 800 ms

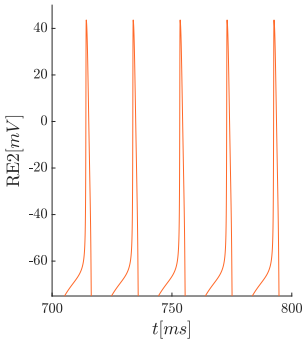

Figure C.2 – Zoom of the evolution of the membrane potential of TRN2 between 700 ms and 800 ms

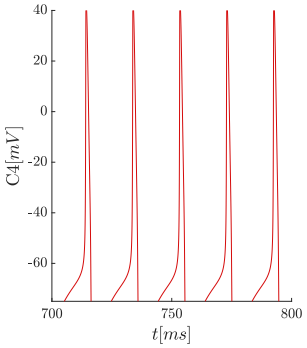

Figure C.3 – Zoom of the evolution of the membrane potential of C4 between 700 ms and 800 ms

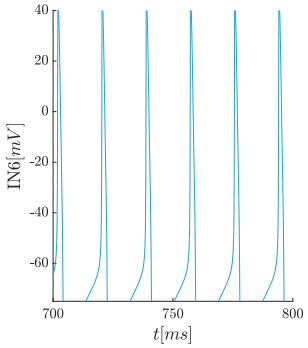

Figure C.4 – Zoom of the evolution of the membrane potential of IN6 between 700 ms and 800 ms

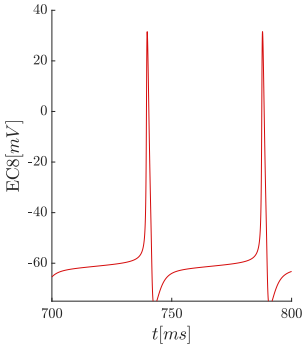

Figure C.5 – Zoom of the evolution of the membrane potential of EC8 between 700 ms and 800 ms

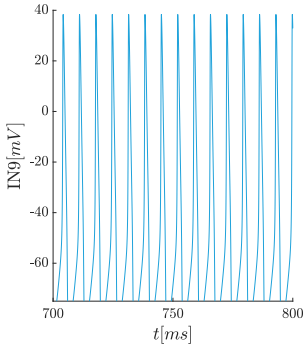

Figure C.6 – Zoom of the evolution of the membrane potential of IN9 between 700 ms and 800 ms

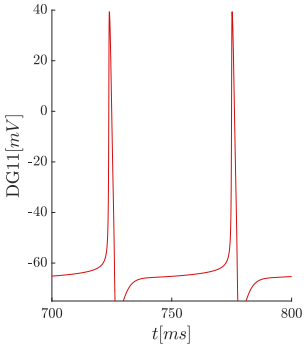

Figure C.7 – Zoom of the evolution of the membrane potential of DG11 between 700 ms and 800 ms

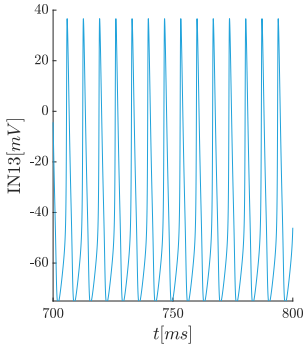

Figure C.8 – Zoom of the evolution of the membrane potential of IN13 between 700 ms and 800 ms

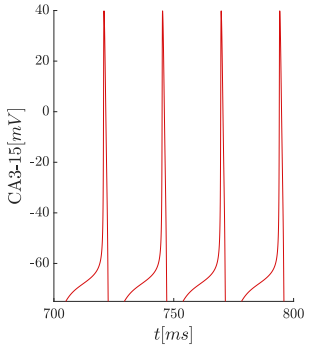

Figure C.9 – Zoom of the evolution of the membrane potential of CA3-14 between 700 ms and 800 ms

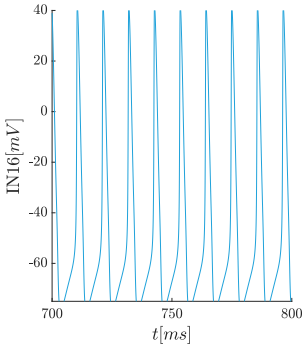

Figure C.10 – Zoom of the evolution of the membrane potential of IN16 between 700 ms and 800 ms

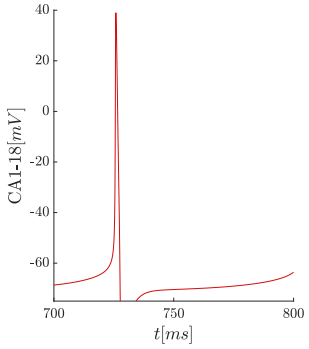

Figure C.11 – Zoom of the evolution of the membrane potential of CA1-18 between 700 ms and 800 ms

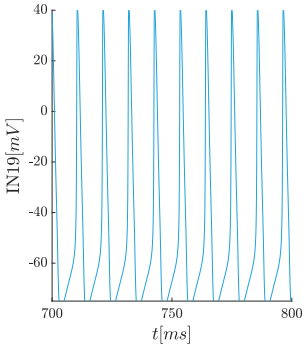

Figure C.12 – Zoom of the evolution of the membrane potential of IN19 between 700 ms and 800 ms

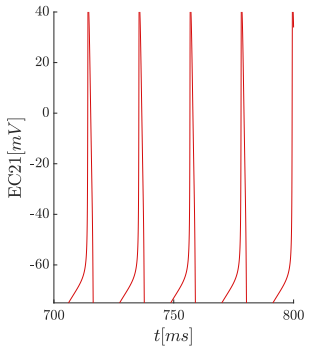

Figure C.13 – Zoom of the evolution of the membrane potential of EC21 between 700 ms and 800 ms

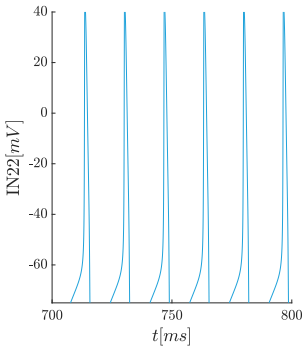

Figure C.14 – Zoom of the evolution of the membrane potential of IN22 between 700 ms and 800 ms

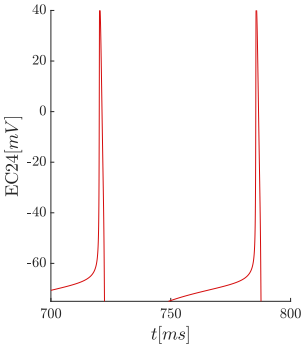

Figure C.15 – Zoom of the evolution of the membrane potential of EC24 between 700 ms and 800 ms

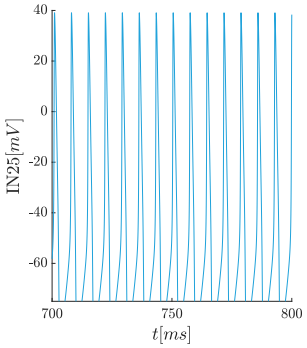

Figure C.16 – Zoom of the evolution of the membrane potential of IN25 between 700 ms and 800 ms

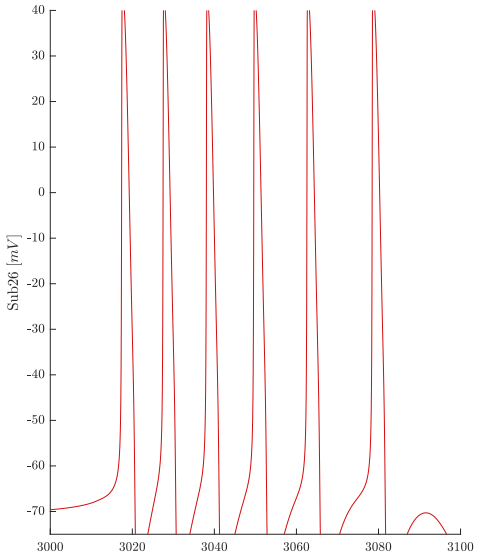

Figure C.17 – Zoom of the evolution of the membrane potential of Sub27 between 3000 ms and 3100 ms (zoom on a burst)

C.22 Entorhinal cortex layer III

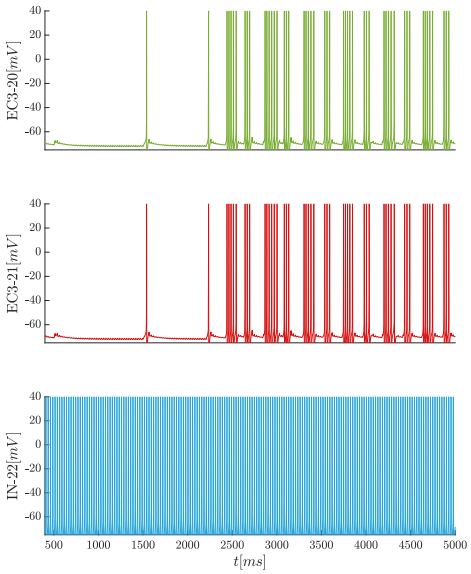

Figure C.18 – Evolution of the potential (in mV) of entorhinal cortex layer III pyramidal cells (in green and red) and interneuron (in blue) according to time (in ms). A spike is appearing at 1500ms

C.23 Variability

C.23.1 Excitatory cells traces

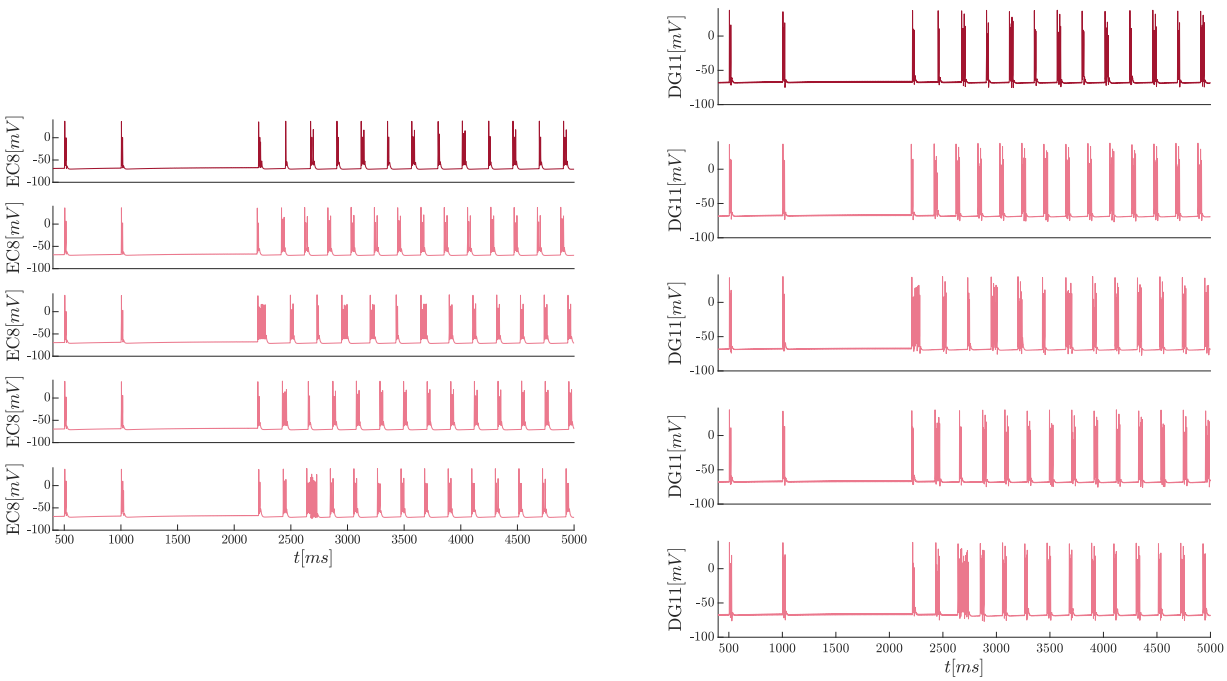

Figure C.19 – Evolution of the membrane potential (in mV) of the EC8 (left) and DG11 (right) in the fully connected model according to time (in ms) with 10% of variability on its ionic conductances. The trace in dark red is the trace without variability and traces in light red corresponds to traces with variability

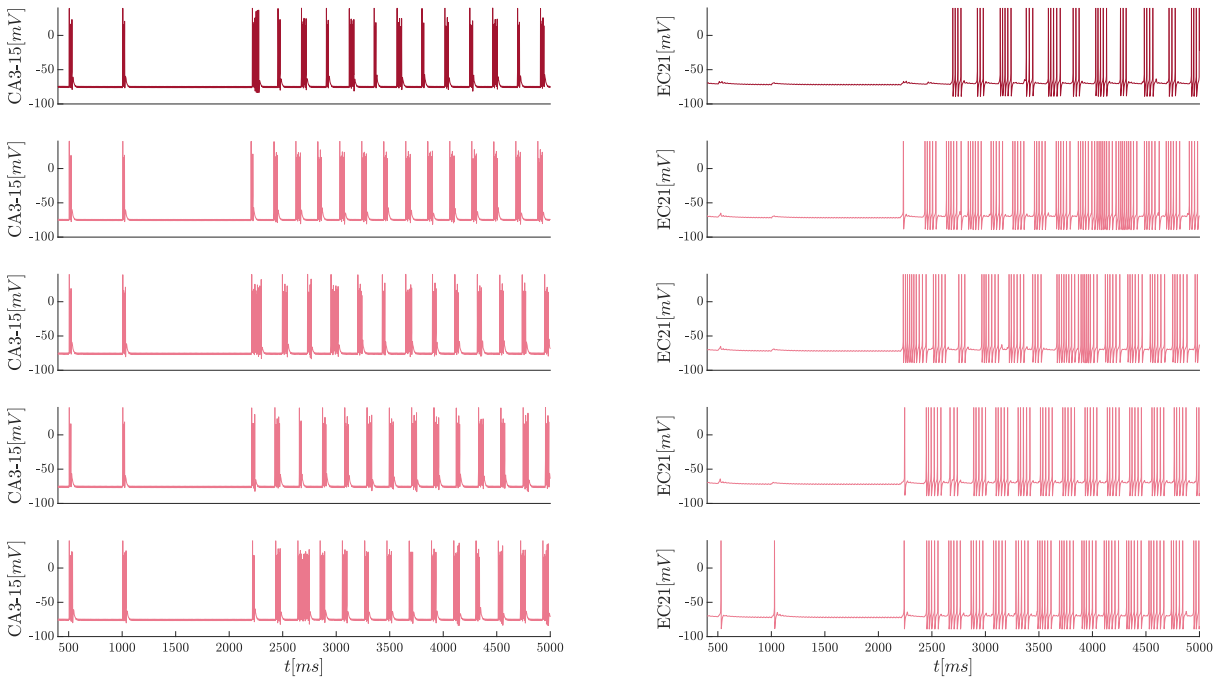

Figure C.20 – Evolution of the membrane potential (in mV) of the CA3-18 (left) and EC21 (right) in the fully connected model according to time (in ms) with 10% of variability on its ionic conductances. The trace in dark red is the trace without variability and traces in light red corresponds to traces with variability

C.23.2 Zoom on excitatory cells traces

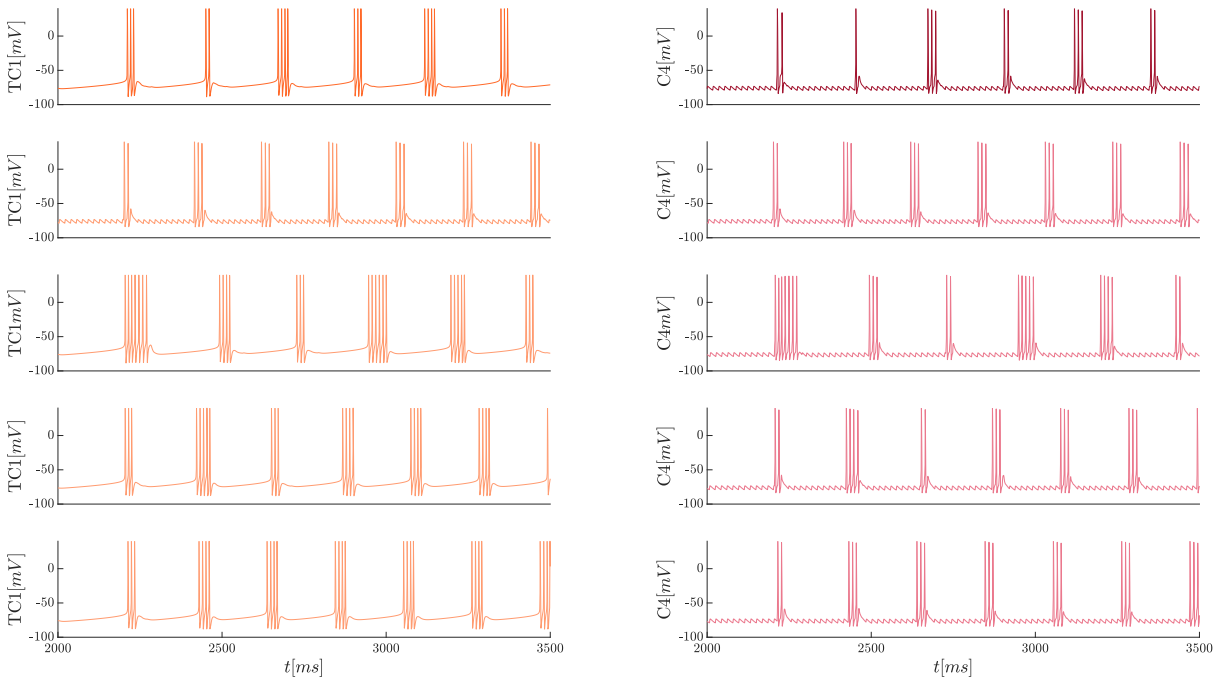

Figure C.21 – Zoom of the evolution of the membrane potential (in mV) of TC1 (left) and C4 (right) in the fully connected model according to time (in ms) between 2000 ms and 3500 ms with 10% of variability on its ionic conductances. The trace in dark orange is the trace without variability and traces in light orange corresponds to traces with variability

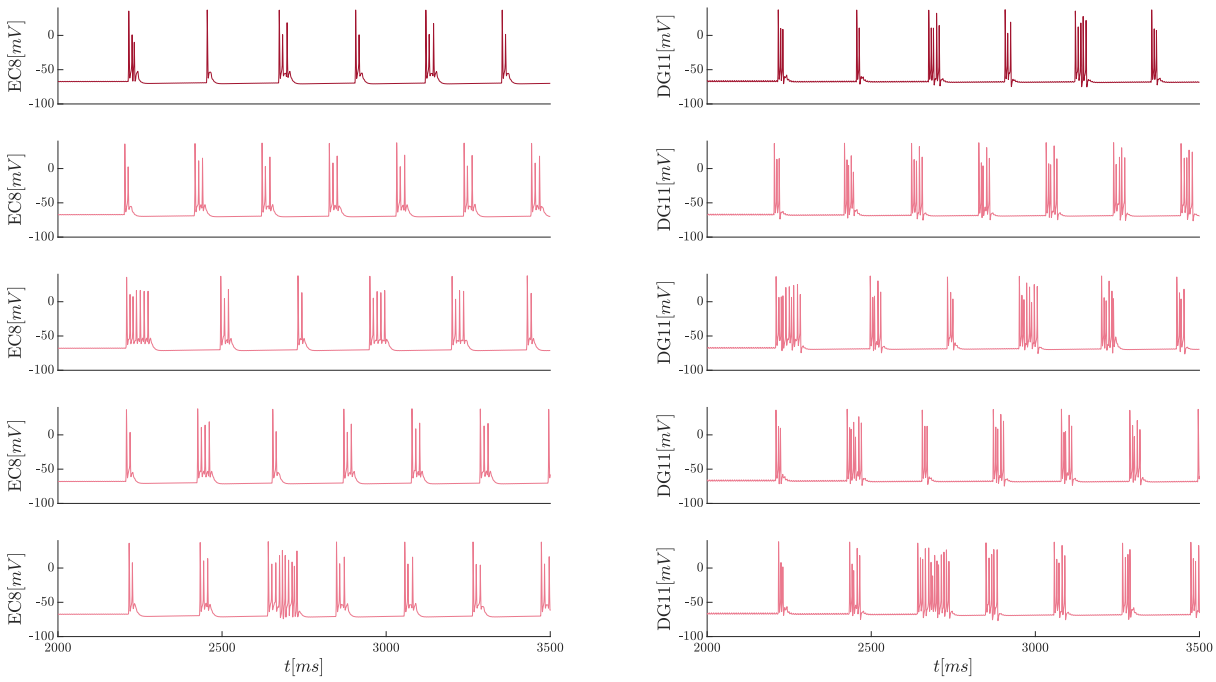

Figure C.22 – Zoom of the evolution of the membrane potential (in mV) of EC8 (left) and DG11 (right) in the fully connected model according to time (in ms) between 2000 ms and 3500 ms with 10% of variability on its ionic conductances. The trace in dark red is the trace without variability and traces in light red corresponds to traces with variability

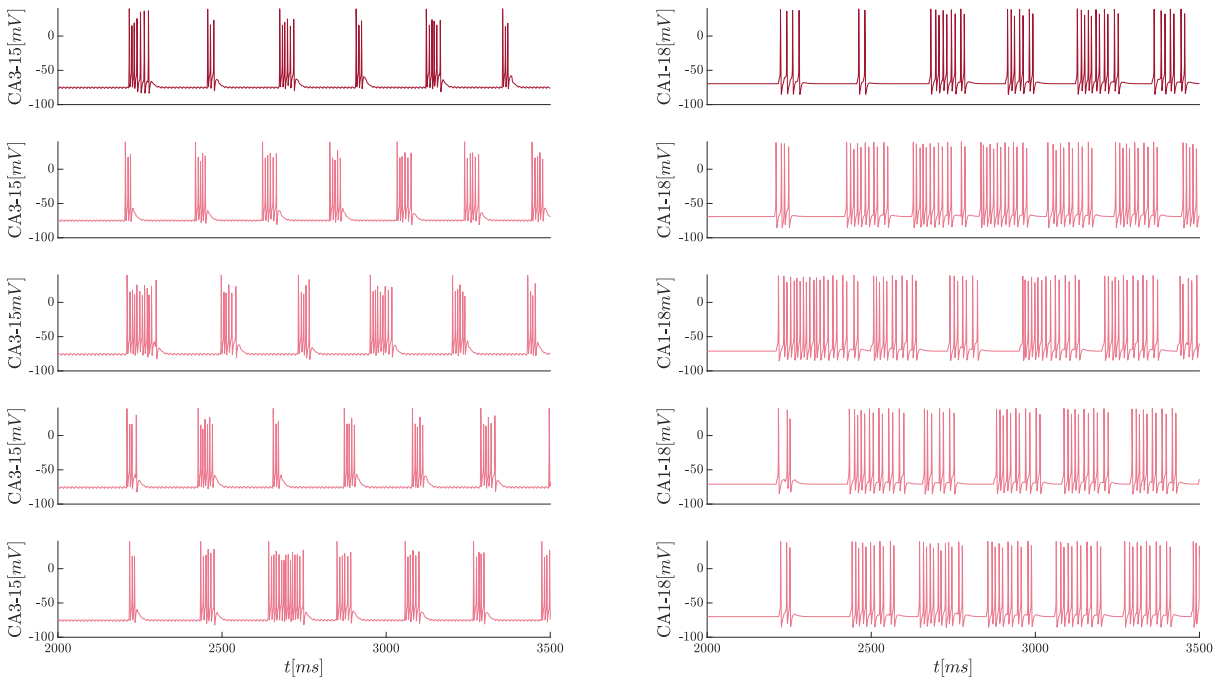

Figure C.23 – Zoom of the evolution of the membrane potential (in mV) of CA3-15 (left) and CA1-18 (right) in the fully connected model according to time (in ms) between 2000 ms and 3500 ms with 10% of variability on its ionic conductances. The trace in dark red is the trace without variability and traces in light red corresponds to traces with variability

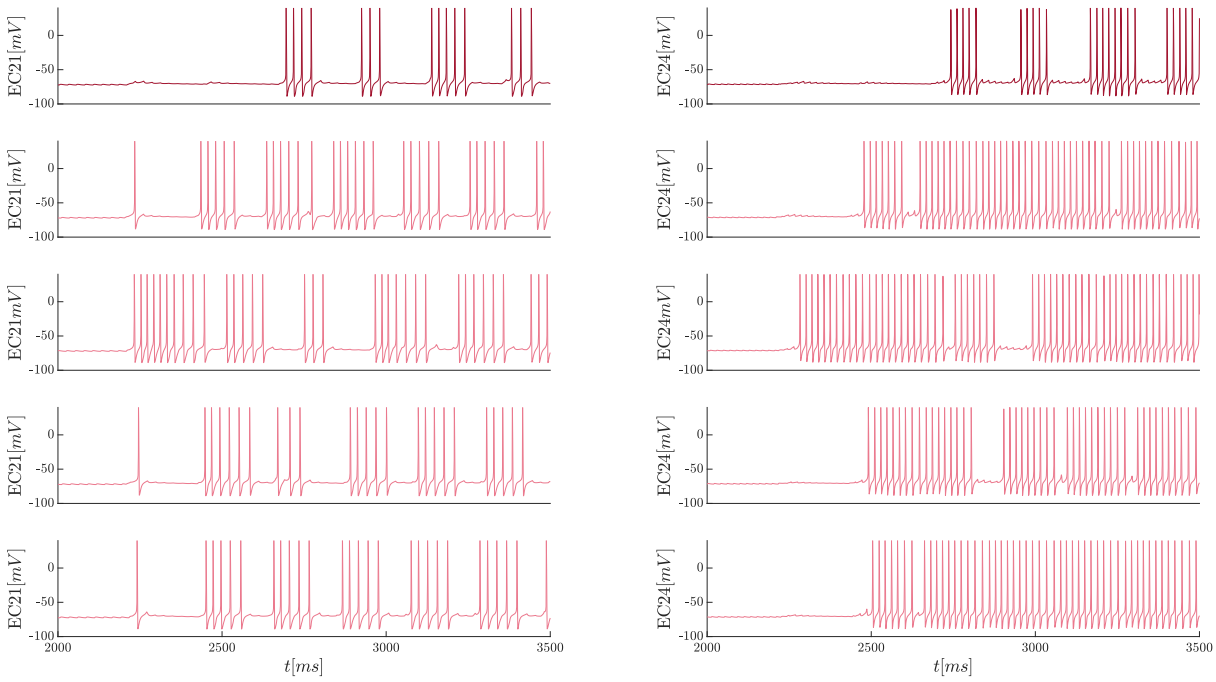

Figure C.24 – Zoom of the evolution of the membrane potential (in mV) of EC21 (left) and EC24 (right) in the fully connected model according to time (in ms) between 2000 ms and 3500 ms with 10% of variability on its ionic conductances. The trace in dark red is the trace without variability and traces in light red corresponds to traces with variability

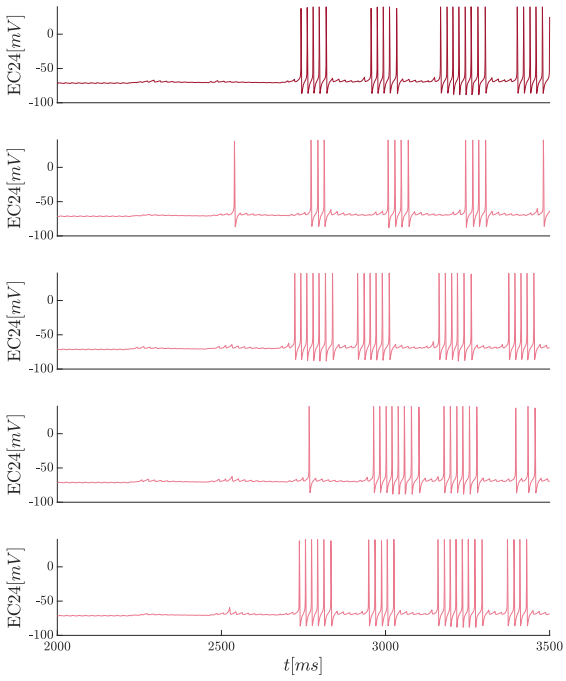

Figure C.25 – Zoom of the evolution of the potential (in mV) of EC24 according to time (in ms) with 5% of variability on its ionic conductances. The trace in dark red is the trace without variability and traces in light red corresponds to traces with variability

C.23.3 Interneuron

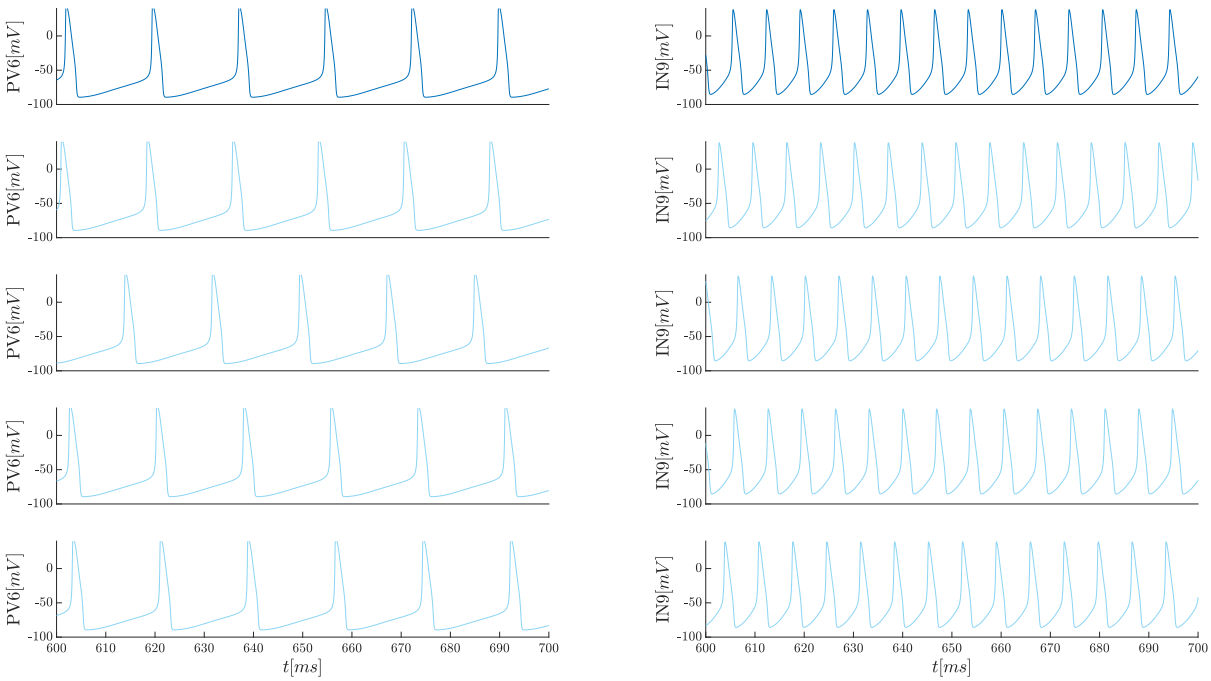

Figure C.26 – Zoom of the evolution of the membrane potential (in mV) of PV6 (left) and IN9 (right) in the fully connected model according to time (in ms) between 700 ms and 800 ms with 10% of variability on its ionic conductances. The trace in dark red is the trace without variability and traces in light red corresponds to traces with variability

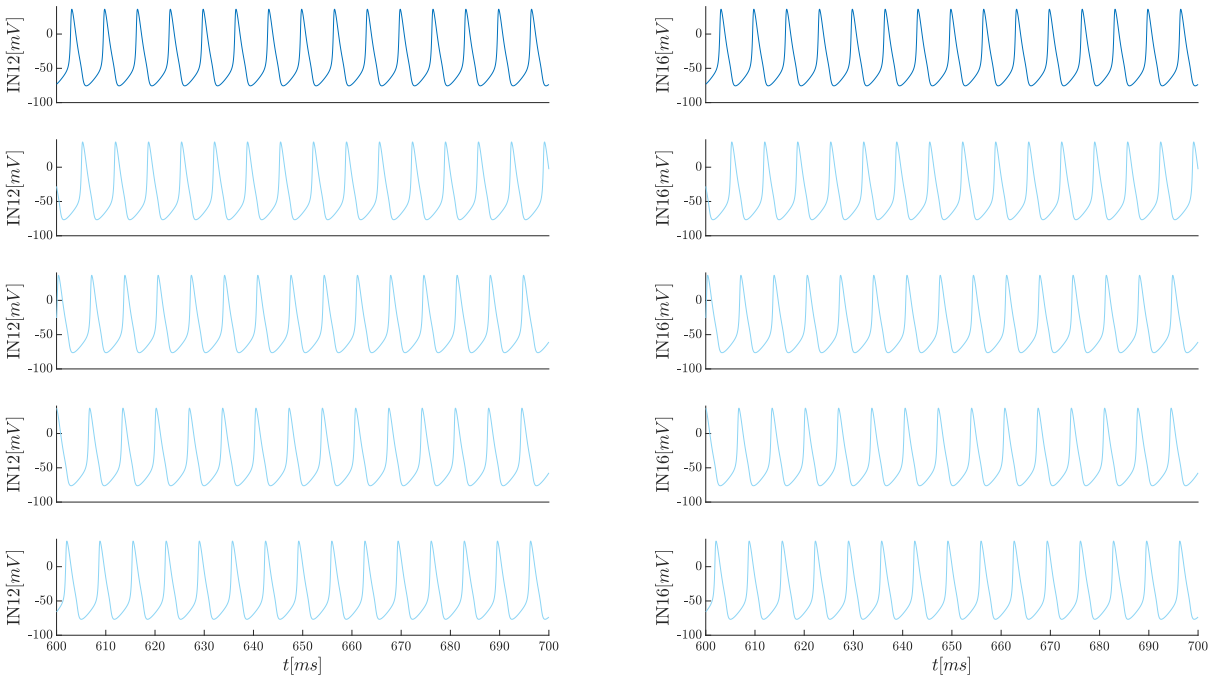

Figure C.27 – Zoom of the evolution of the membrane potential (in mV) of IN12 (left) and IN16 (right) in the fully connected model according to time (in ms) between 700 ms and 800 ms with 10% of variability on its ionic conductances. The trace in dark red is the trace without variability and traces in light red corresponds to traces with variability

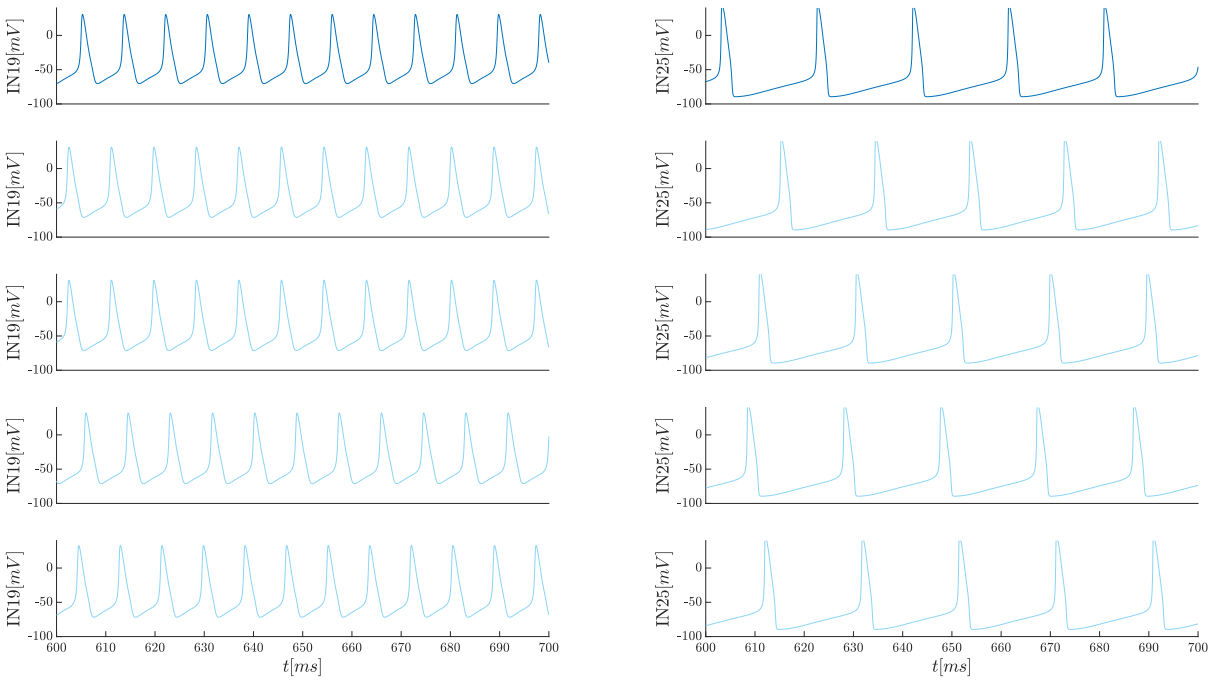

Figure C.28 – Zoom of the evolution of the membrane potential (in mV) of IN19 (left) and IN25 (right) in the fully connected model according to time (in ms) between 700 ms and 800 ms with 10% of variability on its ionic conductances. The trace in dark red is the trace without variability and traces in light red corresponds to traces with variability

Bibliography

Corey D Acker, Nancy Kopell, and John A White. Synchronization of strongly coupled excitatory neurons: relating network behavior to biophysics. *Journal of computational neuroscience*, 15(1): 71–90, 2003.

James B Aimone, Wei Deng, and Fred H Gage. Resolving new memories: a critical look at the dentate gyrus, adult neurogenesis, and pattern separation. *Neuron*, 70(4):589–596, 2011.

Angel Alonso and Ruby Klink. Differential electroresponsiveness of stellate and pyramidal-like cells of medial entorhinal cortex layer ii. *Journal of neurophysiology*, 70(1):128–143, 1993.

David G Amaral, Helen E Scharfman, and Pierre Lavenex. The dentate gyrus: fundamental neuroanatomical organization (dentate gyrus for dummies). *Progress in brain research*, 163:3–790, 2007.

Simone Astori, Ralf D Wimmer, and Anita Lüthi. Manipulating sleep spindles–expanding views on sleep, memory, and disease. *Trends in neurosciences*, 36(12):738–748, 2013.

Amélie Aussel, Laure Buhry, Louise Tyvaert, and Radu Ranta. A detailed anatomical and mathematical model of the hippocampal formation for the generation of sharp-wave ripples and theta-nested gamma oscillations. *Journal of computational neuroscience*, 45(3):207–221, 2018.

Jason S Bant, Kiah Hardcastle, Samuel A Ocko, and Lisa M Giocomo. Topography in the bursting dynamics of entorhinal neurons. *Cell reports*, 30(7):2349–2359, 2020.

Marlene Bartos, Imre Vida, Michael Frotscher, Jörg RP Geiger, and Peter Jonas. Rapid signaling at inhibitory synapses in a dentate gyrus interneuron network. *Journal of Neuroscience*, 21(8): 2687–2698, 2001.

Maxim Bazhenov, Igor Timofeev, Mircea Steriade, and Terrence J Sejnowski. Model of thalamocortical slow-wave sleep oscillations and transitions to activated states. *Journal of neuroscience*, 22(19):8691–8704, 2002.

Mark Bear, Barry Connors, and Michael A Paradiso. *Neuroscience: Exploring the brain*. Jones & Bartlett Learning, LLC, 2016.

Daniela Bianchi, Addolorata Marasco, Alessandro Limongiello, Cristina Marchetti, Helene Marie, Brunello Tirozzi, and Michele Migliore. On the mechanisms underlying the depolarization block in the spiking dynamics of ca1 pyramidal neurons. *Journal of computational neuroscience*, 33(2): 207–225, 2012.

Brain's explained. The neocortex, 2017a. URL https://www.youtube.com/watch?v=fki7AmLma_I. [Accessed: 2021-03-10].

Brain's explained. The thalamus, 2017b. URL https://www.youtube.com/watch?v=fki7AmLma_I. [Accessed: 2021-03-10].

Anatoly Buchin, Anton Chizhov, Gilles Huberfeld, Richard Miles, and Boris S Gutkin. Reduced efficacy of the kcc2 cotransporter promotes epileptic oscillations in a subiculum network model. *Journal of Neuroscience*, 36(46):11619–11633, 2016.

EH Buhl, ZS Han, Z Lorinczi, VV Stezhka, SV Karnup, and P Somogyi. Physiological properties of anatomically identified axo-axonic cells in the rat hippocampus. *Journal of neurophysiology*, 71(4): 1289–1307, 1994.

György Buzsáki. Hippocampal sharp waves: their origin and significance. *Brain research*, 398(2): 242–252, 1986.

György Buzsáki. Two-stage model of memory trace formation: a role for "noisy" brain states. *Neuroscience*, 31(3):551–570, 1989.

György Buzsáki. The hippocampo-neocortical dialogue. *Cerebral cortex*, 6(2):81–92, 1996.

GyÖrgy Buzsáki. Memory consolidation during sleep: a neurophysiological perspective. *Journal of sleep research*, 7(S1):17–23, 1998.

Gyorgy Buzsaki. *Rhythms of the Brain*. Oxford University Press, 2006.

NANCY L Chamberlin, ROGER D Traub, and RAYMOND Dingledine. Role of epsps in initiation of spontaneous synchronized burst firing in rat hippocampal neurons bathed in high potassium. *Journal of neurophysiology*, 64(3):1000–1008, 1990.

Chegg Study. Why are the awake and rem sleep stages both similar in wave patterns observed on an eeg?, 2017. URL https://www.chegg.com/homework-help/questions-and-answers/awake-rem-sleep-stages-similar-wave-patterns-observed-eeg-q74467881. [Accessed: 2021-03-10].

Xiaojing Chen and James J Knierim. It's about time: Temporal dynamics of dentate gyrus pattern separation. *Neuron*, 98(4):681–683, 2018.

James J Chrobak, András Lörincz, and György Buzsáki. Physiological patterns in the hippocampo-entorhinal cortex system. *Hippocampus*, 10(4):457–465, 2000.

Marcos R Costa and Ulrich Müller. Specification of excitatory neurons in the developing cerebral cortex: progenitor diversity and environmental influences. *Frontiers in cellular neuroscience*, 8:449, 2015.

Jozsef Csicsvari, Hajime Hirase, Akira Mamiya, and György Buzsáki. Ensemble patterns of hippocampal ca3-ca1 neurons during sharp wave–associated population events. *Neuron*, 28(2):585–594, 2000.

Vassilis Cutsuridis and Panayiota Poirazi. A computational study on how theta modulated inhibition can account for the long temporal windows in the entorhinal–hippocampal loop. *Neurobiology of learning and memory*, 120:69–83, 2015.

Vassilis Cutsuridis, Bruce P Graham, Stuart Cobb, and Imre Vida. *Hippocampal microcircuits: a computational modeler's resource book*. Springer, 2019.

Vanessa F Descalzo, Lionel G Nowak, Joshua C Brumberg, David A McCormick, and Maria V Sanchez-Vives. Slow adaptation in fast-spiking neurons of visual cortex. *Journal of neurophysiology*, 93(2): 1111–1118, 2005.

Alain Destexhe, Thierry Bal, David A McCormick, and Terrence J Sejnowski. Ionic mechanisms underlying synchronized oscillations and propagating waves in a model of ferret thalamic slices. *Journal of neurophysiology*, 76(3):2049–2070, 1996.

Alain Destexhe, Mike Neubig, Daniel Ulrich, and John Huguenard. Dendritic low-threshold calcium currents in thalamic relay cells. *Journal of Neuroscience*, 18(10):3574–3588, 1998.

Clayton T Dickson, Jacopo Magistretti, Mark Shalinsky, Bassam Hamam, and Angel Alonso. Oscillatory activity in entorhinal neurons and circuits: Mechanisms and function. *Annals of the New York Academy of Sciences*, 911(1):127–150, 2000.

Guillaume Drion. *Regulation of Excitability, Pacemaking, and Bursting: Insights from Dopamine Neuron Electrophysiology.* PhD thesis, Université de Liège, Liège, Belgique, 2013.

Guillaume Drion, Julie Dethier, Alessio Franci, and Rodolphe Sepulchre. Switchable slow cellular conductances determine robustness and tunability of network states. *PLoS computational biology*, 14(4):e1006125, 2018.

Gordon B Feld and Jan Born. Sculpting memory during sleep: concurrent consolidation and forgetting. *Current Opinion in Neurobiology*, 44:20–27, 2017.

Gordon B Feld and Jan Born. Neurochemical mechanisms for memory processing during sleep: basic findings in humans and neuropsychiatric implications. *Neuropsychopharmacology*, 45(1):31–44, 2020.

Laura MJ Fernandez and Anita Lüthi. Sleep spindles: mechanisms and functions. *Physiological reviews*, 100(2):805–868, 2020.

David Ferster. Spatially opponent excitation and inhibition in simple cells of the cat visual cortex. *Journal of Neuroscience*, 8(4):1172–1180, 1988.

Silvana Franceschetti, Ezia Guatteo, Ferruccio Panzica, Giulio Sancini, Enzo Wanke, and Giuliano Avanzini. Ionic mechanisms underlying burst firing in pyramidal neurons: intracellular study in rat sensorimotor cortex. *Brain research*, 696(1-2):127–139, 1995.

RUSSELL A Fricke and DAVID A Prince. Electrophysiology of dentate gyrus granule cells. *Journal of neurophysiology*, 51(2):195–209, 1984.

P. Leprince G. Vandewalle. Introduction aux neurosciences cognitives, Spring 2019.

Francesco Giovannini. *Mathematical Modelling of Neural Oscillations in Hippocampal Memory Networks during Waking and under General Anaesthesia.* PhD thesis, Université de Lorraine, 2017.

Nace L Golding, William L Kath, and Nelson Spruston. Dichotomy of action-potential backpropagation in ca1 pyramidal neuron dendrites. *Journal of neurophysiology*, 86(6):2998–3010, 2001.

David Golomb, Karnit Donner, Liron Shacham, Dan Shlosberg, Yael Amitai, and David Hansel. Mechanisms of firing patterns in fast-spiking cortical interneurons. *PLoS Comput Biol*, 3(8):e156, 2007.

Attila I Gulyás, Gergely G Szabó, István Ulbert, Noémi Holderith, Hannah Monyer, Ferenc Erdélyi, Gábor Szabó, Tamás F Freund, and Norbert Hájos. Parvalbumin-containing fast-spiking basket cells generate the field potential oscillations induced by cholinergic receptor activation in the hippocampus. *Journal of Neuroscience*, 30(45):15134–15145, 2010.

John J Hablitz and Daniel Johnston. Endogenous nature of spontaneous bursting in hippocampal pyramidal neurons. *Cellular and molecular neurobiology*, 1(4):325–334, 1981.

Bassam N Hamam, Timothy E Kennedy, Angel Alonso, and David G Amaral. Morphological and electrophysiological characteristics of layer v neurons of the rat medial entorhinal cortex. *Journal of Comparative Neurology*, 418(4):457–472, 2000.

Michael E Hasselmo. The role of acetylcholine in learning and memory. *Current opinion in neurobiology*, 16(6):710–715, 2006.

Donald Olding Hebb. The organization of behavior; a neuropsycholocigal theory. *A Wiley Book in Clinical Psychology*, 62:78, 1949.

Ruth Heidelberger, Harel Shouval, Robert S Zucker, and John H Byrne. Synaptic plasticity. In *From Molecules to Networks*, pages 533–561. Elsevier, 2014.

Sean Hill and Giulio Tononi. Modeling sleep and wakefulness in the thalamocortical system. *Journal of neurophysiology*, 93(3):1671–1698, 2005.

Michael R Hunsaker, Bart Lee, and Raymond P Kesner. Evaluating the temporal context of episodic memory: the role of ca3 and ca1. *Behavioural brain research*, 188(2):310–315, 2008.

Eugene M Izhikevich. *Dynamical systems in neuroscience*. MIT press, 2007.

Kathleen Jacquerie. Master thesis : Sensitivity and robustness analysis of thalamic neuron models at the cellular and network levels. *Université de Liège, Liège, Belgique*, 2018.

Kathleen Jacquerie and Guillaume Drion. Robust switches in thalamic network activity require a timescale separation between sodium and t-type calcium channel activations. *PLOS Computational Biology*, 17(5):e1008997, 2021.

Tim Jarsky, Rina Mady, Benjamin Kennedy, and Nelson Spruston. Distribution of bursting neurons in the ca1 region and the subiculum of the rat hippocampus. *Journal of Comparative Neurology*, 506 (4):535–547, 2008.

Srdjan M Joksimovic, Pierce Eggan, Yukitoshi Izumi, Sonja Lj Joksimovic, Vesna Tesic, Robert M Dietz, James E Orfila, Michael R DiGruccio, Paco S Herson, Vesna Jevtovic-Todorovic, et al. The role of t-type calcium channels in the subiculum: to burst or not to burst? *The Journal of physiology*, 595(19):6327–6348, 2017.

Barbara E Jones. Neuroscience: what are cortical neurons doing during sleep? *Current Biology*, 26 (21):R1147–R1150, 2016.

Roland SG Jones. Synaptic and intrinsic properties of neurons of origin of the perforant path in layer ii of the rat entorhinal cortex in vitro. *Hippocampus*, 4(3):335–353, 1994.

RSG Jones and EH Bühl. Basket-like interneurones in layer ii of the entorhinal cortex exhibit a powerful nmda-mediated synaptic excitation. *Neuroscience letters*, 149(1):35–39, 1993.

Hae-yoon Jung, Nathan P Staff, and Nelson Spruston. Action potential bursting in subicular pyramidal neurons is driven by a calcium tail current. *Journal of Neuroscience*, 21(10):3312–3321, 2001.

Jens G Klinzing, Niels Niethard, and Jan Born. Mechanisms of systems memory consolidation during sleep. *Nature neuroscience*, 22(10):1598–1610, 2019a.

Jens G Klinzing, Niels Niethard, and Jan Born. Mechanisms of systems memory consolidation during sleep. *Nature neuroscience*, 22(10):1598–1610, 2019b.

Andreas Knopp, Anatol Kivi, Christian Wozny, Uwe Heinemann, and Joachim Behr. Cellular and network properties of the subiculum in the pilocarpine model of temporal lobe epilepsy. *Journal of Comparative Neurology*, 483(4):476–488, 2005.

Giri P Krishnan and Maxim Bazhenov. Ionic dynamics mediate spontaneous termination of seizures and postictal depression state. *Journal of Neuroscience*, 31(24):8870–8882, 2011.

Steve Kunec, Michael E Hasselmo, and Nancy Kopell. Encoding and retrieval in the ca3 region of the hippocampus: a model of theta-phase separation. *Journal of neurophysiology*, 94(1):70–82, 2005.

Jesse J Langille. Remembering to forget: a dual role for sleep oscillations in memory consolidation and forgetting. *Frontiers in cellular neuroscience*, 13:71, 2019.

Pierre Lavenex and David G Amaral. Hippocampal-neocortical interaction: A hierarchy of associativity. *Hippocampus*, 10(4):420–430, 2000.

Rodolfo R Llinas, Anthony A Grace, and Yosef Yarom. In vitro neurons in mammalian cortical layer 4 exhibit intrinsic oscillatory activity in the 10-to 50-hz frequency range. *Proceedings of the National Academy of Sciences*, 88(3):897–901, 1991.

Jacopo Magistretti, David S Ragsdale, and Angel Alonso. High conductance sustained single-channel activity responsible for the low-threshold persistent na+ current in entorhinal cortex neurons. *Journal of Neuroscience*, 19(17):7334–7341, 1999.

David A McCormick and Thierry Bal. Sleep and arousal: thalamocortical mechanisms. *Annual review of neuroscience*, 20(1):185–215, 1997.

David A McCormick and John R Huguenard. A model of the electrophysiological properties of thalamocortical relay neurons. *Journal of neurophysiology*, 68(4):1384–1400, 1992.

David A McCormick, Matthew J McGinley, and David B Salkoff. Brain state dependent activity in the cortex and thalamus. *Current opinion in neurobiology*, 31:133–140, 2015.

Alexia E Metz, Tim Jarsky, Marco Martina, and Nelson Spruston. R-type calcium channels contribute to afterdepolarization and bursting in hippocampal ca1 pyramidal neurons. *Journal of Neuroscience*, 25(24):5763–5773, 2005.

M Migliore, EP Cook, DB Jaffe, DA Turner, and D Johnston. Computer simulations of morphologically reconstructed ca3 hippocampal neurons. *Journal of neurophysiology*, 73(3):1157–1168, 1995.

Giampaolo Milior, Maria Amalia Di Castro, Livio Pepe'Sciarria, Stefano Garofalo, Igor Branchi, Davide Ragozzino, Cristina Limatola, and Laura Maggi. Electrophysiological properties of ca1 pyramidal neurons along the longitudinal axis of the mouse hippocampus. *Scientific reports*, 6(1):1–9, 2016.

Mind fully well. Trauma and the brain. URL https://corkpsychotherapyandtraumacentre.ie/trauma/trauma-and-the-brain/.

Catherine E Myers and Helen E Scharfman. A role for hilar cells in pattern separation in the dentate gyrus: a computational approach. *Hippocampus*, 19(4):321–337, 2009.

Catherine E Myers and Helen E Scharfman. Pattern separation in the dentate gyrus: a role for the ca3 backprojection. *Hippocampus*, 21(11):1190–1215, 2011.

Miguel Navarrete, Mario Valderrama, and Penelope A Lewis. The role of slow-wave sleep rhythms in the cortical-hippocampal loop for memory consolidation. *Current Opinion in Behavioral Sciences*, 32:102–110, 2020.

Neuroscientifically Challenged. 2-minute neuroscience: Gaba, 2018. URL https://www.youtube.com/watch?v=bQIU2KDtHTI). [Accessed: 2021-05-13].

Niels Niethard, Andrea Burgalossi, and Jan Born. Plasticity during sleep is linked to specific regulation of cortical circuit activity. *Frontiers in neural circuits*, 11:65, 2017.

Umberto Olcese, Steve K Esser, and Giulio Tononi. Sleep and synaptic renormalization: a computational study. *Journal of neurophysiology*, 104(6):3476–3493, 2010.

Shane O'Mara. The subiculum: what it does, what it might do, and what neuroanatomy has yet to tell us. *Journal of anatomy*, 207(3):271–282, 2005.

Shane M O'Mara, Sean Commins, and Michael Anderson. Synaptic plasticity in the hippocampal area ca1-subiculum projection: Implications for theories of memory. *Hippocampus*, 10(4):447–456, 2000.

Shane M O'Mara, Sean Commins, Michael Anderson, and John Gigg. The subiculum: a review of form, physiology and function. *Progress in neurobiology*, 64(2):129–155, 2001.

Shane O'Mara. Controlling hippocampal output: the central role of subiculum in hippocampal information processing. *Behavioural brain research*, 174(2):304–312, 2006.

FERENC Pongracz, NICHOLAS P Poolos, JEFFERY D Kocsis, and GORDON M Shepherd. A model of nmda receptor-mediated activity in dendrites of hippocampal ca1 pyramidal neurons. *Journal of neurophysiology*, 68(6):2248–2259, 1992.

Martin Pospischil, Maria Toledo-Rodriguez, Cyril Monier, Zuzanna Piwkowska, Thierry Bal, Yves Frégnac, Henry Markram, and Alain Destexhe. Minimal hodgkin–huxley type models for different classes of cortical and thalamic neurons. *Biological cybernetics*, 99(4):427–441, 2008.

Nadezhda V Povysheva, Aleksey V Zaitsev, Guillermo Gonzalez-Burgos, and David A Lewis. Electrophysiological heterogeneity of fast-spiking interneurons: chandelier versus basket cells. *PloS one*, 8 (8):e70553, 2013.

Björn Rasch and Jan Born. Reactivation and consolidation of memory during sleep. *Current Directions in Psychological Science*, 17(3):188–192, 2008.

Björn Rasch and Jan Born. About sleep's role in memory. *Physiological reviews*, 2013.

Horacio G Rotstein, Tim Oppermann, John A White, and Nancy Kopell. The dynamic structure underlying subthreshold oscillatory activity and the onset of spikes in a model of medial entorhinal cortex stellate cells. *Journal of computational neuroscience*, 21(3):271–292, 2006.

Vijayalakshmi Santhakumar, Ildiko Aradi, and Ivan Soltesz. Role of mossy fiber sprouting and mossy cell loss in hyperexcitability: a network model of the dentate gyrus incorporating cell types and axonal topography. *Journal of neurophysiology*, 93(1):437–453, 2005.

Carla Alessandra Scorza, Bruno Henrique Silva Araujo, LA Leite, Laila Brito Torres, Luis Fernando Pacheco Otalora, Mauro Schneider Oliveira, Emílio Rafael Garrido-Sanabria, and Esper Abrão Cavalheiro. Morphological and electrophysiological properties of pyramidal-like neurons in the stratum oriens of cornu ammonis 1 and cornu ammonis 2 area of proechimys. *Neuroscience*, 177:252–268, 2011.

S Murray Sherman. Tonic and burst firing: dual modes of thalamocortical relay. *Trends in neurosciences*, 24(2):122–126, 2001.

Tristan Shuman, Daniel Aharoni, Denise J Cai, Christopher R Lee, Spyridon Chavlis, Lucia Page-Harley, Lauren M Vetere, Yu Feng, Chen Yi Yang, Irene Mollinedo-Gajate, et al. Breakdown of spatial coding and interneuron synchronization in epileptic mice. *Nature neuroscience*, 23(2):229–238, 2020.

Nathan P Staff, Hae-Yoon Jung, Tara Thiagarajan, Michael Yao, and Nelson Spruston. Resting and active properties of pyramidal neurons in subiculum and ca1 of rat hippocampus. *Journal of neurophysiology*, 84(5):2398–2408, 2000.

Carl E Stafstrom. The role of the subiculum in epilepsy and epileptogenesis. *Epilepsy Currents*, 5(4): 121–129, 2005.

David A Stanley, Sachin S Talathi, Mansi B Parekh, Daniel J Cordiner, Junli Zhou, Thomas H Mareci, William L Ditto, and Paul R Carney. Phase shift in the 24-hour rhythm of hippocampal eeg spiking activity in a rat model of temporal lobe epilepsy. *Journal of neurophysiology*, 110(5):1070–1086, 2013.

Mircea Steriade, David A McCormick, and Terrence J Sejnowski. Thalamocortical oscillations in the sleeping and aroused brain. *Science*, 262(5134):679–685, 1993.

Yanjun Sun, Suoqin Jin, Xiaoxiao Lin, Lujia Chen, Xin Qiao, Li Jiang, Pengcheng Zhou, Kevin G Johnston, Peyman Golshani, Qing Nie, et al. Ca1-projecting subiculum neurons facilitate object–place learning. *Nature neuroscience*, 22(11):1857–1870, 2019.

R. Sépulchre. Gbio0011 modélisation des systèmes biologiques: Notes de cours à l'attention des étudiants. *ULiège*, 2008-2009.

Jeffrey S Taube. Electrophysiological properties of neurons in the rat subiculum in vitro. *Experimental brain research*, 96(2):304–318, 1993.

Jiannis Taxidis, Stephen Coombes, Robert Mason, and Markus R Owen. Modeling sharp wave-ripple complexes through a ca3-ca1 network model with chemical synapses. *Hippocampus*, 22(5):995–1017, 2012.

Jiannis Taxidis, Kenji Mizuseki, Robert Mason, and Markus Roger Owen. Influence of slow oscillation on hippocampal activity and ripples through cortico-hippocampal synaptic interactions, analyzed by a cortical-ca3-ca1 network model. *Frontiers in computational neuroscience*, 7:3, 2013.

Giulio Tononi and Chiara Cirelli. Sleep and the price of plasticity: from synaptic and cellular homeostasis to memory consolidation and integration. *Neuron*, 81(1):12–34, 2014.

Roger D Traub, Robert K Wong, Richard Miles, and Hillary Michelson. A model of a ca3 hippocampal pyramidal neuron incorporating voltage-clamp data on intrinsic conductances. *Journal of neurophysiology*, 66(2):635–650, 1991.

Trusted Neurodiagnostics academy. visual pathway. URL http://www-cs-faculty.stanford.edu/~uno/abcde.html.

Xiao-Jing Wang and György Buzsáki. Gamma oscillation by synaptic inhibition in a hippocampal interneuronal network model. *Journal of neuroscience*, 16(20):6402–6413, 1996.

Yina Wei, Giri P Krishnan, and Maxim Bazhenov. Synaptic mechanisms of memory consolidation during sleep slow oscillations. *Journal of Neuroscience*, 36(15):4231–4247, 2016.

Theodore G Weyand, Michael Boudreaux, and William Guido. Burst and tonic response modes in thalamic neurons during sleep and wakefulness. *Journal of neurophysiology*, 85(3):1107–1118, 2001.

Stephen R Williams and Greg J Stuarty. Mechanisms and consequences of action potential burst firing in rat neocortical pyramidal neurons. *The Journal of physiology*, 521(2):467–482, 1999.

Xiangmin Xu, Yanjun Sun, Todd C Holmes, and Alberto J López. Noncanonical connections between the subiculum and hippocampal ca1. *Journal of Comparative Neurology*, 524(17):3666–3673, 2016.

Edward Zagha and David A McCormick. Neural control of brain state. *Current opinion in neurobiology*, 29:178–186, 2014.